Effect of Molecular Adsorption on the Electronic Structure of Single Walled Carbon Nanotubes

---

Thesis

Submitted in partial fulfillment of the requirements for the degree of

Doctor of Philosophy

By

TALAPUNUR VIKRAMADITYA

ID. No: 2011PHXF009H

Under the Supervision of

Prof. K. SUMITHRA

BIRLA INSTITUTE OF TECHNOLOGY AND SCIENCE, PILANI.

2015

Birla Institute of Technology and Science, Pilani,

Hyderabad Campus, Jawahar Nagar, Shamirpet Mandal, Hyderabad, Telangana State, 500078.

CERTIFICATE

This is to certify that the thesis entitled **"Effect of Molecular Adsorption on the Electronic Structure of Single Walled Carbon Nanotubes"** submitted by Talapunur Vikramaditya, ID.No. 2011PHXF009H for the award of Ph.D degree of the institute embodies the original work done by him under my supervision.

Signature in full of the supervisor -

Name in Capital block letters - K. SUMITHRA

Designation - Associate Professor

Acknowledgements

I am very much indebted to my parents for their immense support and great patience which helped me to successfully complete my doctoral degree.

I thank my Ph.D supervisor Prof. K. Sumithra and feel privileged to work under her guidance and also being her first Ph.D student. Her constant motivation and concern helped me to come out of most difficult times successfully.

I express my gratitude to Prof. V.S. Rao (Director – BITS Pilani Hyderabad campus) and former Vice-Chancellor Prof. B.N. Jain for permitting me to work in the campus.

I thank my Doctoral advisory committee members Prof. Kannan Ramaswamy and Dr. Subhas Ghosal, for their thoughtful inputs and suggestions. I thank Dr. Anupam Bhattacharya, Head of the Department, Chemistry Division, BITS Pilani, Hyderabad campus and also other faculty members.

I express my sincere gratitude to Dean, Academic and Research Division, BITS Pilani, Dean, Sponsored Research and Consultancy Division, Dean, Academic and Research Consultancy Division– BITS Pilani Hyderabad campus for their support and prompt processing of issues concerned.

I sincerely thank Prof. Oded Hod and Dana Krepel, (Tel Aviv University, Israel) for helping me to sort out the queries concerned with Gaussian software package and also the teams of Gaussian help.

I take this opportunity to express my heartfelt thanks to non-teaching staff, Praveen, Bhagya Lakshmi (RCD Division), Ashok, Shanthakumari, Sudheer (Lab technicians - Chemistry Division), Krishna, Anil, Haritha, Madhu, Uday Kumar (Library staff), Hari (Stores), Ramesh (IPC- Division).

I thank all my friends and colleagues Santhanam, K.M.L. Naidu, Mahesh, Yadagiri, Narva Suresh, Amaroju Suresh, Nagesh, Uday, Bharathidasan, Sathvika, Ravikiran, Santhosh, Swapna, Srinivas Rao, Singi Reddy, Praveen, Srikanth, Manoj, Jagan, Subba Rao, Rajesh, Prasad, Meera, Pooja, Sathish, Hemanth, Seshadri, Muthu Kumar, Prathyusha, Rahul, Madhu Poornima, Ravichand, Priyanka, Ram Mishra, Mahibalan, Venkatesh, Ravikrishna and Tripathi.

I specially thank my Junior M. Saisudhakar, for helping me in the work and was very much supportive in all aspects.

It also gives me immense pleasure to thank my teacher during school days Sharma sir and my childhood buddies, Raghavendra and Sankeerth.

I thank my dear sisters Uma, Jyothirmayi, Jwala and Deepthi and my cousins Vamshi, Shyam, Harsha, Chaitanya, Dheeraj, Prithvi, Mourya my aunts Sudha, Chandrika, Manjusha and my uncles, Badrinarayan Rao and Shyam Sunder Rao without these people's support I would not have come up to this stage.

I am grateful towards the funding agency University Grants Commission (UGC), New-Delhi for their financial aid in the form of junior / senior research fellowships.

(T. Vikramaditya)

ABSTRACT

The study of adsorption of various gaseous molecules on Carbon nanotubes (CNTs) are of great importance because of its vast applications in science and technology. Most of these applications are based on electronic and transport property changes as a result of adsorption. Single walled carbon nanotubes (SWCNT) based sensors have gained significant interest especially due to the modification of their electrical properties with adsorption of simple chemical species on the surface. Due to their high surface to volume ratio, they may be able to act as good sensors and also as gas storage materials. It has also been demonstrated experimentally that the electronic properties of SWNTs are very sensitive to the chemical environment. Conventional sensors which are widely used to detect gases are comprised of thin film metal oxides of tin oxide, zinc oxide or indium oxide. These sensors lack flexibility, suffer with poor response times and fails to operate at lower temperatures. Carbon nanotubes can act as a better alternative for these applications because of their unique morphology. The main principle involved in detecting various gases by CNTs is by monitoring the conductance change associated with the charge transfer between CNTs and the adsorbed gases.

Most of the theoretical studies carried out so far to study the adsorption of gases with CNTs are carried out employing the local density approximation (LDA) or generalized gradient approximation (GGA) in the Density functional theory (DFT) framework. It is well reported in the literature that LDA overestimates binding energies and charge transfers, whereas GGA underestimates these quantities. Contradictory results have been published in recent years with respect to the adsorption of few gases with CNTs. We have employed the hybrid functional B3LYP, to investigate the adsorption of various gas molecules on SWCNTs. It has been reported that binding energies, charge transfers and band gaps calculated by this methodology are in good agreement with experimental studies by various groups. In the first Chapter, we discuss the structural and electronic properties of SWCNTs and the literature review on adsorption of gas molecules on CNTs followed by computational methodology employed to study the adsorption of gas molecules along the side walls of SWCNTs in the second Chapter.

Adsorption of various gas molecules like oxygen (in both the spin states), nitrogen, hydrogen, carbon monoxide, water vapor and ammonia with intrinsic as well as doped carbon nanotubes is investigated. Doping the CNTs with hetero atoms like boron and nitrogen helps in

overcoming the serious limitation of passive nature of pristine CNTs. Carbon atoms in CNTs are sp^2 hybridized and incorporation of hetero atoms like boron and nitrogen atoms into the honeycomb lattice results in chemical activation of the rather passive surface of a carbon nanotube and create additional electronic states around the Fermi level.

We have studied the adsorption of oxygen molecule in both the spin singlet and triplet states with intrinsic, boron doped and nitrogen doped SWCNTs. The adsorption patterns of both singlet and a triplet oxygen molecule on carbon nanotubes. Singlet molecule exhibits a strong adsorption with intrinsic and doped SWCNTs, whereas triplet oxygen is found to show a weak physisorption with intrinsic SWCNTs. We find that there is appreciable charge transfer from the nanotube to the singlet oxygen which is also evident from the low lying LUMO of the singlet oxygen. The effect of replacing a single carbon of the semi-conducting nanotube with a boron atom leads to almost the same distances for the singlet molecule, but with less charge transfer, as is expected. The adsorption energy is found to be more for boron doped cases. However doping with nitrogen did not alter the electronic properties of SWCNTs. The triplet oxygen adsorptions mentioned in the literature reports only weak van der Waals interactions with pristine nanotubes. Our results support this and we also propose the idea of nanoscale sensor devices that can detect the oxygen molecule in its natural state in transient proximity. The boron doped semi-conducting tubes show very good affinity towards triplet oxygen and is found to be at distances of 1.5 – 1.6 Å. The results of oxygen adsorption are discussed in detail in Chapter 3.

We have also investigated the adsorption of various other gaseous molecules like hydrogen, nitrogen, carbon monoxide and water vapor. We have found that hydrogen, nitrogen and carbon monoxide did not exhibit any significant binding with intrinsic and boron doped SWCNTs. Water vapor on the other hand show weak binding with intrinsic SWCNTs but exhibited a binding energy of -0.239, -0.244, -0.542 eV with (5,0), (5,5) and (8,0) boron doped SWCNTs respectively. The charge transfer is found to be from the water molecule to the electron deficient boron doped CNT. From the density of states plots of (8,0) intrinsic and boron doped SWCNTs, we observe that the band gaps remain unaltered in the case of intrinsic SWCNTs whereas it is increased with doped system. This can be understood from the fact that there is negligible charge transfer between intrinsic (8,0) SWCNT and water whereas 0.258 e charge transfer is observed in the case of (8,0) boron doped SWCNT. All the other gaseous molecules studied are found to be passive with respect to binding on both intrinsic and boron doped SWCNTs. The results of adsorption of environmentally relevant

molecules like hydrogen, nitrogen, carbon monoxide and water vapor on SWCNTs are discussed in Chapter 4.

We have also studied the effect of ammonia adsorption on semi-conducting SWCNTs of various diameters and have found that the electronic properties and affinity towards ammonia appreciably change upon substitutionally doping the SWCNT with boron. This is reflected in the increased charge transfer, ammonia-nanotube distance and binding energies. In order to understand the accurate conductivity changes, we have employed periodic boundary conditions (PBC) and studied the doping and adsorption characteristics for an infinite system. We find that doping of the nanotubes leads to lowering of the direct band gap thus making the semi-conducting SWCNT to a semi-metal nanotube with a direct band gap of about 0.365 eV and a negative indirect band gap of -1.14 eV. After binding with ammonia the band gap opens up and the tube becomes more semi-conducting with an increase in band gap from 0.365 to 1.24 eV which can be understood by the charge transfer phenomenon. The doped nanotube has hole carriers and ammonia would reduce the hole concentration by transferring its electrons to the nanotube thus increasing the band gap and reducing the conductivity. Thus by detecting the conductivity changes of the boron-doped systems before and after adsorption of ammonia the presence of this molecule can be detected. We have also found that the electronic charge transfer is an important mechanism which brings about a change in conductivity in the doped SWCNT on adsorption of ammonia. These findings are discussed in Chapter 5.

In order to understand the interaction of simple amino acids with nanotubes the adsorption of bio-molecules like glycine in both non-ionic and zwitter-ionic forms with intrinsic and functionalized SWCNTs is investigated. Glycine in both non-ionic and zwitter-ionic states is found to exhibit weak binding energies with intrinsic SWCNT, with the zwitter-ionic interaction being more favorable. In the case of functionalized SWCNT, COOH-CNT exhibited higher binding energies compared to the hydroxyl and amino functionalized SWCNTs in both the states of glycine. Doubly functionalized SWCNT with carboxylic and amino groups exhibited higher binding energy in gas phase compared to the singly functionalized SWCNTs. In all cases charge transfer is observed to be weak, with charge being transferred from glycine to the SWCNT. Glycine shows better interaction, in both non-ionic and zwitter-ionic states with functionalized SWCNTs compared to that of intrinsic SWCNT and binding energy is found to be enhanced in the aqueous media. Zwitter-ions are found to adsorb stronger than their nonionic counterparts and physisorption is strongest

through the active carbonyl oxygen site for the zwitter-ionic-glycine amino acid, in contrast to the non-ionic case. Interaction of glycine with intrinsic and functionalized SWCNTs is discussed in Chapter 6.

Understanding the nature of band gap whether direct or indirect is very much important since it affects the device performance in organic electronics. In order to understand whether the nature of band gap is direct or indirect upon doping, we have performed band structure studies on boron and nitrogen doped SWCNTs. Semi-conducting (8,0) SWCNTs are found to be conducting upon doping with boron and nitrogen. We observed that unsymmetrical doping results in slight increase in band gap which could be due to the increase in strain energy of SWCNT these results are discussed in Chapter 7. A brief summary and conclusions are discussed in Chapter 8.

LIST OF ABBREVIATIONS

- AO – Atomic orbitals
- B3LYP – Becke 3Lee Yang Parr
- CGTO – Contracted Gaussian type of orbitals
- CNT - Carbon nanotube
- CPU – Central processing unit
- CVD – Chemical Vapor Deposition
- DFT – Density functional theory
- DFTB – Density functional based tight binding
- DOS – Density of states
- ESP – Electrostatic potential mapped surfaces
- Exc – Exchange correlation energy
- GGA – Generalized gradient approximation
- GTO – Gaussian type of orbitals
- HF – Hartree Fock
- HOCO – Highest occupied crystal orbital
- HOMO –Highest occupied molecular orbital
- KS – Kohn sham
- LDA – Local density approximation
- LSDA – Local spin density approximation
- LUCO – Lowest unoccupied crystal orbital
- LUMO – Lowest unoccupied molecular orbital
- MGGA – Meta generalized gradient approximation
- MO – Molecular orbital
- MOT – Molecular orbital theory
- MWCNT – Multi walled carbon nanotube
- NAO – Natural atomic orbitals
- NBO – Natural bond orbital

- NHO – Natural hybrid orbitals
- NLMO – Natural semi-localized molecular orbital
- NMR – Nuclear magnetic resonance
- NPA – Natural population analysis
- PBC – Periodic boundary conditions
- PES – Potential energy surface
- PPB – Parts per billion
- PPM – Parts per million
- SALC – Symmetry adapted linear combination
- STO – Slater type of orbital
- SWCNT – Single walled carbon nanotube
- TEM – Transmission electron microscopy

LIST OF FIGURES

LIST OF TABLES

TABLE OF CONTENTS

Contents

CHAPTER 1

An Introduction to Carbon Nanotubes

1.1. Introduction of Carbon Nanotubes

Low dimensional carbon nanomaterials form an important class of materials due to their unique all carbon structure and versatile properties. Carbon nanotubes (CNTs), one of the allotropes of carbon, belong to the family of these materials with a single dimensional sp^2 carbon structure. The studies of CNTs have attracted the attention of both experimental and theoretical front owing to their exceptional electronic, optical and mechanical properties [1-3]. CNTs exhibit an unique morphology wherein a graphene sheet is rolled to form a cylindrical shape of uni-dimensional material, with very high surface area to volume ratio where the length to diameter ratio is about 132, 000, 000:1 [4]. Unique electronic properties offered by CNTs like thermal conductivity greater than diamond [5], mechanical properties like stiffness, resilience and strength exceeding any current known materials provides tremendous opportunities to develop them as new material systems. Exceptional mechanical properties coupled with superior thermal and electric properties make them a unique material. They are thermally stable up to 2800^0C in vacuum and have current carrying capacity almost 1000 times higher than copper wires [6]. Carbon nanotubes exhibit unique transport properties and at low temperatures act as quantum wires in which the electrons move without being scattered by scattering centers [3]. Due to these peculiar properties, CNTs are considered as potential candidates in a wide variety of applications like nano electronic devices, solar cells, hydrogen storage, gas sensors, optics, drug delivery etc. and hence are extensively investigated both theoretically and experimentally over the past few years [7-11]. Unique and tunable properties of CNTs exploiting their electronic, physical and chemical properties open new doors for their application in these diverse areas.

The synthesis of nanotubes of carbon of 50 nm diameters was published as early as in 1952 by Radushkevich *et al.,* [12] which went largely unnoticed. In the year 1976, Oberlin and co-workers synthesized hollow carbon fibers with nanoscale diameters and elucidated the structures of single walled carbon nanotubes (SWCNTs) with transmission electron microscopy (TEM) images [13]. Later different groups [14,15] synthesized and characterized CNTs however, it is in 1991, following Iijima's synthesis of MWCNTs [16] and his prediction of its remarkable transport properties that CNTs were brought into the lime light of scientific community. Since then extensive work, both theoretical and experimental have

been carried out to investigate its possible applications in the frontier areas of energy and materials.

CNTs consist of all carbon sp^2 hybrid structure with aromatic six membered rings. CNTs possess a low density of 1.3-1.4 g/cm^3, and a high tensile strength of around 63 Giga Pascals [17]. Computational studies [18] with quantum and atomistic models show that the strength of SWCNTs can be as high as 100 Giga Pascals, which is in good agreement with experiments. The deformation of the 2D- graphene sheet in the third dimension to form CNTs does not significantly alter the bond lengths in the hexagonal rings within the sheet. CNTs are classified into two categories based on their structural aspects, as single walled carbon nanotubes (SWCNTs) and multi walled carbon nanotubes (MWCNTs). If a single layer graphene sheet is rolled in the cylindrical form, it gives a SWCNT and if "n" number of graphene sheets are rolled one over the other, it forms MWCNTs (where $n > 1$). The basic structures of both these forms are shown in Figure 1.1. In MWCNTs the layers are held together by van der Waals forces of attraction because of π-π stacking and an interlayer spacing of 0.34 - 0.36 nm is observed. In order to understand their magnificent behavior, their physical properties are compiled and are given in Table 1.1 [19]. Specific surface area of SWCNTs is much larger compared to MWCNTs which is an important factor for many processes that may happen on the surfaces. One such process is the physical and chemical adsorption of various moieties on the sidewalls of SWCNTs.

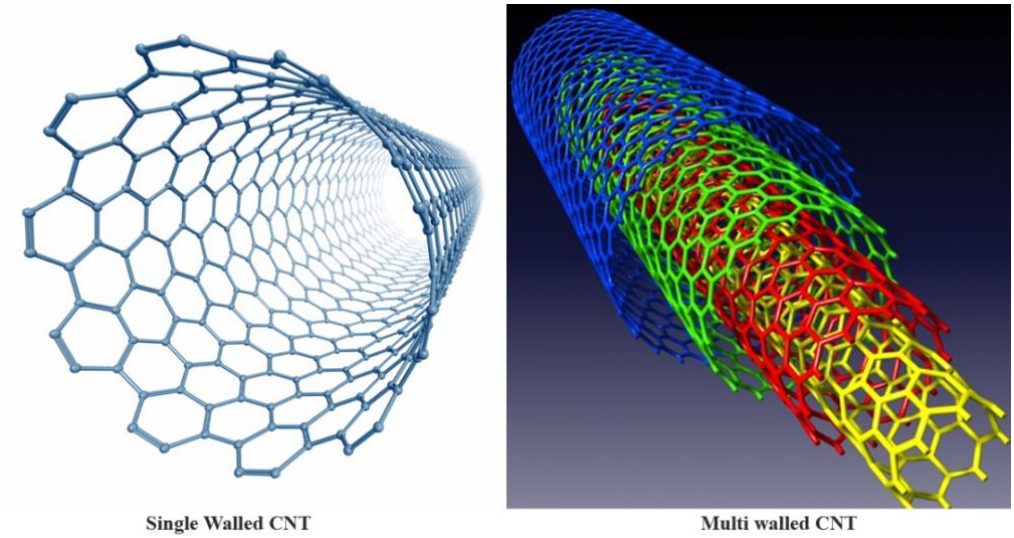

Figure 1.1. Single-walled and Multi-walled carbon nanotubes (open ended) are shown.

Table 1.1. Established physical properties of SWCNTs and MWCNTs [19].

Properties	**SWCNTs**	**MWCNTs**
Specific Gravity	0.8 g/cm^3	1.8 g/cm^3
Elastic Modulus	~1 TPa	~0.3 - 1 TPa
Strength	50 - 500 GPa	10 - 60 GPa
Resistivity	5 - 50 μΩcm	5 - 50 μΩcm
Thermal conductivity	3000 W m^{-1} K^{-1}	3000 W m^{-1} K^{-1}
Thermal stability	>700^{0}C (in air)	>700^{0}C (in air)
Specific surface area	~400-900 m^2/gm	~200-400 m^2/gm

1.2. Theoretical and Structural Aspects of Single Walled Carbon Nanotubes

SWCNT is defined as a graphene sheet which is rolled into a cylindrical shape such that the structure is one dimensional with axial symmetry exhibiting a spiral conformation called chirality [3]. The basic symmetry classification of a SWCNT is defined as either chiral or achiral. An achiral CNT can be defined as the CNT whose mirror image is identical with the original structure. The way in which graphene sheets are wrapped up to give arm-chair, zig-zag and chiral nanotubes are shown in Figures 1.2. The only two possible achiral SWCNTs are arm-chair SWCNTs and zig-zag SWCNTs. Chiral SWCNTs exhibit spiral symmetry and its mirror image cannot be superimposed on the original. SWCNTs are represented by the indices (n,m) and these indices represent the number of unit vectors along two directions in the honey comb crystal lattice of graphene as shown in Figure 1.3. If n = m they form arm-chair nanotubes, if m = 0 zig-zag nanotubes, and if m ≠ n or 0 then the nanotubes formed are chiral. Arm-chair CNTs are metallic and most of the zig-zag CNTs are semi-conducting. Semi-conducting and chiral SWCNTs who's (n–m) difference corresponds to the multiple of three are metallic CNTs and if not they are semi-conducting [3].

The most conventional types of defects, like vacancies and interstitials, are unlikely to be found in pristine CNTs [20]. Defects in CNTs are present in the form of pentagons and heptagons. Pentagons produce positive curvature, heptagon produce a negative curvature on the graphene layer which is mostly found at the cap for the closed ended nanotubes.

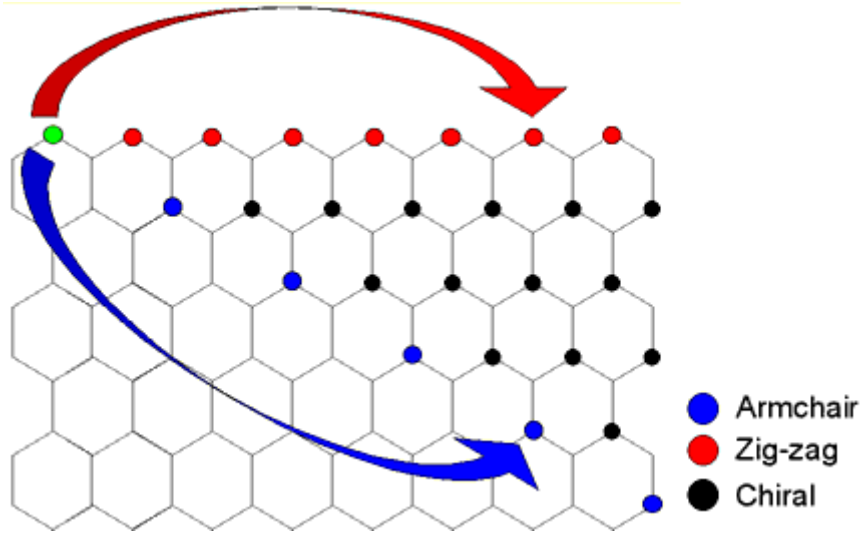

Figure 1.2. The way in which graphene sheet is rolled up to give arm-chair, zig-zag and chiral single walled carbon nanotubes is depicted. Starting from the green point and rolling the graphene sheet with the end points blue, red and black give arm-chair, zig-zag and chiral SWCNTs respectively.

Such kinds of defects are known as Stone-Wales defect [20] and some examples are shown in Figure 1.3. In the Figure 1.3 (a) represents defect free intrinsic benzene rings in carbon nanotube (b) represents Stone-Wales defect. A_0 and B_0 positions shown in (a) are distorted to give rise to two pentagons and two heptagons shown in (b).

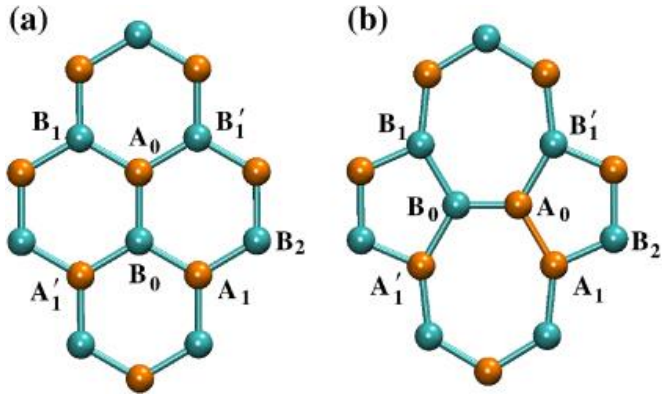

Figure 1.3. Defect free hexagonal benzene rings of intrinsic nanotube shown in (a). Stone-Wales defect shown in (b).

The Stone-Wales is also represented by 5-7-7-5 configuration where 5 imply a pentagon and 7 implies a heptagon is unique to graphitic systems and is predicted to be a relatively common type of defect in CNTs [20].

1.3. Electronic Structure of Single Walled Carbon Nanotubes

CNTs are described by the chiral vector (n,m), where n,m are the integers of the vector equation $\bar{C}_h = n\hat{a}_1 + n\hat{a}_2$ shown in Figure 1.4., where a_1 and a_2 are two unit vectors with an opening of 120°. The chiral angle "θ" is defined as the angle between the vectors "C_h" and a_1, where the range of θ varies between 0° - 30° due to the hexagonal symmetry of the honeycomb lattice. This angle relates the integers (n,m) defined in the chiral vector as,

$$\cos\theta = \frac{2n + m}{2\sqrt{n^2 + m^2 + nm}}. \quad (1.1)$$

This chiral angle denotes the tilt angle of the hexagons with respect to the direction of the nanotube axis. If θ corresponds to 0° we obtain zig-zag CNT and if it corresponds to 30° we get arm-chair CNTs and if it is in between this range we derive chiral SWCNTs. The translation vector "T" is defined as the unit vector of one dimensional CNT. The vector "T" is perpendicular to the chiral vector and parallel to the nanotube axis in the honeycomb lattice.

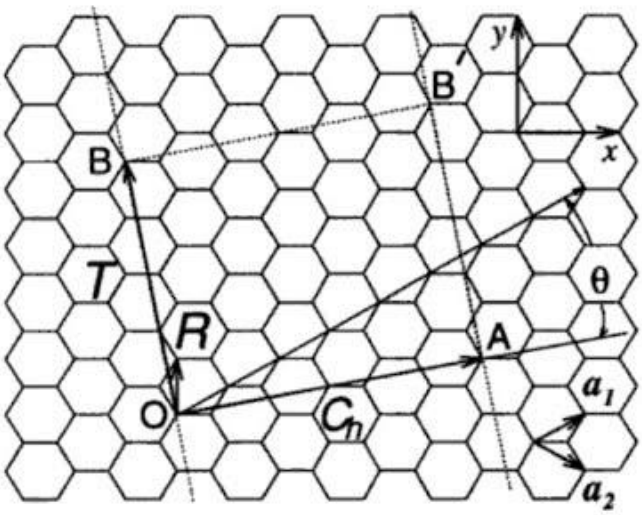

Figure 1.4. Translation vector (T) along the direction OB and chiral vector C_h perpendicular to translation vector along the direction OA, chiral angle θ, unit vectors a_1 and a_2 are shown.

The lattice vector $\bar{T}$ is defined in terms of the basis vectors a_1 and a_2 as

$$\bar{T} = t_1\hat{a}_1 + t_2\hat{a}_2. \quad (1.2)$$

where, t_1, t_2 are integers.

First lattice point on the 2-D graphene sheet corresponds to the translation vector "T". The area of the nanotube unit cell is given by

$$\text{Area} = |\bar{C}_h \times \bar{T}|. \tag{1.3}$$

The number of hexagons (N) per unit cell is given by the expression,

$$N = \left| \frac{\bar{C}_h \times \bar{T}}{\hat{a}_1 \times \hat{a}_2} \right|. \tag{1.4}$$

Electronic structure of SWCNTs is obtained from the graphene (Folding the graphene sheet along the chiral vector and applying periodic boundary conditions along the translational vector). When the graphene sheet is wrapped along the direction of chiral vector connecting any two points from O along the direction of C_h vector, it forms a cylindrical tube of fixed diameter. Electronic structure of Carbon nanotubes can be explained in a much more simple way using real-space orbital representations and traditional concepts of aromaticity, orbital symmetry and frontier orbitals, rather than complicated band structure representation in reciprocal space [20]. Semi-conducting carbon nanotubes are analogous to (4n+2) annulenes, (4n+2) represent number of π electrons, where "n" corresponds to an integer; annulenes represent a class of macrocyclic organic molecules) which are considered as aromatic by the Hückel rule, whereas metallic nanotubes are analogous to (4n) annulenes, which are anti-aromatic. Rolling up the graphene sheet to form a nanotube imposes periodic boundary conditions on the system given by $C_h.k = 2\pi q$, where C_h is the roll-up vector (or chiral vector) which becomes the circumference of the nanotube, where "q" is an integer.

Molecular orbitals formed by linear combination of atomic orbitals (LCAO) of graphene, corresponding to the Γ, M and K points of the band structure are shown in Figure 1.5 [20]. These localized representations can be generated as linear combinations of degenerate Bloch functions [20]. There can be infinite number of valid combinations, but the molecular orbitals formed by the linear combination in the corresponding points shown have real solutions. The LCAO coefficients formed by summing up of sine or cosine functions of the position with the directions and periodicities that correspond to the different Γ, M and K wave vectors in the first Brilloiun zone. The degree of bonding varies from the most bonding at the bottom to the most antibonding at the top. The two degenerate orbitals in the middle are nonbonding designate Fermi level. The symmetry of these orbitals determines the properties of the nanotube.

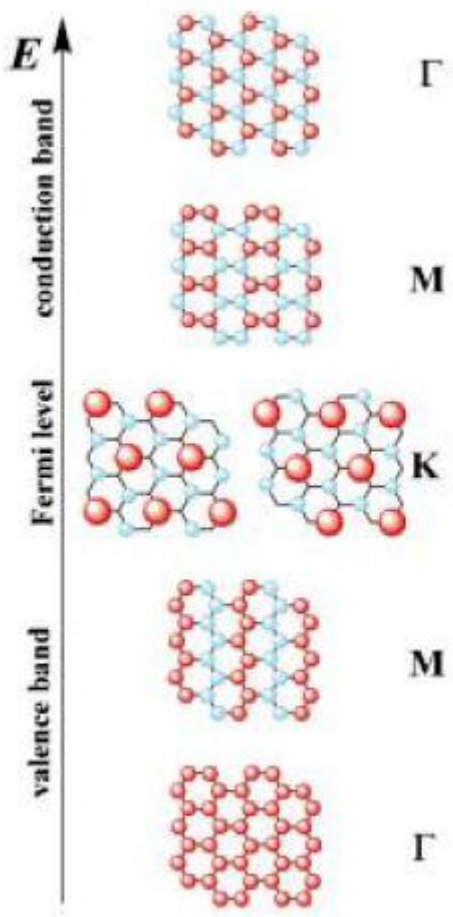

Figure 1.5. Real space LCAO representations of molecular orbitals in graphene corresponding to Γ, M and K points. Red and blue circles correspond to positive and negative LCAO coefficients of p_z orbitals contributing to the molecular orbitals.

If the graphene sheet is rolled up to form a CNT in such a way, so that carbons with similar LCAO coefficients (red with red or blue with blue shown in Figure 1.6) [20] then the periodicity of the orbital will be conserved in the nanotube and there will be allowed states at the Fermi level and the corresponding nanotube formed will be metallic. If the graphene sheet is rolled in such a way where carbon atoms with different LCAO coefficients overlap, the orbital symmetry conservation rule will not allow this orbital to exist in the CNT and there will be a gap at the Fermi level and the nanotube is semi-conducting. LCAO coefficients repeat themselves every three translations by any of the lattice basis vectors, hence a nanotube is metallic when the difference between the indices is multiple of 3 (Figure 1.6.) (a), otherwise (b) semi-conducting.

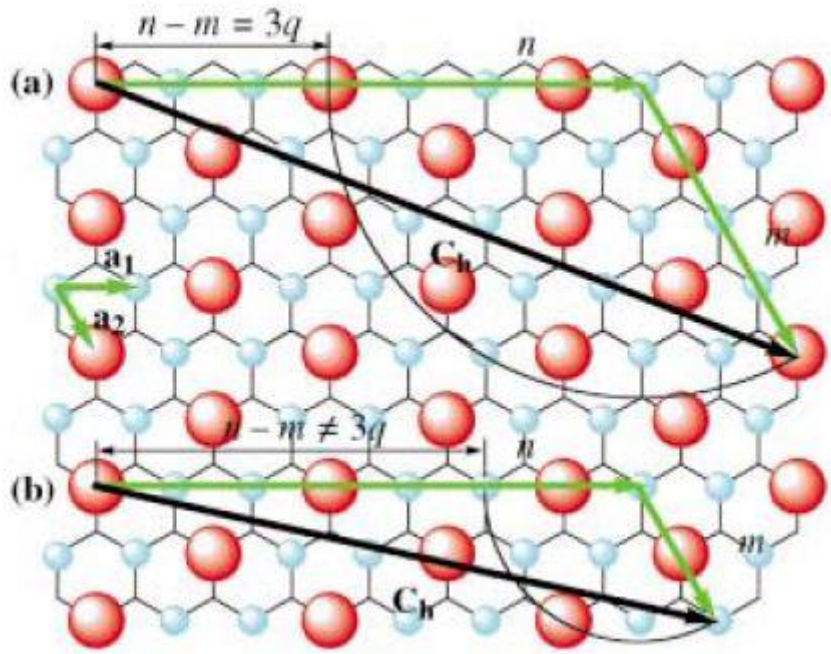

Figure 1.6. Rolling up of graphene sheet with carbon atoms having similar LCAO coefficients (red to red or blue to blue) are shown. C_h represent chiral vector, a_1, a_2 are lattice vectors with coefficients n and m. C_h is given by na_1+ma_2.

1.4. Methods of Preparation

The most popular methods [3] available to prepare CNTs are Arc-discharge method, Laser ablation technique and Chemical vapor deposition (CVD) method. In the first method, carbon electrodes are used which act as carbon source in a vacuum chamber in an inert atmosphere which enhances carbon deposition. When high dc voltage is applied between the carbon anode and cathode, inert gas of plasma is generated which evaporates the carbon atoms. Thus the carbon atoms ejected are deposited on the negative electrode forming the nanotubes. High quality CNTs including both SWCNTs and MWCNTs with almost perfect structures can be prepared using this methodology [20,21]. In the laser ablation technique, the source of carbon is ablated employing intense laser pulses in a furnace in an inert atmosphere employing a catalyst. Both these methodologies require very high temperatures of about 3000-4000^{0}C to evaporate carbon atoms from the solid source. In the CVD technique, the source of carbon is usually a hydrocarbon (methane, acetylene or ethylene) which flows into the reaction chamber. A temperature in the range of 550-1000^{0}C is employed which breaks the reactive species in the presence of catalyst like Ni, Fe or Co leading to the formation of CNTs. Compared to the arc discharge and laser ablation

techniques this method is widely used because of the efficiency in the process due to the ambient temperature range.

From the above mentioned methodologies CNTs produced will come up with mostly metallic and carbonaceous impurities. For the elimination of carbonaceous impurities oxidation technique is used with either, gas phase purification or liquid phase purification. Gas phase method usually gives low yields since it involves high temperature. In liquid phase purification CNTs are washed with acids like nitric acid and sulfuric acid. Using these techniques and optimizing conditions CNTs with purity of about 99.6% can be obtained [21].

1.5. Adsorption of Gas Molecules on Carbon Nanotubes – An Overview

Due to the unique features like large surface to volume ratio, hollow geometry, CNTs are considered as prime materials for gas sensing and also as gas storage materials. Conventional widely used sensors like tin oxide, zinc oxide and indium oxide [22] lack flexibility suffer with poor response times and fail to operate at lower temperatures [23]. Basic criteria for a system to act as an efficient sensor are

- Reasonable selectivity towards certain gases.
- Sensitive towards the exposed gases i.e., low analyte consumption.
- Fast response and recovery times.
- Low operating temperatures and
- Stable performance.

It has been demonstrated experimentally that the electronic properties of SWNTs are very sensitive to the chemical environment [24-26]. The main principle involved in detecting various gases by CNTs is by monitoring the conductance change associated with the charge transfer between CNTs and the adsorbed gases. Collins *et al.,* [24] have experimentally shown that SWCNTs are extremely sensitive to the exposure of air; their conductivities are dramatically altered with the exposure of air or oxygen. They measured the electrical resistance, thermoelectric power, local density of states by transport measurement and scanning tunneling spectroscopy. They have concluded that isolated semi-conducting nanotubes can be converted into metallic systems upon exposure to small concentrations of oxygen [24]. Nuclear magnetic resonance spectroscopy (NMR) studies proved that the spin lattice relaxation rates of the CNTs are increased upon exposure to oxygen [25]. Sumanasekera *et al.,* [26] demonstrated experimentally that the thermoelectric power and the

resistance of the SWCNTs are very sensitive to inert gases like nitrogen and helium. Jhi *et al.,* [27] theoretically studied electronic and magnetic properties of oxidized CNTs employing *ab initio* pseudo potential total energy method. They concluded that oxygen is weakly bound to the CNT with charge transfer being observed from the CNT to the oxygen resulting in increased spin lattice relaxations of oxidized CNTs which are consistent with the observed experimental findings [27]. Kong *et al.,* proposed CNTs as gas sensors based on change in electrical conductivity upon exposure with gases like nitrogen dioxide and ammonia [10]. Many experimental studies have been carried out in order to determine the sensitivity of carbon nanotubes with respect to various gas molecules like hydrogen, methane, nitrogen monoxide, ammonia, nitrogen dioxide, oxygen etc [28-34].

By exploiting its versatile properties new materials like CNTS can serve as an alternate option overcoming the shortcomings of the conventional sensors [35]. CNTs are found to exhibit very good sensitivities and recovery times with sensitivity varying in the range from parts per billion (ppb) to parts per million (ppm) and recovery times from seconds to hours depending upon the type of gas molecule [6,9,10,24]. Although CNTs have been demonstrated to act as very good sensors, their sensitivity is confined to very few molecules [6,9,24,26]. Intrinsic CNTs are capable of detecting gases which have large binding energies and higher charge transfers with CNTs. Many of the gas molecules like water vapor, carbon monoxide (H_2O, CO) are not detected using intrinsic CNTs since they do not adsorb on the side walls of CNTs. In order to overcome the deficiency of passiveness of intrinsic CNTs, Peng and Cho [36] proposed that CNTs substitutionally doped with boron and nitrogen can act as better adsorbents. Intrinsic CNTs are inert with sp^2 aromatic carbons throughout the structure and doping the CNTs with impurities like boron and nitrogen makes the CNT walls reactive; this is partially due to the electronegativity difference arising from substituted doped atoms and carbon atoms of CNTs. Boron and nitrogen are the most preferred choices to substitutionally dope CNTs because they only differ by one valence electron compared to that of carbon atom which allows them to easily incorporate into the honey comb lattice. Nitrogen atom when substituted in graphite is found to differ by 0.01 Å from the equilibrium position of the carbon of graphite [37]. On the other hand boron atoms which are comparatively bigger than the carbon atoms are found to produce a higher strain thus deviating from the atomic potential of the carbon [38]. Different methodologies like decorating CNTs with metal atoms to detect or enhance the sensitivity have also been proposed by various theoretical studies [39-41].

Doped CNTs of various concentrations $B_xC_yN_z$ have been synthesized where x,y,z indicates the percentage of doping [42]. Pure CNTs can be doped partially or totally by boron upon reaction with B_2O_3 with intrinsic CNTs under inert atmosphere [38]. Substitution with nitrogen is carried out by chemical vapor deposition employing imidazole as the carbon-nitrogen precursor using ferrocene as the catalyst [43]. In this thesis work we have mainly focused the attention on understanding the interaction of various gas molecules with pristine and doped CNTs using most reliable theoretical methodology in the DFT frame work employing the hybrid functional B3LYP [44,45]. In addition to this interaction of amino acid glycine in both non-ionic and zwitter-ionic form have also been carried out. Existing experimental and theoretical studies are incomplete and contradictory with respect to adsorption of various gases with CNTs [24-43]. Few studies suggest that CNTs can act as sensors with very high sensitivity and few others report that intrinsic CNTs do not exhibit sensitivity and that doping is required in order to improve their sensitivity [24-43, 46-66]. Therefore in order to find out whether CNTs are capable to act as sensors, we have carried out the investigation of adsorption of various gases like oxygen, nitrogen, hydrogen, carbon monoxide, water vapor, ammonia along the side walls of SWCNTs. We have also investigated the adsorption of these gases with doped SWCNTs with dopants like boron and nitrogen to understand whether the doped CNTs can act as better sensors compared to intrinsic CNTs.

1.6. Literature Review

There are few studies reported on adsorption of ground state oxygen molecule on CNTs [27,46-48]. Most of the theoretical studies carried out so far are studied employing the local density approximation in DFT formalism [27,46-51]. Peng and Cho [36] observed that molecular oxygen weakly physisorbs on the outer surface of a (10,0) zig-zag semi-conducting nanotube. Calculations carried out by Jhi *et al.,* [27] employing local density approximations (LDA) of DFT formalism concluded that oxygen binds to a semi-conducting (8,0) nanotube with binding energy of 0.25 eV at a distance of 2.7 Å. In a similar study, by Giannozzi *et al.,* [51] based on LDA reported a binding energy of oxygen with CNT as 0.08 eV at a distance of 2.9 Å, and employing gradient functional methods (PBE), yielded binding energy of 0.004 eV and distances of 3.68–3.70 Å [51]. Oxygen molecule was found to be at a distance 2.3–2.5 Å with a binding energy of 0.5 eV with various semi-conducting SWCNTs employing DFT using LDA reported by Zhao *et al.,* [46]. All these previous results suggest that oxygen in its ground state i.e., in the triplet spin state weakly adsorbs with the CNTs

although there is non-concurrence in binding energies estimated by different groups. This can be partially attributed to the different theoretical methodologies with insufficient models and functionals and also due to different diameters of CNTs considered for the investigation.

Most of the existing theoretical and experimental methods focus only on triplet oxygen adsorption which binds only weakly to the nanotubes [27,46-51]. Recently, Kinoshita and coworkers [52] studied the adsorption of singlet oxygen onto surfaces of graphene-like aromatic hydrocarbon molecules and observed that singlet oxygen has the potential to bind strongly with benzene, naphthalene and pyrene. Recent applications of singlet oxygen in photodynamic therapy makes the study of singlet adsorption very interesting [53]. This current research reveals the application of oxygen adsorption on CNTs in radiotherapy that the carbon nanotubes can adsorb oxygen and deliver it to the oxygen deficient tumor cells [53]. The spin state play a crucial role in these applications as singlet oxygen can cure cancerous tissues and can find application as an alternate to photodynamic therapy [54]. The serious limitation of photodynamic therapy is that the photosensitizer is unable to penetrate into the thick cell walls of the tissues and cure the tumor cells. CNTs on the other hand with their needle like geometry can reach the tumor affected cells and can deliver oxygen. Behaviour of singlet oxygen near CNT surfaces is unknown but it is very interesting from the fundamental point of view. Thus CNTs if found selectively bind to the singlet oxygen can pave way to great applications in the field of medicine.

In Chapter 3, we discuss the adsorption behavior of oxygen in both singlet and triplet spin states with both intrinsic and doped zig-zag and arm-chair nanotubes employing density functional calculations. Doping the CNTs with hetero atoms like boron and nitrogen helps in overcoming the serious limitation of passivity of pristine CNTs. Carbon atoms in CNTs are sp^2 hybridized and inert, incorporation of hetero atoms like boron and nitrogen atoms into the honeycomb lattice results in chemical activation of the rather passive surface of a carbon nanotube and create additional electronic states around the Fermi level [38]. In few cases we have also carried out adsorption studies on gas molecules like hydrogen, nitrogen, carbon monoxide and water, to understand, whether the SWCNTs exhibit sensitivity with respect to the gas molecules these results of this investigation are discussed in Chapter 4.

In addition to the molecules studied in chapter 3 and 4, we have also explored the adsorption behaviour of another environmentally important molecule, ammonia. In many areas like industry, environment, and life sciences the detection of pollutant molecules with

great sensitivity is of crucial interest. Ammonia is a significant pollutant and its emissions are difficult to model and measure, leading to large uncertainties in global and regional inventories [55]. But unfortunately, from the past few years the amount of reactive nitrogen entering the environment has significantly increased thus leading to a host of ecological problems [55]. Ammonia sensors are very important for monitoring its ambient concentrations since it is related to many environmental issues such as human health, acidification, climate change through particle formation etc. [56,57]. Ammonium aerosols may influence global climate by altering the transmission of atmospheric and terrestrial radiation. Thus, ammonia sensors, can find their application in many fields like monitoring the environment gases, in chemical industry, automobile industry, medical applications etc. [22,58].

There have been few scientific findings on the interaction of ammonia with intrinsic SWCNTs and the results employing various computational methods are inconsistent. For example Kong *et al.,* [10] reported that electrical resistance of semi-conducting pristine SWCNTs is dramatically altered on adsorption of ammonia. On the other hand, ammonia is found to be weakly physisorbed on intrinsic CNTs by weak van der Waals force of attraction leading to a small charge transfer of about 0.04 e by earlier theoretical studies [27,59-61]. These theoretical observations are further supported by the experimental findings [62,63] that there is no conductance change observed upon adsorption of ammonia with CNTs. Some of the previous studies suggest that the interaction of ammonia with the CNTs is also moisture sensitive [38,62]. With the increase in presence of moisture, the interaction with the SWCNT and ammonia has been enhanced in their investigations. Picaud *et al.,* found that SWCNTs are slightly more sensitive to ammonia than MWCNTs [60]. Experimentally, it is found that SWCNTs exhibit sensitivity with a response time in minutes with parts per million (ppm) concentrations of ammonia [62]. This can be understood by the low charge transfer between ammonia and CNT due to weak physisorption. A chemical modification in CNT is required to enhance the sensitivity with faster response time with lower concentrations of ammonia. Substitutional doping can alter the local chemical reactivity thus making the surface of CNT slightly more reactive.

Existing theoretical and experimental findings suggest that the intrinsic SWCNTs show a weak physisorption toward ammonia and functionalized nanotubes are found to be slightly more sensitive to ammonia adsorption compared to that of intrinsic CNTs [65]. Using generalized gradient approximation (GGA), Bai and Zhou [66] have studied the

interaction of ammonia and nitric oxide on boron and nitrogen doped SWCNTs using GGA. Matsuda *et al.*, [67] reported that LDA and GGA methodologies underestimate the band gaps up to 70–100%. They have also suggested the superiority of B3LYP functional over LDA and GGA in calculating the band gaps of SWCNTs. In Chapter 5, we discuss the adsorption of ammonia with intrinsic and boron doped SWCNTs with various diameters. Band structure calculations are carried out employing periodic boundary conditions (PBC) to probe the electronic changes. Natural Bond orbital (NBO) analysis is carried out to understand the favorability of charge transfer. Semi-conducting SWCNTs of various diameters are chosen to study the diameter effects on adsorption of ammonia.

In this thesis we have also studied the interaction of glycine in neutral form and zwitter- ionic form along the side walls with intrinsic and various functionalized SWCNTs. The interaction between SWCNTs and typical amino acids is therefore very important in understanding and exploring possible biological applications. It has been established that nucleotides and proteins can be immobilized either inside [68,69] or outside [70–73] the SWCNTs without losing their properties. Considerable changes in conductivity of CNTs are reported as these biomolecules are immobilized on the surface of the SWCNT [74–76]. Needle like geometry of CNTs help them to penetrate well and delivers the drug and thus finds application in the field of medicine. It has already been established that the use of SWCNTs as liquid filled nanoparticles for drug delivery [77], thus attracting interest in the potential application of CNTs as drug or vaccine carriers in medicine. Interaction of amino acids with carbon nanotubes is a topic of interest since, non-covalent interactions play a key role to predict ligand binding and structural aspects of proteins [78-82]. Rajesh *et al.*, [82] investigated the interaction of amino acids with graphene and SWCNTs to understand the effect of curvature on the non-covalent interactions. CNTs application as biological transporters and in cancer cell destruction has been demonstrated by Salvador *et al.*, [83] and Shi *et al*.[84]. Bianco *et al.*, [85] reported that functionalized CNTs can be used as templates for delivering bioactive peptides to the immune system. The changes in electrical conductance of CNTs when proteins are immobilized on their side walls facilitate applications in chemistry and biology as sensors [71-74,86]. CNTs can be structurally modified and the properties can be altered which offer better properties compared to that of quantum dots in nanostructured biological devices [82]. Intrinsic CNTs are passive towards many of the gases and biological species and in addition are insoluble in water which is a main hindrance for biological application according to the studies reported earlier [87].

Chemical functionalization of CNTs makes them not only soluble but also helps in reducing their toxic levels according to the studies reported earlier [87]. It has been reported that functionalization of CNTs improved the application of CNTs in various biological components [88-94]. Previous studies [88,89] have evaluated the cytotoxicity of fullerenes and found that it decreased appreciably with degree of functionalization in addition to improved solubility in water.

Despite the huge interest there are only a few studies of interaction of amino acids with SWCNTs in neutral and zwitter-ionic forms [90]. Previous studies of interaction of glycine with CNTs suggests that it shows weak binding energy with intrinsic SWCNTs and strong binding with doped and functionalized CNTs [90-94]. Roman *et al*., [90] have carried out adsorption of glycine in both neutral form and zwitter ionic form with conducting (3,3) CNTs and predicted that the zwitter-ionic form exhibited a binding energy of 0.53 eV compared to the value of 0.10 eV of the neutral form employing the generalized gradient approximation (GGA) of density functional theory (DFT). Recently Ganji [93] investigated the interaction of glycine with functionalized SWCNTs employing self-consistent charge density- functional based tight-binding (DFTB) approach. This investigation carried out on (6,6) conducting CNTs with glycine conclude that intrinsic CNTs exhibit weak binding interactions of 0.17 eV with glycine and stronger interaction with functionalized CNT with a binding energy of 0.69 eV. The previous investigations were carried out employing GGA and DFTB which gave similar results to that of Local Density Approximation (LDA)/GGA. It is well known that the binding energies calculated by LDA formalism are overestimated and by GGA formalism are underestimated [94].

Moreover, previous theoretical studies [90,91,93] are carried out in gas phase where solvent interactions are neglected. Glycine exists as zwitter ion in aqueous medium and therefore the solvent effects cannot be neglected. We have studied the interaction of glycine in both non-ionic and zwitter-ionic states with semi-conducting, intrinsic as well as SWCNTs functionalized with amino, hydroxyl and carboxylic groups. SWCNTs doubly functionalized with both amino and carboxylic group are also considered. Although real protein systems are much complicated than the model studied, all proteins contain amino nitrogen, carbonyl oxygen and hydroxyl oxygen active sites and therefore it is of interest to study the nature of binding of glycine with the nanotube walls. Interaction of glycine in neutral (gas phase) and zwitter ionic state (aqueous phase) with intrinsic and functionalized (8,0) SWCNTs are discussed in detail in Chapter 6.

Nature of band gaps whether direct or indirect is crucial since it determines the material efficiencies in LEDs, solar cells and laser applications [95,96]. In order to understand whether the semi-conducting SWCNTs exhibit direct or indirect band gaps, we have performed band structure studies on boron and nitrogen doped (8,0) semi-conducting SWCNTs. The nature of band gaps and the conductivity changes upon doping with various concentrations are discussed in Chapter 7.

Reference

1. Z. Yao, W. Jinquan, V. Robert, A. Pulickel, B. Enrique V. *Scientific Reports – Nature,* 1, 83, 2011.
2. R. Bhandavat, A. Feldman, C. Cromer, J. Lehman, G. Singh. *ACS Applied Materials & Interfaces,* 5, 2354, 2013.
3. R. Saito, G. Dresselhaus, M. S. Dresselhaus. *Physical properties of carbon nanotubes*, Imperial College press, UK, 1998.
4. X. Wang, L. Qunqing, X. Jing, J. Zhong, W. Jinyong, L. Yan, J. Kaili, F. Shoushan. *Nano Letters*, 9, 3137, 2009.
5. E. T. Thostensona, Z. Renb, T.W. Choua. *Composites Science and Technology*, 61, 1899, 2001.
6. P. G. Collins, P. Avouris. *Scientific American*, 283, 62, 2000.
7. W. Ch. P. Henk, T. Teepen, Z. Yao, M. Grifoni, C. Dekker. *Science*, 293, 76, 2001.
8. J. Wei, Y. Jia, Q. Shu, Z. Gu, K. Wang, D. Zhuang, G. Zhang, Z. Wang, J. Luo, A. Cao, D. Wu. *Nano Lett*. 7, 2317, 2007.
9. A. C. Dillon, K. M. Jones, T. A. Bekkedahl, C. H. Kiang, D. S. Bethune, M. J. Heben. *Nature*, 386, 377, 1997.
10. J. Kong, N. R. Franklin, C. Zhou, M. G. Chapline, S. Peng, K. Cho, H. Dai. *Science*, 287, 622, 2000.
11. P. Cherukuri, S. M. Bachilo, S. H. Litovsky, R. B. Weisman. *J. Am. Soc.* 126, 15638, 2004.
12. L. V. Radushkevich, V. M. Lukyanovich. *Soviet Journal of Physical Chemistry*, 26, 88, 1952.
13. A. Oberlin, M. Endo, T. Koyama. *Journal of Crystal Growth*, 32, 335, 1976;
14. I. A. Nauk SSSR, *Metals*. 3, 12, 1982.
15. A. John, W. G. Peter, R. L., Brian. *Carbon* 37, 1873, 1999.
16. S. Iijima. *Nature*, 354, 56, 1991.

17. M. F. Yu, O. Lourie, M. J. Dyer, K. Moloni, T. F. Kelly, R. S. Ruoff. *Science*, 287, 637, 2000.
18. B. Peng, L. Mark, Z. Peter, L. Shuyou, M. Steven, S. George, E. Horacio. *Nature Nanotechnology*, 3, 626, 2008.
19. X. L. Xie, Y. W. Mai, X. P. Zhou. *Materials Science and Engineering R: Reports*, 49, 4, 2005.
20. A. V. Narlikar, Y.Y. Fu, Eds. *Oxford Handbook of Nanoscience and Technology: Frontiers and Advances*. Oxford Univ. Press, Oxford, 2009; E. Joselevich, *Chem Phys Chem*, 5, 619, 2004.
21. J. Li, Y. Lu, Q. Ye, M. Cinke , J. Han, M. Meyyappan. *Nano Lett*. 3, 929, 2003.
22. T. Bjorn, O. Wouter, A. V. D. Berg. *Sens. Actuat. B*, 107, 666, 2005.
23. S. K. Koh, H. J. Jung, S. K. Song, W. K. Choi, D. Choi, J. S. Jeon - Sensor having tin oxide thin film for detecting methane gas and propane gas and process for manufacturing thereof, US patent 6, 059, 937, 2000.
24. P. G. Collins, K. Bradley, K. Ishigami, M. Zettl. *Science*, 287, 1801, 2000.
25. X. P. Tang, A. Kleinhammes, H. Shimoda, L. Fleming, K. Y. Bennoune, S. Sinha, C. Bower, O. Zhou, Y. Wu. *Science*, 228, 492, 2000.
26. G. U. Sumanasekera, C. K. W. Adu, S. Fang, P. C. Eklund. *Phys. Rev. Lett*. 85, 1096, 2000.
27. S. H. Jhi, S. G. Louie, M. L. Cohen. *Phys. Rev. Lett*. 85, 1710, 2000; Y. Wu (private communication)
28. C. Cantalini, L. Valentini, L. Lozzi, I. Armentano, J. M. Kenny, S. Santucci. *Sensors and Actuators B*, 93, 333, 2003.
29. A. Kuznetsova, J. T. Yates, J. Liu, and R. E. Smalley. *J. Chem. Phys.*112, 9590, 2000.
30. O. Byl, P. Kondratyuk, S. T. Forth, S. A. Fitzgerald, L. Chen, J. K.Johnson, J. T. Yates. *J. Am. Chem. Soc.* 125, 5889, 2003.
31. A. C. Dillon, M. J. Heben. *Appl. Phys. A.* 72, 133, 2001.
32. G. E. Froudakis. *J. Phys. Condens. Matter* 14, 453, 2002.
33. A. Lubezky, L. Chechelnitsky, M. Folman. *J. Chem. Soc. Faraday Trans.* 92, 2269, 1996.
34. M. Fastow, Y. Kozirovski, M. Folman, J. Heidberg. *J. Phys. Chem*. 96, 6126, 1992.
35. S. K. Koh, H. J. Jung, S. K. Song, W. K. Choi, D. Choi, J. S. Jeon - Sensor having tin oxide thin film for detecting methane gas and propane gas and process for manufacturing thereof, US patent 6, 059, 937, 2000.
36. S. Peng, K. Cho. *Nano Lett*. 3, 513, 2003.

37. A. H. Nevidomskyy, G. Csanyi, M. C. Payne. *Phys. Rev. Lett.* 91, 105502, 2003.
38. M. Glerup, V. Krstic, C. Ewels, M. Holzinger, G. V. Lier. *Doping of carbon nanotubes, in Doped Nanomaterials and Nanodevices*, American Scientific Publishers, USA, 2010.
39. Z. Zanolli, R. Leghrib, A. Felten, J. J. Piereaux, E. Llobet, J. C. Charlier. *ACS Nano*, 5, 4592, 2011.
40. R. Wang, D. Zhang, W. Sum, Z. Han, C. Liu. *Journal of Molecular structure: THEOCHEM*, 806, 93, 2007.
41. A. Z. Sadek, C. Zhang, Z. Hu, J. G. Partridge, D. G. McCulloch, W. Wlodarski, K. K. Zadeh. *Jour. Phys. Chem. C*, 114, 238, 2010.
42. W. Han, J. Cumings, X. Huong, K. Bradlay, A. Zettl. *Chem. Phys. Lett.* 346, 368, 2001.
43. Z. Mo, S. Liao, Y. Zheng, Z. Fu. *Carbon*, 50, 2620, 2012.
44. A. D. J. Becke. *J. Chem. Phys.* 98, 5648, 1993.
45. C. Lee, W. Yang, R. G. Parr. *Phys. Rev. B.* 37, 785, 1988.
46. J. Zhao, A. Buldum, J. Han, J. P. Lu. *Nanotechnology*, 13, 195, 2002.
47. C. Kim, Y. S. Choi. *J. Am. Chem. Soc.* 124, 9906, 2002.
48. A. Tchernatinsky, S. Desai, G. U. Sumanasekera, C. S. Jayanthi, S. Y. Wu. *J. Appl. Phys.* 99, 034306, 2006.
49. X. Y. Zhu, S. M. Lee, Y. H. Lee, T. Frauenheim. *Phys. Rev. Lett*. 85, 2757, 2000.
50. D. C. Sorescu, K. D. Jordan, P. Avouris. *J. Phys. Chem. B*. 105, 11227, 2001.
51. P. Giannozzi, R. Car, G. Scoles. *J. Chem. Phys.* 118, 1003, 2002.
52. K. Kinoshita, T. Saito, I. Akira, K. Takashi, K. Yasutaka, Y. Shusuke, Y. Kizashi, O. Mitsutaka. *Polyhedron*, 30, 3249, 2011.
53. J. Yang, W. Li, Q. Li, S. Wu, B. Yu, X. Jing, W. Li, *IET Nanobiotech*. 1, 10, 2007.
54. R. M. Howes. *Internet J. Alt. Med*. 8, 1, 2010.
55. L. Myles. *Nat. Geosci*. 2, 461, 2009.
56. V. P. Aneja, W. H. Schlesinger, J. W. Erisman. *Nature Geosci*. 1, 409, 2008.
57. J. N. Galloway, J. D. Aber, J. W. Erisman, S. P.Seitzinger, R. W. Howarth, E. B. Cowling, B. J. Cosby. *Bioscience*, 53, 341, 2003.
58. W. Ament, J. R. Huizenga, E. Kort, T. W. V. D. Mark, R. G. Grevink, G. J. Verkerke. *Int. J. Sports Med*. 20, 71, 1999.
59. H. Chang, J. D. Lee, S. M. Lee, Y. H. Lee. *Appl. Phys. Lett*. 79, 3863, 2001.
60. F. Picaud, C. Girardetand, A. M. Rao. *J. Appl. Phys.* 105, 014315, 2009.
61. C. W. Bauschlicher, Jr., A. Ricca. *Phys. Rev. B.* 70, 115409, 2004.
62. S. Chopra, A. Pham, J. Gaillard, A. Parker, A. M. Rao. *Appl. Phys. Lett*. 80, 4632, 2002.

63. K. Bradley, J. Christophe, P. Gabriel, M. Briman, A. Star, G. Gruner. *Phys. Rev. Lett*. 91, 218301, 2003.
64. B. B. Shirvani, J. Beheshtian, G. Parasar, N. L. Hadipour. *Comput. Mater. Sci.* 48, 655, 2010.
65. X. Feng, S. Irle, H. Witek, K. Morokuma, R. Vidic, E. Borguet. *J. Am. Chem. Soc*. 127, 10533, 2005.
66. L. Bai, Z. Zhou. *Carbon*, 45, 2105, 2007.
67. Y. Matsuda, J. Tahir-Kheli, W. A. Goddard, III. *J. Phys. Chem. Lett.* 1, 2946, 2010.
68. J. J. Davis, M. L. H. Green, O. A. H. Hill, Y. C. Leung, P. J. Sadler, J. Sloan, A. V. Xavier, S. C. Tsang. *Inorg. Chim. Acta*. 272, 261, 1998.
69. B. S. Paratala, B. Sitharaman. *Carbon Nanotubes for Biomedical Applications, Carbon Nanostructures*, Springer-Verlag, Berlin Heidelberg, 2011.
70. Z. Guo, P. J. Sandler, S. C. Tsang. *Adv. Mater.* 10, 701, 1998.
71. F. Balavoine, P. Schultz, C. Richard, V. Mallouh, T. W. C. Mioskowski. *Angew. Chem. Int. Ed*. 38, 1912, 1999.
72. S. C. Tsang, J. J. Davis, L. Malcolm, H. Green, H. Allen, O. Hill, Y. C. Leung, P. J. Sadler. *Chem. Comm*. 17, 1803, 1995.
73. S. C. Tsang, Z. Guo, Y. K. Chen, M. L. H. Green, H. Allen, O. Hill, T. W. Hambley, P. J. Sadler. *Angew. Chem. Int. Ed. Engl*. 36, 2198, 1997.
74. R. J. Chen, S. Bangsaruntip, K. A. Drouvalakis, N. W. S. Kam,M. Shim, Y. Li, W. Kim, P. Utz, H. Dai. *Proc. Natl. Acad. Sci*.100, 4984, 2003.
75. K. Besteman, J. Lee, F. G. M. Wiertz, H. Heering, C. Dekker. *Nano Lett*. 3, 727, 2003.
76. A. Star, J. C. P. Gabriel, K. Bradley, G. Gruner. *Nano Lett.* 3, 459, 2003.
77. N. Venkatesan, J. Yoshimitsu, Y. Ito, N. Shibata, K. Takada. *Biomaterials* 26, 7154, 2005.
78. G. Weber, *Protein Interactions*, Chapman and Hall, London 1992.
79. H. Rubin. *Touchstone of Life: Molecular Information, Cell Communication and the Foundations of Life*, Oxford University Press, New York, 1999.
80. S. Jones, J. M. Thornton. *Proc. Natl. Acad. Sci*. 93, 13, 1996.
81. D. A. Dougherty. *Science*, 271, 163, 1996.
82. C. Rajesh, C. Majumder, H. Mizuseki, Y. Kawazoe. *J. Chem. Phys*. 130, 124911, 2009.
83. C. Salvador-Morales, P. Townsend, E. Flahaut, C. Venien-Bryan, A. Vlandas, M. L. H. Green, R. B. Sim. *Carbon*. 45, 607, 2007.

84. N. W. Shi Kam, M. O' Connell, J. A. Wisdom, H. Dai. *Proc. Natl. Acad. Sci*. U.S.A. 102, 11600, 2005.
85. A. Bianco, K. Kostarelos, C. D. Partidos, M. Prato. *Chem. Commun*. 571, 11, 2005.
86. R. J. Chen, H. C. Choi, S. Bangsaruntip, E. Yenilmez, X. Tang, Q. Wang, Y. Chang, H. Dai. *J. Am. Soc.* 126, 1563, 2004.
87. N. Sinha, J. T. W. Yeow. *IEEE Transactions on Nanobioscience* 4, 180, 2005.
88. M. Mananghaya, E. Rodulfo, G. Nonato Santos, A. R. Villagracia. *Jour. of Nanotech.* 2012, 6, 2011.
89. A. Srivastava, J. Srashti, A. K. Nagawat. *Quantum Matter*, 2, 469, 2013.
90. T. Roman, W. A. Dino, H. Nakanishi, H. Kasai. *Thin Solid Films*, 509, 218, 2006.
91. A. Mavrandonakis, S. C. Farantos, G. E. Froudakis. *J. Phys. Chem. B.* 110, 6048, 2006.
92. W. Sun, Y. Bu, Y. Wang. *J. Phys. Chem. B.* 112, 15442, 2008.
93. M. D. Ganji, A. Bakhshandeh. *Physica B: Condensed Matter*, 406, 4453, 2011.
94. A. Grob. *Theoretical Surface Science–A Microscopic Prospective*, Springer Verlag, Berlin Heidelberg 2009.
95. Green, Martin A. *Solar Cells: Operating Principles, Technology, and System Applications.* Englewood Cliffs: Prentice-Hall, Inc., 1982.
96. X. Peng, Q. Wei, A. Copple. *Phys. Rev. B.* 90, 085402, 2014.

CHAPTER 2

Computational Methodology

2.1. Introduction

Adsorption of gas molecules on carbon nanotubes can be investigated employing various *ab-initio* electronic structure calculations. Density functional theory (DFT) is the most popular choice currently employed to study the various properties like binding energy, tube-molecule distance, band gaps and charge transfers [1-9]. It offers the advantage of low computational cost (~Hartree Fock) and accuracy up to the level of Mϕller Plesset (MP2) calculations taking into the consideration of exchange-correlation effects [10-12]. Theoretical studies aid the experimentalists to understand the various factors which contribute to the efficient binding, charge transfer and conductance change thoroughly. Most popular theoretical methods which are widely used in order to determine the adsorption properties of CNTs with various gases are Local Density Approximation (LDA) and Generalized Gradient Approximation (GGA) in the DFT frame work [1-5]. Although these DFT methodologies are widely used (LDA and GGA) the main drawback associated with these techniques is that LDA overestimate the binding energies and charge transfers whereas GGA underestimates the same [1-5]. We have employed the hybrid functional B3LYP in the DFT framework to investigate the adsorption properties of various molecules along the sidewalls of SWCNTs. B3LYP is found to be a reliable methodology to study the adsorption properties [6-8] and investigations by Matsuda *et al.,* confirms the superiority of B3LYP functional over various LDA and GGA functionals in predicting the band gaps of SWCNTs of various diameters [9]. In this chapter we briefly discuss the basic aspects of DFT and various approximation techniques to calculate exchange and correlation energy, calculation of charge transfers by Mulliken population analysis and Natural population analysis (or Natural bond orbital analysis) and band structure calculations.

2.2. Density Functional Theory (DFT) – Thomas Fermi Model

Ground state properties of an atom or molecule can be determined accurately if the exact electron density is known. DFT is based on electron probability density $\rho(x,y,z)$ which is derived from Hohenberg-Kohn theorems. *Ab-initio* approaches use wave function which cannot be physically measured; DFT techniques on the other hand use electron density which can be measured employing techniques like X-ray diffraction or electron diffraction [10]. The advantage of DFT over wave-function based approach is that electron density is a

function of only three variables (x,y,z) irrespective of the size of the molecule [11,12]. Wave function based approaches depend on 4n variables, where "n" represent number of electrons. Therefore the wave function of an atom with ten electrons will have 40 variables whereas the electron density is a function of three variables simplifying the matter in DFT and provides an advantage over the wave function based procedures.

The predecessor to the current DFT [11-12] is the Thomas-Fermi model developed independently by Thomas and Fermi in 1927. However this model failed miserably to explain the properties of molecules because earlier DFT techniques employ orbital free models, where the energy functional is divided into three parts, kinetic energy, T[ρ], attraction between the nuclei and electrons, $E_{ne}[\rho]$, and electron–electron repulsion, $E_{ee}[\rho]$. The $E_{ee}[\rho]$ term is further divided into coulomb and exchange parts, J[ρ] and K[ρ], including correlation energy in all the terms. Kinetic and exchange energies considered based on uniform electron gas.

$$T_\rho = \pi \frac{3}{10} (3\pi^2)^{\frac{2}{3}} \int \rho^{\frac{5}{3}}(r) dr. \tag{2.1}$$

$$E_{ne}[\rho] = \sum_{a}^{N_{nuclie}} \int \frac{Z_e\,(R_a)\rho(r)}{|R_a - r|}\, dr. \tag{2.2}$$

$$E_{ee}[\rho] = \frac{1}{2} \iint \frac{\rho\,(r)\rho\,(r)'}{|r - r'|} dr\, dr'. \tag{2.3}$$

Calculations obtained from this orbital free model, where the energy components obtained from the functional of electron density, yielded poor results and hence wave function based approaches were preferred to DFT calculations. In 1965 Kohn and Sham suggested that the electron kinetic energy should be calculated from auxiliary set of orbitals which represent the electron density. This approach gave satisfactory results with the experiments and laid to the foundation of modern Density functional theory based on Kohn-Sham orbitals. In the Kohn-Sham formalism, kinetic energy functional is split into two parts, one can be calculated exactly and the other is the correction term (Explained in section 2.3). But kinetic energy calculated from the auxiliary set of orbitals again introduces the complexity from 3 to 3N variables.

2.3. DFT : Kohn-Sham approach

In this approach fictitious non-interacting reference system is defined in which electrons do not interact with each other. Ground sate electron density ρ_r is considered to be exactly the same as the real ground state system ρ_o ($\rho_r = \rho_o$). Since the electrons are non-interacting they can be treated exactly and any deviation in energy caused due to the assumption of non-interacting electrons can be added further by exchange-correlation term (correction term) which is rather a small fraction compared to the total energy.

Electronic ground state energy of the real molecule is given by the sum of electron kinetic energy, nucleus-electron attraction energies and electron-electron repulsion energies and is given by

$$E_0 = < T[\rho_0] > + < V_{Ne}[\rho_0] > + < V_{ee}[\rho_0] >. \quad (2.4)$$

The first term ($T[\rho_0]$) in the Eq. (2.4) represents kinetic energy of the electrons, the second term ($V_{Ne}[\rho_0]$) represents Columbic attraction between nucleus and electron and the last term ($V_{ee}[\rho_0]$) represents Columbic repulsions between the electrons. The second term is given by the expression,

$$V_{Ne}[\rho_0] = \sum_{i=1}^{2n} \sum_{\text{nuclei A}} \frac{Z_A}{r_{iA}} = \sum_{i=1}^{2n} v\,(r_i). \quad (2.5)$$

Z_A/r_{iA} is the potential energy due to interaction of electron "i" with nucleus "A" at the varying distance r; $v(r_i)$ is the external potential for the attraction of electron "i" to all the nuclei. The density function $\rho(r)$ can be introduced into $<V_{Ne}>$ (in the Eq. 2.5) by using the fact that [13]

$$\int \psi \sum_{i=1}^{2n} f(r_i)\psi \, d\tau = \int \rho(r) f(r) dr. \quad (2.6)$$

Here $f(r_i)$ is a function of the spatial coordinates of electron "i" of the system and "ψ" is the total wavefunction. Eq. (2.6) represents the Columbic force of attraction between electrons and the nuclei in terms of $\rho(r)$. Now the total energy is given by,

$$E_0 = < T[\rho_0] > + \int \rho(r) v(r) dr + < V_{ee}[\rho_0] >. \quad (2.7)$$

But the Eq. (2.7) cannot be used to calculate the energy because the functionals corresponding to first (kinetic energy) and last term i.e., the Columbic force of repulsion between electrons in the Eq. (2.7) are unknown. Moreover the Eq. (2.7) is built on the assumption that electrons are non-interacting, thus the energy calculated using the above formula does not give proper results. Therefore Eq. (2.7) has to be modified taking into account the corrections of first and last terms. In the real systems electrons are interacting, therefore there will be the difference in kinetic energy calculated with respect to the real systems and the kinetic energy calculated for the reference system where the electrons are non-interacting. Kinetic energy deviation for the real and the reference system is given by

$$\Delta< T[\rho_0] > \equiv\ T[\rho_{\text{real}}] - T[\rho_{\text{reference}}]. \tag{2.8}$$

The deviation of Columbic repulsion is given as follows, the classical electrostatic repulsion energy is the summation of the repulsion energies for pairs of infinitesimal volume elements $\rho(r_1)dr_1$ and $\rho(r_2)dr_2$ separated by a distance r_{12}, multiplied by one-half. Similarly the deviation in Columbic repulsion is given by

$$\Delta< V_{ee}[\rho_0] > \equiv < V_{ee}[\rho_0] >_{\text{real}} - \frac{1}{2} \iint \frac{\rho_0\,(r_1)\rho_0\,(r_2)}{r_{12}} dr_1\, dr_2. \tag{2.9}$$

Employing the classical charge-cloud repulsion formula, it gives inappropriate picture of electrons in that smearing an electron out into a cloud forces it to repel itself, as any two regions of the cloud interact repulsively. This physically incorrect electron self-interaction can be compensated by using a good-correlation functional. Now the modified ground state electronic energy is given by,

$$E_0 =< T[\rho_0] >_{\text{ref}} + \int \rho(r)v(r)dr\ + \frac{1}{2} \iint \frac{\rho_0\,(r_1)\rho_0\,(r_2)}{r_{12}} dr_1\, dr_2 + \Delta< T[\rho_0] > \ + \Delta< V_{ee}[\rho_0] >. \tag{2.10}$$

The sum of the kinetic energy deviation from the reference system and the electron–electron repulsion energy deviation from the classical system is called the Exchange-correlation energy (E_{XC}) represented by,

$$E_{XC} = \Delta< T[\rho_0] > \ + \Delta< V_{ee}[\rho_0] >. \tag{2.11}$$

Incorporating this (E_{XC}) in the equation Eq. (2.10), we get

$$E_0 = \int \rho(r)v(r)dr + < T[\rho_0] >_{\text{ref}}\ + \frac{1}{2} \iint \frac{\rho_0\,(r_1)\rho_0\,(r_2)}{r_{12}} dr_1\, dr_2 + E_{XC}. \tag{2.12}$$

The first term in the Eq. (2.12) is the sum of Columbic force of attraction of nuclei with infinitesimal charge cloud which can be calculated from ρ_0 employing the expression,

$$\int \rho(r)v(r)dr = -\sum_{a}^{N_{nucleus}} Z_A \int \frac{\rho_{r1}}{r_{1A}}\, dr_1. \qquad (2.13)$$

The second term in the Eq. (2.12) is the kinetic energy of non-interacting electrons of the reference system, given by the expression,

$$< T[\rho_0] >_{ref} = -\frac{1}{2}\sum_{i=1}^{2n} < \psi_1^{KS}(1)|\nabla_1^2|\psi_1^{KS}(1) >. \qquad (2.14)$$

The expected kinetic energy of non-interacting electrons is given by Eq. (2.14), as the electrons are non-interacting and the wavefunction can be written as a single Slater determinant similar to the wavefunction constructed in the Hartree-Fock methodology. The only difference in the DFT is that the orbitals involved in the construction are Kohn Sham (KS) orbitals. The third term in the Eq. (2.12) represents the Columbic force or repulsion between the electrons, which can be calculated using the classical formula, if the density ρ_0 is known. The only term which is unknown is the exchange-correlation term functional E_{XC} which is smaller compared to the first three terms; since the exact functional is unknown, the most approximate functional is to be devised appropriate to the systems under consideration.

2.4. Exchange and correlation energy (E_{XC})

In calculating the energy using Eq. (2.12), it is assumed that electrons are non-interacting with each other, thus leading to a functional, which compensates the effect. In the real systems, since electrons owe charge, they repel each other, represented classically in the energy equation. Quantum mechanically, this repulsion must be modified to take into account the spin of electrons. Pauli's principle suggests that, two fermions (particles with half-integer spin) cannot occupy the same spatial position, or the total wave function must be anti-symmetric upon interchange of any two particles. This leads to the exchange energy which can be considered as a quantum correction to the classical Coulomb repulsion. The exchange term is present in Hartree–Fock theory, and can also be incorporated into DFT as Hybrid functionals. There is a dynamical effect where electrons tend to avoid each other more than given by an HF wave function, and this is the correlation energy. The basic problem with the DFT is the inability to account exact exchange-correlation energy. DFT definitions of

exchange-correlation energy (described earlier) is not exactly the same as its wave-mechanical counterparts like HF theory [14]. The expectation energy in HF is given by

$$< E >= \int \psi^* \hat{H} \psi \, d\tau \tag{2.15}$$

where, $\hat{H}$ is the electronic Hamiltonian given by

$$\hat{H} = \sum_{i=1}^{2n} -\frac{1}{2} \nabla_i^2 - \sum_{\text{all } \mu,i} \frac{z_\mu}{r_{\mu i}} + \sum_{\text{All } i,j} \frac{1}{r_{i,j}}. \tag{2.16}$$

First term in the Eq. (2.16) represents kinetic energy of electrons, second term the Columbic forces of attraction with the nuclei and the third term represents the Columbic forces of repulsion between the electrons. Substituting the Slater determinant and Hamiltonian in the equation after the algebraic manipulation transforms Eq. (2.15) (For eg. For the 2n electron system) as,

$$E = 2\sum_{i=1}^{n} H_{ii} + \sum_{i=1}^{n}\sum_{j=1}^{n} (2J_{ij} - K_{ij}) \tag{2.17}$$

with, $$H_{ii} = \int \psi_i^*(1) \, \hat{H}_{core} \, \psi_i \, dv. \tag{2.18}$$

and, $$\hat{H} \text{ core } (1) = -\frac{1}{2}\nabla_1^2 - \sum_{\text{all } \mu} \frac{Z_\mu}{r_{\mu 1}}. \tag{2.19}$$

Here $\hat{H}$ core (1) represents the kinetic energy of electron one plus the potential energy (PE) of attraction of that electron with each of the nuclei μ. One in the parentheses indicates that the same electron is being considered. In the Eq. (2.17) J represent Coulomb integral and K represent exchange integral. "J" represents the electrostatic repulsion between the charge clouds of orbitals ψ_i and ψ_j. Exchange integral "K" arises from Slater determinant, no physical interpretation can be defined but from Eq. (2.17), it can be understood that "K" is the correction to reduce the effect of "J" reducing its effect. This arises due to the fact that electrons possess spin. (2J - K) can be considered to be the true Columbic repulsion (within the charge cloud model), corrected for electron spin (Pauli Exclusion Principle effect). The J integrals represent interactions between electrons in different spatial orbitals and the K integrals represent interactions between electrons of the same spin.

The basic difference between wave function based methods and DFT is that wave mechanics considers the exact Hamiltonian operator but makes approximations of wave function, whereas in DFT, it makes approximations in the Hamiltonian, but allow the electron density to vary. The exchange energy in DFT and HF is represented by the same formula, but in DFT we employ Kohn-Sham orbitals which leads to a non-local potential, i.e. the exchange potential at a given point will be strongly dependent on the density at distant points. The probability of finding an electron at a given point will be independent of the position of second electron if the electrons do not have charge or spin and the electron pair density ρ_2 will be represented as a simple product of two one-electron densities ρ_1, with a proper normalization factor.

$$\rho_2^{\text{indep}}(r_1, r_2) = \frac{N_{ele} - 1}{N_{ele}} \rho_1(r_1)\rho_1(r_2) = \left(1 - \frac{1}{N_{ele}}\right) \rho_1(r_1)\rho_1(r_2). \qquad (2.20)$$

But there is a reduced probability of finding an electron near the other, this can be formally written in terms of conditional probability factor $h_{xc}(r_1, r_2)$ (N_{ele} represents number of electrons in the Eq. 2.20). This conditional probability factor can be represented as follows,

$$\rho(r_1, r_2) = \rho_1(r_1)\rho_1(r_2) + \rho_1(r_1)h_{xc}(r_1, r_2) \qquad (2.21)$$

where, $h_{xc}(r_1,r_2)$ is given by

$$h_{xc}(r_1, r_2) = \frac{\rho_2(r_1, r_2)}{\rho_1(r_1)} - \rho_1(r_1). \qquad (2.22)$$

The exchange–correlation hole gives the reduced probability of finding electron 2 at a position ρ_2 given that electron 1 is located at ρ_1. The exchange part of h_{xc} is called the Fermi hole, and the dynamical correlation gives the Coulomb hole. The Fermi (exchange) hole describes the static reduction in the probability function corresponding to one electron. While the Coulomb (correlation) function, reduces the probability of finding an electron near the reference electron, but increases the probability of finding it away from the reference electron. The exchange energy in Hartree–Fock theory is a non-local whereas in DFT it is a local function which is the main difference between wave function and DFT approaches. However there are some limitations with this model. The Coulomb energy functional given in Eq. (2.3) depends only on ρ_1. This suggests that the density arising from a single electron will interact with itself (self-interaction), and this self-repulsion is non-physical. The HF

model takes care of this problem elegantly, as the exchange energy cancels the Coulomb self-interaction.

2.5. Exchange and correlation Functionals

Exchange correlation functions are represented by mathematical forms containing different parameters. These parameters are evaluated based on the functional's requirement to satisfy the conditions like; the energy functional should be self-interaction-free; when the density becomes constant, the uniform electron gas result should be recovered, etc [12] or by fitting the parameters to experimental data. But in practice a combination of these approaches is often used.

2.6. Local Density Approximation (LDA)

The simplest model in the approximation is Local density approximation [12], where the electron density is assumed to be varying slowly. Exchange-correlation energy can be calculated from the formulae derived for a uniform electron density in this methodology. It is based on the assumption that at every point in the molecule the energy density is given by a homogeneous electron gas which had the same electron density ρ at that point. It is the energy density i.e., the energy (exchange plus correlation) per electron. LDA does not assume that the electron density in a molecule as homogeneous; it arises only in Thomas-Fermi molecule.

2.7. Local Spin Density Approximation (LSDA)

The electrons of opposite spin are placed in different Kohn–Sham orbitals, similar to the unrestricted Hartree–Fock (UHF) method. The advantage of LSDA [12] is that it can handle systems with one or more unpaired electrons like radicals. For species in which all the electrons are paired, the LSDA is equivalent to the LDA. LSDA geometries, frequencies and electron-distribution properties are found to be reasonably good, but the dissociation energies, including atomization energies, are very poor.

2.8. Gradient-Corrected Functionals

Modern DFT calculations use gradient corrected functionals which use both electron density and its gradient (the first derivative of ρ with respect to its position). These functionals are called generalized gradient approximations (GGA). In Generalized Gradient Approximation (GGA) methods, the first derivative of the density is included as a variable, and in addition

the Fermi and Coulomb holes integrate to the required values of −1 and 0. Exchange-correlation functionals can be further improved by making functionals depend on higher order derivatives of electron density. Functionals which use the second derivative of ρ are called meta- generalized gradient corrected (MGGA) functionals [12]. Although this functional improves the accuracy of results, but functionals are dependent on Laplacian of ρ at present. MGGA functionals side skips the problem by not depending on ρ but on KE density τ. This can be obtained as

$$\tau(r) = \frac{1}{2} \sum_{i=1}^{\text{occupied}} \left|\nabla \psi_i^{KS}(r)\right|^2, \qquad (2.23)$$

where, ψ_i^{KS} represent Kohn Sham orbitals.

Exchange energy corresponding to HF is added in these functionals. These are also called adiabatic correction methods. In the adiabatic process of wave function approach, wave function remains the same on potential energy surface (PES). Adiabatic correction method shows that the exchange-correlation energy $E_{XC}(\rho)$ can be taken as a weighted sum of the DFT exchange-correlation energy and HF exchange energy. Hybrid DFT functionals which include an energy contribution from HF-type electron exchange, calculated from the KS wave function of the non-interacting electrons. Since these electrons have no Coulomb interaction, but electrons with a spin of one-half, show "Pauli repulsion" represented by the exchange K integral. Hybrid functionals are functionals (of the GGA level or higher) that contain HF exchange, the correction energy to the classical Coulomb repulsion [12]. The percentage of HF exchange energy to use is a main characteristic of the various hybrid functionals.

2.9. Hybrid functional B3LYP

There are two methodologies for assigning values of parameters for exchange-correlation functional either by requiring the functional to fulfill the criteria discussed above or by fitting the parameters to experimental data, but in practice a combination of these approaches is often used. The B3LYP functional has a total of eight purely empirical parameters. This exchange-energy functional was developed by Becke [15] with Lee, Yang and Paar with three parameters (LYP) [16]

$$E_{XC} = a_0 E_{X,HF} + (1 - a_0) E_{X,Slater} + a_X \Delta E_{X\,Becke88} + (1 - a_C) E_{c,VWN} + a_C \Delta E_{C,LYP}. \qquad (2.24)$$

$E_{x,HF}$ is the HF exchange energy based on Kohn-Sham orbitals, $E_{x,Slater}$ is the uniform electron gas exchange-correlation energy, $\Delta E_{xBecke88}$ is Becke's 1988 generalized gradient approximation (GGA) for exchange [17] $E_{c,VWN}$ is Vosko-Wilk-Nusair 1980 correlation functional [18] and $\Delta E_{c,LYP}$ is the LYP correlation functional. The parameters $a_o = 0.20$, $a_x = 0.72$ and $a_c = 0.81$ are determined by Becke using a least square fit to 56 experimental values of atomization energies, 42 ionization potentials and 8 proton affinities.

2.10. Basis sets

Basis functions approximate orbitals of atoms in molecule and linear combination of basis functions approximates total electronic wavefunction. Atomic orbitals are represented by atom-centered Gaussians in most quantum chemistry programs for example in Gaussian09 [19]. Slater type of orbitals (STO) represents electron density well in valence region and beyond (not so well near nucleus) however evaluating these STOs are difficult because a typical STO function is given below,

$$\emptyset_{abc}^{STO}(x,y,z) = N\, x^a y^b z^c e^{-\zeta r}. \tag{2.25}$$

"N" represents the normalization constant, a,b,c control angular momentum (L = a+b+c) and Zeta (ζ) controls the width of the orbital (the function is difficult to solve mathematically). Gaussian types of orbitals (GTO) are used in the place of Slater type of orbitals where they can be mimicked by using linear combination of Gaussian functions. Gaussian type of orbitals are given by the Eq. (2.26)

$$\emptyset_{abc}^{GTO}(x,y,z) = N\, x^a y^b z^c e^{-\zeta r^2}. \tag{2.26}$$

A combination of "n" Gaussians to mimic an STO is often called an "STO-nG" basis, even though it is made of contracted GTO's (CGTO) given by,

$$\emptyset_{abc}^{CGTO}(x,y,z) = N \sum_{i=1}^{n} c_i x^a y^b z^c e^{-\zeta r^2}. \tag{2.27}$$

where c_i represent contraction coefficient. We have used Pople basis sets in our calculations developed by late Nobel Laurate John Pople [20] which are based upon CGTOs. In most of our calculations we used 6-31G (d) basis sets, where 6 represent the core orbital which is a CGTO made of 6 Gaussians, and the valence orbitals are described by two orbitals — one CGTO made of 3 Gaussians, and the other with one single Gaussian. "d" indicates the

polarization functions on non-hydrogen atoms. Adding more basis functions per atom allow orbitals to "change size" and adding polarization functions allow orbitals to change shape.

2.11. Population Analysis

In order to understand the important phenomenon of charge transfer between CNTs and various adsorbate molecules, population analysis is carried out. In population analysis the idea is to accurately model partial charge magnitude and location within a molecule. Partial atomic charges are not observable characteristics of molecules, to assign charges to atoms; one must define the spatial region of those atoms, then add up all the charge in that region and integrate charge density over the volume [21].

2.12. Mulliken Population analysis

One of the oldest and widely used methodologies to determine the partial charges of atoms in the molecule is Mulliken Population analysis. It is based on the linear combination of atomic orbitals where the electrons are partitioned to the atoms based on the nature of the atomic orbitals' contribution to the molecular wave function [21]. Generally, the total number of electrons in the molecule N can be expressed as

$$N = \sum_{J}^{\text{Electrons}} \int \psi_j(r_j)\psi_j(r_j)\, dr_j. \tag{2.28}$$

$$N = \sum_{j}^{\text{Electrons}} \sum_{r,s} \int c_{jr}\, \emptyset_r(r_j) c_{js} \emptyset_s dr_j. \tag{2.29}$$

$$N = \sum_{j}^{\text{Electrons}} \left(\sum_{r} c_{jr}^2 + \sum_{r \neq s} c_{jr}\, c_{js} S_{rs} \right). \tag{2.30}$$

Here r and s index the AO basis functions φ, c_{jr} are coefficients of the basis function "r" in the MO "j", and "S" is the overlap matrix. The total number of electrons can be divided into two sums (Eq. (2.30)): the first one including only squares of single AO basis function (r), and the other one products of two different AO functions (r and s). The first term represents electrons belonging to the particular atom. It is the second term that causes problems – since there is no best way to divide the shared electrons between the two atoms. Mulliken

suggested splitting the shared density 50:50. Then the electrons associated with the atom "k" are given by

$$N_k = \sum_{j}^{\text{Electrons}} \sum_{r\in k} c_{jr}^2 + \sum_{r,s\in k, r\neq s} c_{jr}\, c_{js} S_{rs} + \sum_{r\in k, s\notin k} c_{jr}\, c_{js} S_{rs}. \qquad (2.31)$$

The first two terms come from the basis functions on the kth atom and the last term is the part shared with all other atoms. The partial charge on the atom k is given by

$$q_k = Z_k - N_k. \qquad (2.32)$$

where "Z" represents atomic number of the atom.

The partial charges assigned to atoms using Mulliken population analysis vary significantly for the same system when different size basis sets are used. This instability of charge with increasing basis set size is a major drawback of this analysis [21].

2.13. Natural Population Analysis (NPA)

NPA [22] is based on the Natural Bond Orbital (NBO) [23] scheme. Natural bond analysis classifies the orbitals into three distinct groups: non-bonding natural atomic orbitals (NAOs), orbitals involved in bonding and antibonding (NBOs), and Rydberg type orbitals. The Rydberg type orbitals and NAOs are made up of basis sets of single atoms and the NBOs are a combination of basis set atomic orbitals of two atoms. This is similar to the notion of core electrons, lone pairs of electrons, and valence electrons, and works under the assumption that only the bonding orbitals should be made by combinations of two atoms' basis sets. Based on this model of electron partitioning, Natural Population Analysis then treats the NBOs as the Mulliken method treats all the orbitals. NPA procedure thus eliminates most of the problems associated with the Mulliken Analysis and provides a marked improvement over it [22].

The concept of natural orbitals was introduced by Löwdin [24] in 1955. Natural orbitals (like the canonical molecular orbitals of Hartree-Fock theory) are symmetry adapted. Let us consider wavefunction (Ψ_2) of two hydrogen atoms with H, H' separated by infinite distance.

$$\Psi_2 = \Psi(H, H'). \qquad (2.33)$$

On physical grounds, we can expect the wavefunction Ψ_2 to be nearly identical to corresponding localized wavefunctions. However, Ψ_2 must incorporate the superposition symmetry [25] between hydrogen wavefunctions (although these atoms have no interactions of physical significance); the natural orbitals of Ψ_2 will be found to differ qualitatively from the wavefunctions of two hydrogen atoms. This result in the consequence of making orbitals more delocalized which in turn misses the simplicities associated with chemical bonding. Similar spurious mixings result when the atoms are merely separated by a few links of an alkane chain [26]. To remove spurious effects associated with symmetry adaptation, we can formulate [27,28] a localized criterion for orbitals that have the analogous maximum-occupancy (natural) character in localized 1-center and 2-center regions of the molecule, since the maximum occupancy of an orbital is limited to a pair of electrons by the Pauli exclusion principle. Natural bond orbitals (NBOs) provide the most accurate natural Lewis structure picture of wavefunction Ψ, as all orbital details (atomic hybrid compositions, polarization coefficients etc.) are mathematically chosen which include the highest possible percentage of the electron density. This percentage gives an intrinsic measure of the accuracy of the natural Lewis structure picture, and is found to be > 99% for common organic molecules [26].

The NBOs are the intermediate between basis AOs and molecular orbitals (MOs). Sequence of natural localized orbital sets include natural atomic (NAO), hybrid (NHO), natural bond orbitals (NBO), (semi) Natural localized molecular orbital (NLMO) and molecular orbitals (MOs). AOs → NAOs → NHOs → NBOs → NLMOs → MOs.

In accordance with the simple bond orbital picture [26] each bonding NBO, σAB can be written in terms of two directed valence hybrids (NHOs) h_A, h_B on atoms A and B, with corresponding polarization coefficients C_A, C_B as,

$$\sigma_{AB} = C_A h_A + C_B h_B. \tag{2.34}$$

Each valence bonding NBO (Eq. (2.34)) must in turn be paired with a corresponding valence antibonding NBO in Eq. (2.35),

$$\sigma^*_{AB} = C_A h_A + C_B h_B. \tag{2.35}$$

The "Lewis" type (donor) NBOs (Eq. (2.34)) is thereby complemented by the "non-Lewis"-type (acceptor) NBOs (Eq. (2.35)) that are formally empty in an idealized Lewis structure. Weak occupancies of the valence antibonding (Eq. (2.35)) suggest irreducible departures

from an idealized localized Lewis structure picture, in other words true delocalization effects [26]. The energetic stabilization associated due to $\sigma \rightarrow \sigma^*$ donor acceptor interactions can be estimated by 2nd-order perturbation theory, viz., for the $\sigma_i \rightarrow \sigma_j^*$ interaction given by,

$$\Delta E_{i \rightarrow j^*}^{(2)} = -2 \frac{< \sigma_i | \hat{F} | \sigma_j^* >^2}{\varepsilon_{j^*} - \varepsilon_i}. \quad (2.36)$$

where $\hat{F}$ is the effective orbital Hamiltonian (Fock or Kohn-Sham operator) and ϵ_i and ϵ_j are the respective orbital energies of donor and acceptor NBOs.

2.14. Band structure studies

Molecular orbital theory (MOT) describes the electronic energy levels of isolated molecules. But in solid state materials, interactions between neighboring molecules become very important. Many of the important properties like superconductivity, magnetism, metallic conductivity, etc. depend upon intermolecular interactions. The solid state equivalent to a molecular orbital (MO) diagram is called the band structure diagram [29]. Electronic band structure provides the insight and understanding of very important physical properties of solids. Similar to the molecular orbital theory where the energy levels in a MO diagram are dependent upon the energy levels of the atomic orbitals, the symmetry and interatomic distances in a molecule, the electronic band structure depends on the energy levels of the constituent atomic orbitals and the crystal structure. Band structure is mostly studied by physicists and the terminology of physicists differs from the chemists. A rough comparison of the way chemists and physicists view solids is given in the table below.

Table 2.1. Terminology in Band structure used by chemists and physicists.

Chemist	Physicist
MO Diagram	Band Structure Diagram
Molecular Orbital	Wave vector
Chemical bonding	Potentials
Qualitative	Quantitative (Mathematical)

2.15. Preliminaries of Band structure - Let us consider a simple 1-D chain of hydrogen atoms. If there are N atoms in the chain there will be N energy levels and N electronic states or N “MOs". The wavefunction of the electronic state [29] is given by Eq. (2.37),

$$\Psi_k = \sum e^{ikna} \chi_n. \tag{2.37}$$

Here "a" corresponds to the lattice constant (spacing between H atoms) and n is a counter for each atomic orbital in the chain. χ represents basis functions and n corresponds to number of atoms in the chain. Each Ψ_k is a symmetry adapted linear combination (SALC) of AOs, where the symmetry operator in this case is translational symmetry. The process of symmetry adaption is called in the solid-state physics as, "forming Bloch functions" [30,31]. The variable k represents the labels of respective SALCs, it also gives the information about phase of the orbitals as shown in Figure 2.1 [29].

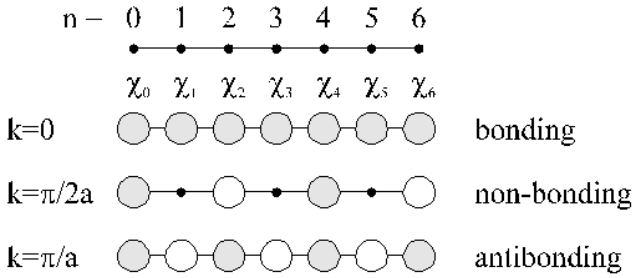

Figure 2.1. Illustration of bonding at different k points forming bonding, non-bonding and antibonding orbitals.

At k = 0 all of the orbitals are in phase, while at k = π/a the orbitals are out of phase, at intermediate values the phase of the orbitals are different. The value of k also is related to the wavelength of the wave packet (λ) which in turn describes an electron in a given state, Ψ_k, given by the relationship,

$$\lambda = \frac{2\pi}{k}. \tag{2.38}$$

The unique values of k are in the interval $-\pi/a \leq k \leq \pi/a$ or $|k| \leq \pi/a$, called the first Brillouin zone. An example of a typical Band structure diagram [29] is shown below (Figure 2.2). Here we observe (Figure 2.2) the lowest energy orbital is at k=0 and highest energy orbital at k=π/a. One of the interesting features of bands is how they "run". Let us consider the band structure diagram [29] of sigma interaction of "p" functions shown below (Figure 2.3). From the Figure 2.3. it is clear that k = 0 correspond to highest energy and π/a the lowest. Another important feature of band structure plots is it gives the information about

bonding interactions between orbitals in the case of polymer or crystal the overlap is considered between neighboring unit cells.

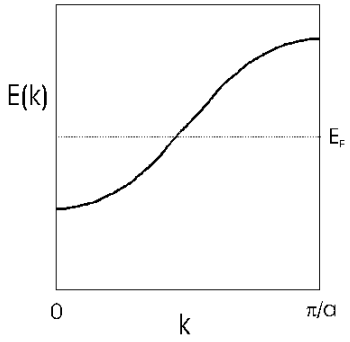

Figure 2.2. Band structure diagram Energy vs k vector in the first Brillouin zone is shown.

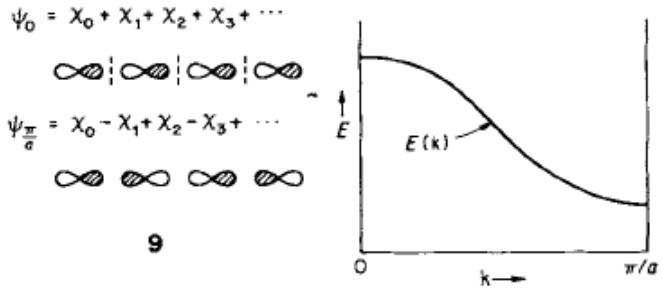

Figure 2.3. Band structure diagram formed by "p" functions (frontier orbitals). Overlap of frontier orbitals at k points 0, π/a is also shown.

Band width is defined as the energy gap between the lowest and highest energy orbital. As the orbital overlap is increased (decreasing the interatomic spacing) the bonding interaction is stabilized while the antibonding is further destabilized. This will cause the band width to increase.

2.16. Band structure studies of Carbon Nanotubes

SWCNT are formed by rolling up 2-D graphite sheet as a hollow cylindrical shape of one layering of cyclic carbon array shape as 1-D tube axis infinity extension. Quantum chemistry calculations cannot simulate the real infinite length SWNT model owing to the large requirements of memory and CPU speed. Periodic boundary condition (PBC) model has been proposed that could solve the discrete MO model into the continuous bands [32-34].

Scuseria *et al.*, [35] used the DFT-PBC method to optimize the geometrical structure and to generate the energies of [5,0] zigzag SWNTs. The PBC model in Gaussian 09 package is based on Gaussian type orbitals (GTOs), to transform GTOs into "Crystalline orbitals" for calculating with periodic boundary conditions, modulated by a phase factor e^{ikl}. These functions are known as Bloch functions,

$$\Psi_k = \sum_l \left[\frac{1}{\sqrt{N}} e^{ikl}\right].\Psi_l. \qquad (2.39)$$

Here k=(k_x,k_y,k_z) correspond to the reciprocal-lattice vector, which classifies periodic orbitals by their irreducible representations of the infinite translation group, Ψ_l is an orbital Ψ located in cell "*l*", and "i" is the imaginary unit. Orbitals which belong to different k do not interact directly with each other and this allow to solve the self-consistent-field equations separately for each k point with,

$$C_k = S_k C_k E_k. \qquad (2.40)$$

F_k represents Fock matrix or Kohn Sham matrix, C_k is the matrix of coefficients of crystalline orbitals, S_k represents overlap matrix and E_k represents crystalline orbital energies in the Eq. (2.40). The exponent in the Bloch orbital definition in the Eq. (2.39) introduces complex factors. Hence, all matrices in Eq. (2.40) are, in general, complex. Matrix elements between periodic orbitals defined in Eq. (2.39) can be computed from matrix elements for localized GTOs employing,

$$\langle\Phi_k|A|\Psi_k\rangle = \sum_l \langle\Phi_k|A|\Psi_k\rangle e^{ik.l} = \sum_l A^{0l}_{\Phi\Psi} e^{ikl}. \qquad (2.41)$$

In this Eq. (2.41), $A^{0l}{}_{\Phi\Psi}$ represent the matrix element of operator A between the Gaussian atomic orbitals Φ located in the central cell "0" and Ψ located in cell "*l*". The Kohn-Sham Hamiltonian matrix elements (or Fock matrix elements in the HF case), $F^{0l}{}_{\mu\nu}$, include several contributions

$$F^{0l}_{\mu\nu} = T^{0l}_{\mu\nu} + U^{0l}_{\mu\nu} + J^{0l}_{\mu\nu} + E^{0l,xc}_{\mu\nu}. \qquad (2.42)$$

In the equation $T^{0l}{}_{\mu\nu}$ represents the electronic kinetic energy term, $U^{0l}{}_{\mu\nu}$ represents the electron-nuclear attraction term, $J^{0l}{}_{\mu\nu}$ defines the electron-electron repulsion term, and $E^{0l,xc}{}_{\mu\nu}$ denotes the contribution from the DFT exchange-correlation potential. $T^{0l}{}_{\mu\nu}$ and $U^{0l}{}_{\mu\nu}$ terms

do not depend on the density matrix, whereas $J^{0l}{}_{\mu\nu}$ and $E^{0l,\ xc}{}_{\mu\nu}$ do. The Kohn-Sham Hamiltonian matrix elements, $F^{0l}{}_{\mu\nu}$, is their exponential decay with respect to the increasing separation between the μ and ν GTOs. This arises from the individual decay of the kinetic energy term, the exchange-correlation potential term, and the exponential decay of the combined electrostatic terms. Thus Eq. (2.42) is quite similar to analogous terms in molecular calculations. The electrostatic terms ($U^{0l}{}_{\mu\nu}$ and $J^{0l}{}_{\mu\nu}$) considers the interactions of a given pair of basis functions with charge distributions of the system. In the PBC the number of such interactions is infinite, and hence different from the molecular case. The infinite sums can be handled employing the Ewald summation techniques [36] or by using periodic fast multipole method [35]. The real-space density-matrix elements $P^{0l}{}_{\lambda\sigma}$ which is required for the construction of the Coulomb, exchange, and correlation contributions can be derived by integrating the complex density $P^{k}{}_{\lambda\sigma}$ in reciprocal space as,

$$P^{0l}_{\lambda\sigma} = \frac{1}{V_k} \int P^{k}_{\lambda\sigma}\, e^{ik.l}\ dk. \tag{2.43}$$

In Eq. (2.43), V_k corresponds to the volume of the unit cell in k space. The matrix P^k is derived from the orbital coefficients C_k, which are the solutions to the eigenvalue Eq. (2.40). The transformation described by Eq. (2.43) is the only coupling of different k points during the SCF procedure. The energy per unit cell can be given as,

$$E = \sum_{\mu\in 0}\sum_{l}\sum_{\nu\in l} P^{0l}_{\mu\nu}\left(T^{0l}_{\mu\nu} + U^{0l}_{\mu\nu} + \frac{1}{2}J^{0l}_{\mu\nu}\right) + E_{xc} + E_{NR}. \tag{2.44}$$

Here in the equation Eq. (2.44) E_{xc} gives the exchange-correlation energy and E_{NR} gives the nuclear repulsion energy. The triple sums in Eq. (2.44) are abbreviated as $\sum_{\mu\nu l}$ for simplicity in the following equations. To avoid the convergence problems and to maximize accuracy, it is essential that electrostatic terms be grouped together as electronic E_e and nuclear E_N terms given in Eqs. (2.45) and Eq. (2.46) as,

$$E_e = \frac{1}{2}\sum_{\mu\nu l}\left(U^{0l}_{\mu\nu} + J^{0l}_{\mu\nu}\right)P^{0l}_{\mu\nu} \quad \text{and} \tag{2.45}$$

$$E_N = \frac{1}{2}\sum_{\mu\nu l} U^{0l}_{\mu\nu}P^{0l}_{\mu\nu} + E_{NR}. \tag{2.46}$$

After the successful optimization, it is possible to obtain the converged density from available charge density and to compute the gradient of total energy with respect to nuclear displacements to plot the band structure.

Reference

1. X. Zhou, T. Zifer, B. M. Wong, K. L. Krafcik, F. Leonard, A. L. Vance. *Nano Lett.* 9, 1028, 2009.
2. S. Grimme, J. Antony, T. Schwabe, C. M. Lichtenfeld. *Org. Biomol. Chem.* 5, 741, 2007.
3. M. Chi, Y. P. Zhao. *Comp. Mat. Sci.* 46, 1085, 2009.
4. P. V. Avramov, K. N. Kudin, G.E. Scuseria. *Chem. Phys. Lett.* 370, 597, 2003.
5. L. Jeloaica, V. Sidis. *Chem. Phys. Lett.* 300, 157, 1999.
6. L. Gan, J. Zhao. *Physica E*, 41, 1249, 2009.
7. L. Chen, C. Xu, X. F. Zhang, T. Zhou. *Physica E*, 41, 852, 2009.
8. A. Ahmadi, J. Behestian, N.L. Hadipour. *Structural Chemistry*, 22, 183, 2011.
9. Y. Matsuda, J. Tahir-Kheli, W. A. Goddard, III. *J. Phys. Chem. Lett.* 1, 2946, 2010.
10. R. F. W. Bader. *Atoms in molecules*. Oxford, New York, 1990.
11. E. G. Lewars. *Computational Chemistry-Introduction to the Theory and Applications of Molecular and Quantum Mechanics*, Springer, Dordrecht Heidelberg, London, New York, 2011.
12. Frank Jensen. *Introduction to Computational Chemistry*, John Wiley & Sons Ltd, England, 2007.
13. I. N. Levine. *Quantum chemistry*, Prentice Hall, Upper Saddle River, NJ, 2000.
14. O. V. Gritsenko, P. R. T. Schippen, E. J. Baerends. *J. Chem. Phys.* 107, 5007, 1997.
15. A. D. Becke. *J. Chem. Phys*. 98, 5648, 1993.
16. C. Lee, W. Yang, R. G. Parr. *Phys. Rev. B.* 37, 785, 1988.
17. A. D. Becke. *Phys. Rev. A*. 38, 3098, 1988.
18. S. H. Vosko, L. Wilk, M. Nusair. *Can. J. Phys*. *58*, 1200, 1980.
19. M. J. Frisch, G. W. Trucks, H. B. Schlegel, G. E. Scuseria, M. A. Robb, J. R. Cheeseman, J. A. Montgomery Jr., T. Vreven, K. N. Kudin, J. C. Burant, J. M. Millam, S. S. Iyengar, J. Tomasi, V. Barone, B. Mennucci, M. Cossi, G. Scalmani, N. Rega, G.A. Petersson, H. Nakatsuji, M. Hada, M. Ehara, K. Toyota, R. Fukuda, J. Hasegawa, M. Ishida, T. Nakajima, Y. Honda, O. Kitao, H. Nakai, M. Klene, X. Li, J. E. Knox, H. P. Hratchian, J. B. Cross, V. Bakken, C. Adamo, J. Jaramillo, R.

Gomperts, R.E. Stratmann, O. Yazyev, A. J. Austin, R. Cammi, C. Pomelli, J. W. Ochterski, P.Y. Ayala, K. Morokuma, G. A. Voth, P. Salvador, J. J. Dannenberg, V. G. Zakrzewski, S. Dapprich, A. D. Daniels, M. C. Strain, O. Farkas, D. K. Malick, A. D Rabuck, K. Raghavachari, J. B. Foresman, J. Ortiz, Q. Cui, A. G Baboul, S. Clifford, J. Cioslowski, B. B. Stefanov, G. Liu, A. Liashenko, P. Piskorz, I. Komaromi, R. L. Martin, D. J. Fox, T. Keith, M. A. Al-Laham, C. Y. Peng, A. Nanayakkara, M. Challacombe, P. M. W. Gill, B. Johnson, W. Chen, M. W. Wong, C. Gonzalez, J. A. Pople, *Gaussian Inc, Gaussian 09*, Revision A.1, Wallingford, CT, 2009.

20. J. B. Foresman, A. Frisch, *Exploring Chemistry with Electronic Structure Methods: A Guide to using Gaussian*, Pittsburgh, 1996.
21. K.I. Ramachandran, G. Deepa, K. Namboori. *Computational Chemistry and Molecular Modeling: Principle and Applications.* Springer, Berlin Heidelberg, 2008.
22. K. B. Wiberg, P. R. Ruben. *J. Comput. Chem*. 14, 1504, 1993.
23. F. Weinhold. *Discovering Chemistry with Natural Bond Orbitals*; Wiley, New Jersey, 2012.
24. P. O. Löwdin. *Phys. Rev.* 97, 1474, 1955.
25. F. Weinhold. *J. Chem. Ed*. 76, 1141, 1999.
26. F. Weilhold, C. R. Landis, *Chemistry Education: Research and practice in Europe*, 2, 91, 2001.
27. J. P. Foster and F. Weinhold. *J. Am. Chem. Soc.* 102, 7211, 1980.
28. A. E. Reed, L. A. Curtiss, F. Weinhold. *Chem. Rev.* 88, 899, 1988.
29. R. Hoffmann. *Angew. Chem. Int. Ed. Engl.* 26,846, 1987.
30. J. K. Burdett. *Prog. Solid State Chem.* 15, 173, 1984.
31. T. A. Albright, J. K. Burdett, M. H. Whangbo. *Orbital Interactions in Chemistry*, Wiley-Interscience, New York, 1985.
32. K. N. Kudin, G. Scuseria. *Phys. Rev. B.* 61, 16440, 2000.
33. S. Erkoc, *International J. Mode. Phys*. 11, 547, 2000.
34. H Cao, J. Ma, G. Zhang, Y. Jiang. *Macromolecules*, 38, 1123, 2005.
35. K. N. Kudin, G. Scuseria. *Chem. Phys. Lett*. 289, 611, 1998.
36. H. D. Herce, A. E. Garcia, T. Darden. *J. Chem. Phys.* 126, 124106, 2007.

CHAPTER 3

Oxygen Adsorption on Intrinsic Pristine and Doped Zig-zag and Arm-chair SWCNTs

3.1. Introduction

Interest in gas adsorption by carbon nanotubes at ambient conditions has been initiated by the demonstrations of the potential of SWCNT based sensors, [1-5] especially the establishment of the mutual dependence between gas adsorption and transport properties. In this context Oxygen sensors find application in many areas like cement and steel industries, biological and food-processing industries, chemical plants, automobiles etc. [1]. Currently used oxygen sensors are broadly divided into three types namely, potentiometric sensors, amperometric sensors and semi-conducting metal oxide sensors [2]. But most of these sensors, for example, potentiometric sensors and metal oxide sensors require high operating temperatures of 300-1000^{0}C whereas amperometric sensors have complicated design [2]. Monitoring oxygen under ambient conditions is necessary in medical, food processing and waste management industries [2]. Currently available sensors which operate at ambient conditions are optical sensors, but the main drawback associated with these sensors is the slower response time (around 40 seconds) and high power consumption [3]. SWCNTs have been found to be very sensitive to gas molecule adsorption exhibiting great sensitivities in addition operating at ambient conditions [4,5].

Adsorption of oxygen on SWCNTs was first reported by Kong *et al.,* [4] showing that conductivity of CNTs dramatically being altered on exposure to air or oxygen. Since then various groups studied the adsorption of oxygen both theoretically and experimentally and many divergent reports have been published [4-15]. Studies based on Local density Approximation (LDA) predicted a weak hybridization between semi-conducting SWCNTs and oxygen with a weak charge transfer of 0.1 e leading to a binding of oxygen at a distance of less than 3 Å from the nanotube [10,12]. On the other hand studies based on gradient corrected methods predicted a very weak bonding with equilibrium distance between SWCNT and oxygen at ~4 Å without any charge transfer [11,13,15]. Current literature mostly focusses on adsorption of triplet oxygen [4-15].

In order to obtain a consistent idea of the adsorption of oxygen by individual SWCNT, we have conducted a diligent theoretical investigation of adsorption of oxygen. In

the current Chapter, we discuss the adsorption of oxygen in both the spin states singlet and triplet along the sidewalls of semi-conducting and arm-chair SWCNTs. To shed light on the nature of adsorption and its effects on the transport properties of SWCNTs, we study the adsorption properties of oxygen on intrinsic, boron doped and nitrogen doped SWCNTS in both zig-zag and arm-chair forms. Binding energies, charge transfer calculations and equilibrium bond distances are calculated to understand the adsorption patterns.

3.2. Results and Discussion

Hybrid functional B3LYP with 6-31G (d) basis set is employed for optimization studies of oxygen gas molecules along the side walls of SWCNTs. In order to predict the properties of adsorption of gases along sidewalls of SWCNTs correctly, one require a nanotube of size of at least 70 atoms if finite structures are chosen instead of infinite structures [16]. Semi-conducting zig-zag (5,0), metallic arm-chair (5,5) SWCNTs with eight layers constituting 80 carbon atoms and (8,0) semi-conducting zig-zag SWCNT with 6 layers constituting 96 carbon atoms are considered and end carbon atoms of the tube are saturated with hydrogen atoms in order to satisfy the valence in all the cases.

3.3. Adsorption on pristine nanotubes

We have studied the behavior of oxygen in its singlet and triplet forms on the side walls of (5,0), (8,0) and (5,5) nanotubes. The results of these calculations binding energy (i.e., adsorption energy) in eV per mole, distance of the molecule from the nanotube (Å) and charge transfer employing Mulliken population analysis are given in Table 3.1. Negative sign indicates charge transfer from the nanotube to gas molecule and positive sign indicates charge transfer from the gas molecule to the nanotube. Binding energy is calculated by the formula

Binding energy = (Energy of SWCNT + Gas molecule) – (Energy of SWCNT + Energy of Gas molecule) **Note**: (Energy of the combined moiety in optimized orientation minus Energy of individual SWCNT and gas molecule)

The singlet oxygen is found to be at a distance of 1.46, 1.47 Å from the pristine (5,0) and (8,0) semi-conducting CNTs respectively which shows very good affinity and there is significant charge transfer from the nanotube to the molecule, of the order of ~0.6 e. Molecular oxygen in its singlet state is found to adsorb strongly on semi-conducting nanotube surfaces with appreciable binding energies.

Table 3.1. Calculated data of binding energy distance from the walls and charge transfer of singlet and triplet oxygen on semi-conducting and metallic nanotubes.

SWCNT	Binding energy (eV)		Distance (Å)		Charge transfer (e)	
	Singlet	Triplet	Singlet	Triplet	Singlet	Triplet
(5,0)	-1.418	-0.026	1.46	3.31	-0.608	-0.002
(8,0)	-0.880	-0.040	1.47	3.37	-0.631	-0.004
(5,5)	-0.348	0.004	2.52	3.50	-0.258	-0.003

All the adsorption processes examined are found to be exothermic from the adsorption energy values. The singlet oxygen near the metallic tube is found to be at a distance of 2.52 Å from the surface. This is very much in contrast with the behavior of singlet oxygen near the semi-conducting tubes. In the case of the semi-conducting tubes, the charge transfer is more as is evident from the closer tube-molecular distance. The negative value of the charge transfer suggests that the charge transfer is from the nanotube to the molecule. Table 3.1. also describes the adsorption characteristics of the triplet oxygen. It is found to be at physisorption range for all the nanotubes, at distances 3.3 – 3.5 Å with very low binding energies and negligible charge transfer, for both semi-conducting and metallic nanotubes.

The geometry optimized structure of the singlet oxygen molecule near the (8,0) tube at a distance of 1.47 Å and the triplet oxygen at a distance of 3.37 Å are shown in Figures. 3.1, and 3.2, respectively. This difference in behaviour of singlet and triplet forms is a very interesting finding. We find that singlet oxygen has more potential for chemisorption onto the nanotube walls than the triplet oxygen which only weakly physisorbs. In a recent study [17], it is found that singlet oxygen chemically bonding on hydrocarbon molecules to form metastable structures whereas the triplet form adsorbs only weakly. Our study is also in accordance with the experimental finding that the semi-conducting nanotubes show affinity towards oxygen molecule [18]. It has been established in the literature by experiments and theory that the oxygen has very little affinity or only weakly physisorbs on graphite surfaces and also on carbon nanotubes [11,12,19]. However the oxygen mentioned in these works refer to ground state oxygen. In our calculations also we find that triplet oxygen has only weak affinity to intrinsic CNTs. The adsorption energy curve shows interesting results for both the cases. Single point energy calculations at various distances are calculated and the potential energy variation as a function of the distance of singlet oxygen and triplet oxygen

from the (5,0) surface is given in Figure. 3.3. It shows a clear minimum for the singlet oxygen adsorption at a distance of about 1.46 Å. On the other hand, the curve for triplet case has no well-defined minimum which clearly shows that the tube-molecule interaction is less and therefore can be identified as physisorption.

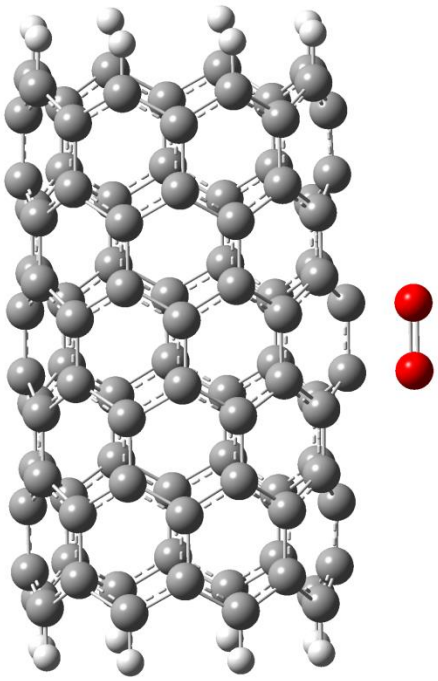

Figure 3.1. Optimized orientation of singlet oxygen with intrinsic (8,0) SWCNT. Grey, white and red colours indicate carbon, hydrogen and oxygen atoms respectively. The closest distance between singlet oxygen from the nanotube surface is 1.47 Å.

We also prove that the singlet oxygen is getting dissociatively chemisorbing on to the walls of the zig-zag tubes. In order to confirm that singlet oxygen molecule indeed dissociate near the semi-conducting tube and getting chemically adsorbed on to the walls, we have done the calculations with the oxidized (8,0) nanotube with the structure as shown in Figure. 3.4. Both the configurations, i.e., the structure with singlet oxygen at a distance of 1.47 Å in Figure. 3.1. and the oxidized form in Figure. 3.4. are found to have the same energy. The O-O bond length in the ring structure in Figure. 3.4. and also in the Figure.3.1, is found to match at a distance of 1.49 Å, compared to the bond distance of 1.21 Å in bare oxygen molecule. This is very clear from the charge transfer calculations where we see that there is a charge transfer of about ~0.631 e (according to Mulliken population analysis) for (8,0) tube, thus showing increase in its single bond character.

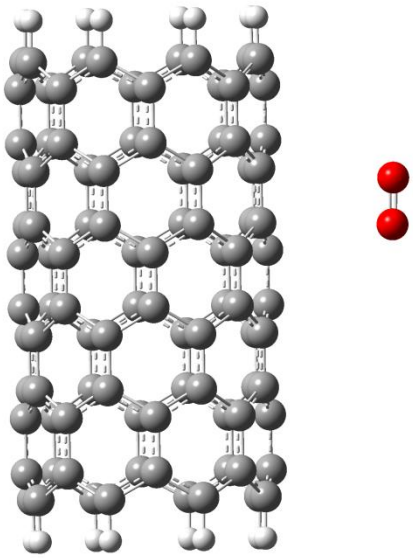

Figure 3.2. Optimized orientation of triplet oxygen with intrinsic (8,0) SWCNT. Grey, white and red colours indicate carbon, hydrogen and oxygen atoms respectively.

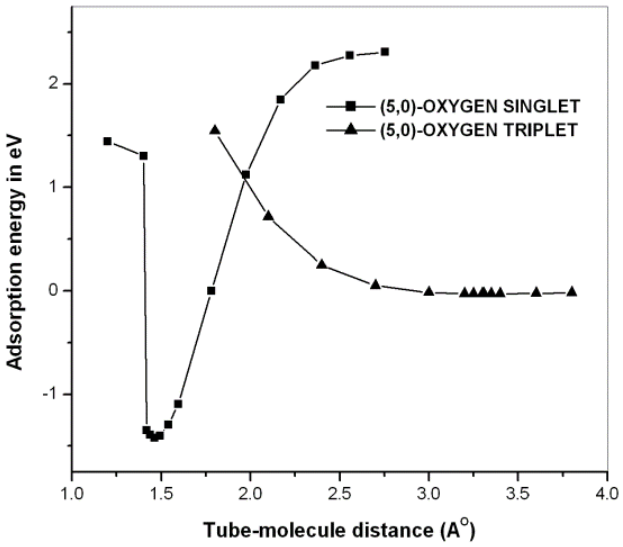

Figure. 3.3. Adsorption energy (eV) of singlet and triplet oxygen on (5,0) SWCNT as a function of tube-molecule distance (Å).

Chemisorbed oxygen is accompanied by a significant amount of charge transfer between the molecule and the nanotube. It is interesting as oxidation can happen on the surface easily

resulting in a dioxetane structure similar to one mentioned by Sorescu *et al.*, [11] in their work on singlet oxygen near graphite surface.

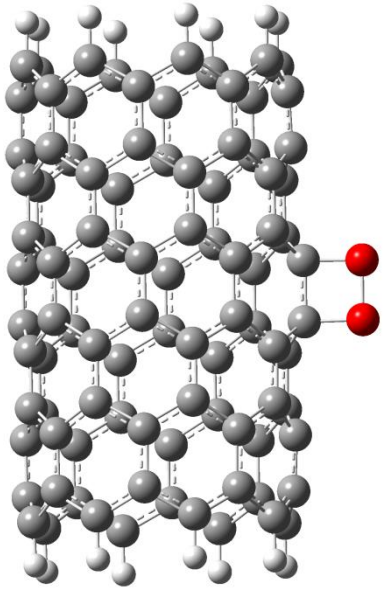

Figure 3.4. Optimized configuration for the chemisorption of singlet oxygen adsorbed on the surface of (8,0) single walled carbon nanotube.

It has been found in recent calculations that singlet oxygen can form metastable structures with graphite [11,17]. This difference in interaction of triplet and singlet forms is also clearly visible in the electrostatic potential (ESP) mapped density surfaces shown in Figurs 3.5. and 3.6. (Default iso-value settings of 0.0004 is taken throughout while plotting ESPs in the thesis) ESP maps illustrate the charge distributions of molecules three dimensionally which allows us to visualize variably charged regions of a molecule, using colour codes [20]. The coloured display of the electrostatic charge computed by DFT has been superimposed on an electron isodensity surface. The red region indicate the higher negative electrostatic potential indicating favorable interaction energy with electron density acceptors and the highest positive potential is represented by blue colour. The positive and negative regions of the molecule show where polar reactions might be more or less likely [20]. From this density mapped surfaces of the singlet oxygen adsorption in Figure. 3.5. We see distinct colour changes for the singlet oxygen near the nanotubes, indicating a higher density on the oxygen, whereas it is absent in the triplet case. This result of the singlet oxygen adsorption is very interesting and is very much different from the behavior of the triplet case. The existing theoretical prediction of triplet oxygen at a distance of about 2.7 Å near (8,0) semi-

conducting nanotubes employing LDA using DFT with binding energy of 0.25 eV [13] is slightly different from our calculations with distance of 3.31 Å is shown in Figure. 3.6.

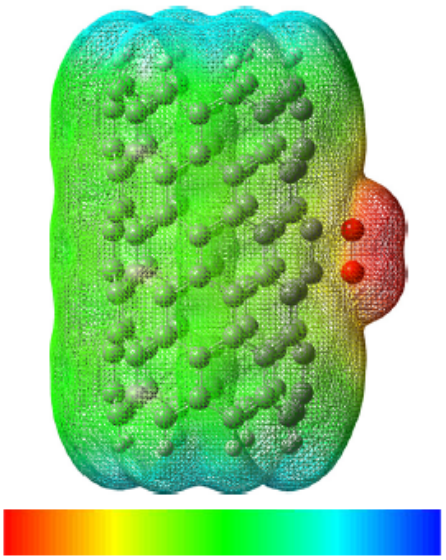

Figure. 3.5. Electrostatic potential (ESP) mapped surface of (8,0) carbon nanotube with singlet oxygen. Red to blue regions indicates the change in the electrostatic potential in the increasing order.

This difference is understandable from the prediction that the LDA overestimates the binding energy values. In our calculations for the same system, this is found to have adsorption energy of 0.04 eV and is weakly physisorbed with negligible charge transfer.

The high affinity of the singlet oxygen on the nanotube can be explained on the basis of molecular orbital theory. It is evident from the molecular orbital theory of singlet oxygen that it has a low lying LUMO compared to triplet oxygen. This makes it highly electrophilic and hence it reacts more readily with electron rich double bonds, but slowly or not at all with electron poor ones. Therefore, a charge transfer can take place effectively from the HOMO of the nanotube to the LUMO of the singlet oxygen. It is also well known in the literature [17] that singlet oxygen reacts rapidly with olefinic bonds with concerted addition reactions. Singlet oxygen is an electrophile with chemistry unique from that of ground state triplet oxygen which is nucleophilic. It is also well understood that because of the electrophilicity, the singlet oxygen acts as both an oxidizing as well as oxygenating agent in chemical and biological environments [17].

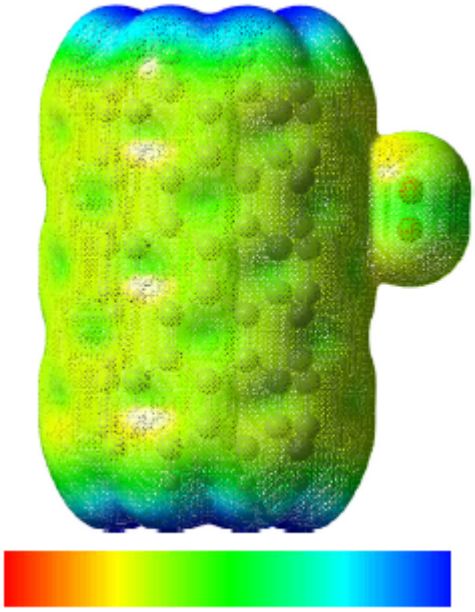

Figure. 3.6. Electrostatic potential (ESP) mapped surface of (8,0) carbon nanotube with triplet oxygen. Red to blue regions indicates the change in the electrostatic potential in increasing order.

Table 3.2. HOMO, LUMO energies and band gaps of oxygen and SWCNTs

System	HOMO (eV)	LUMO (eV)	HOMO-LUMO Gap (eV)
Singlet	-12.800	0.746	13.546
Triplet	-15.093 (alpha) -15.590(beta)	11.451(alpha) 3.028 (beta)	26.544 18.618
(5,0)	-3.815	-0.225	3.59
(8,0)	-3.286	-2.116	1.17
(5,0)-Oxygen singlet	-4.046	-0.2112	3.835
(5,0)-Oxygen triplet	-3.817(α) -3.817(β)	-0.257(α) -0.259(β)	3.56 3.558

In order to understand it quantitatively, we have calculated the highest occupied molecular orbital (HOMO) and the lowest unoccupied molecular orbital (LUMO) for few cases using Hartree–Fock theory with 6-31G (d) basis set. This level of theory, synonymous with molecular orbital theory is regarded as much more meaningful and accurate compared to the

molecular orbital calculations using DFT method. The calculated HOMO–LUMO values are given in Table 3.2.

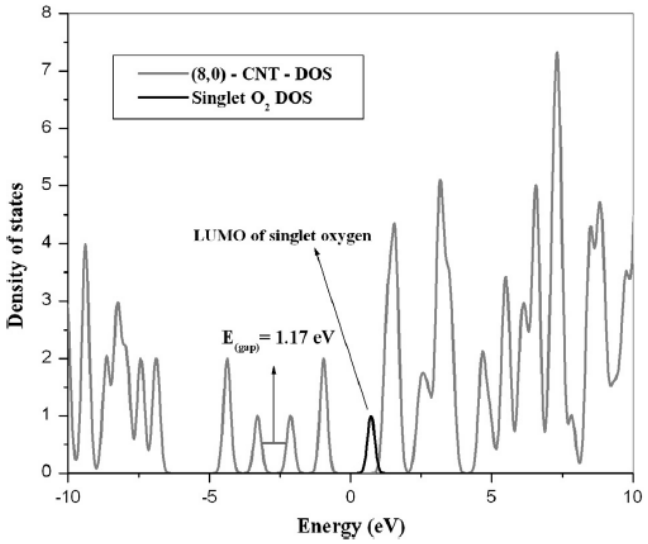

Figure 3.7. The density of states (DOS) spectrum of intrinsic (8,0) SWCNT and the DOS peak of the low lying LUMO of the singlet oxygen.

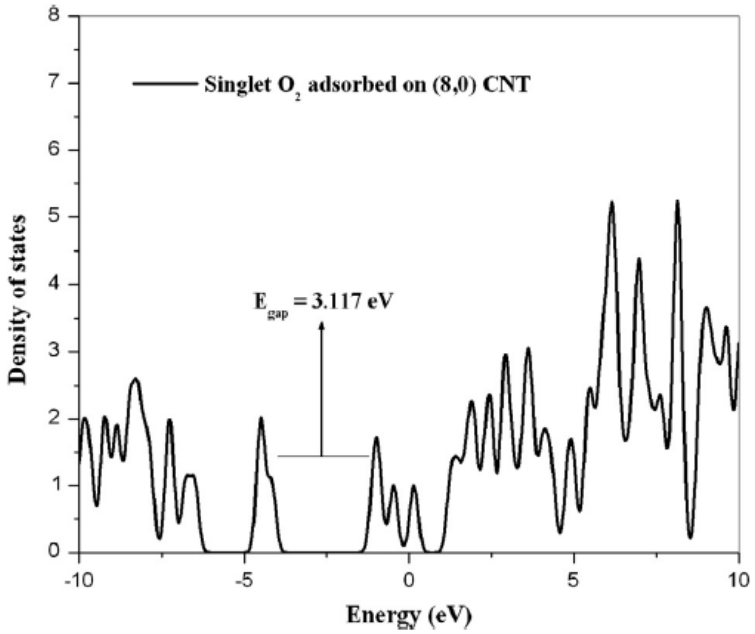

Figure 3.8. The density of states (DOS) spectrum of singlet oxygen adsorbed on intrinsic (8,0) single walled semi-conducting carbon nanotube.

The LUMO of the singlet is at 0.746 eV compared to 3.028 of β-LUMO and 11.451 of α-LUMO of the triplet oxygen. The HOMO of the different nanotubes studied are also given.

It is clear that the charge transfer can occur very effectively from the HOMO of the nanotube (8,0) (-3.286 eV) to the LUMO of singlet oxygen as the gap is much smaller compared to all other cases. The strong affinity of the singlet oxygen is visible also from the density of states (DOS) spectrum calculated using the Hartree-Fock method. The DOS spectrum for intrinsic (8,0) CNT and CNT with singlet oxygen molecule are shown in Figures. 3.7. and 3.8. respectively. We have also included the relevant part from singlet oxygen in Figure. 3.7. It is clear that electrons can be conveniently transferred to these levels. HOMO of the CNT preferably donates electron to the low lying LUMO of the singlet oxygen. As a result of this strong adsorption, there is increased band gap in Figure. 3.8.

3.4. Adsorption of oxygen on boron and nitrogen doped SWCNTs

The unique morphology of nanotubes indicates that there are a wide variety of possible approaches to dope them and thereby change their physical and electronic properties.

Table 3.3. The values of binding energy, distance from the walls and charge transfer of singlet and triplet oxygen with pure and boron doped CNTs.

System	Binding energy (eV)		Distance (Å)		Charge transfer (e)	
	Singlet	Triplet	Singlet	Triplet	Singlet	Triplet
(5,0)-SWCNT	-1.418	-0.026	1.460	3.310	-0.608	-0.002
(8,0)-SWCNT	-0.880	-0.040	1.470	3.370	-0.631	-0.004
(5,5)-SWCNT	-0.348	0.004	2.520	3.500	-0.258	-0.003
(5,0)-B-SWCNT	-2.387	-0.707	1.508	1.503	-0.489	-0.485
(8,0)-B-SWCNT	-1.622	-0.087	1.533	1.530	-0.495	-0.497
(5,5)-B-SWCNT	-1.737	-0.008	1.569	3.480	-0.464	0.004

Many of these take advantage of the molecular nature of the nanotubes; however it is also possible to dope in the more traditional semi-conductor industry sense, *i.e.,* by deliberately replacing or substituting carbon atoms with impurities such as nitrogen and boron. In our studies, we have replaced a single carbon atom of the semi-conducting and also conducting nanotube with boron and nitrogen. The results of adsorption of both singlet and triplet oxygen on pristine nanotubes and doped systems are summarized in Tables 3.3. and 3.4.

Table 3.4. The values of binding energy, distance from the walls and charge transfer of singlet and triplet oxygen with pure and nitrogen doped CNTs.

System	Binding energy (eV)		Distance (Å)		Charge transfer (e)	
	Singlet	Triplet	Singlet	Triplet	Singlet	Triplet
(5,0)-SWCNT	-1.418	-0.026	1.460	3.310	-0.608	-0.002
(8,0)-SWCNT	-0.880	-0.040	1.470	3.370	-0.631	-0.004
(5,5)-SWCNT	-0.348	0.004	2.520	3.500	-0.258	-0.003
(5,0)-N-SWCNT	-1.444	-0.141	1.514	3.337	-0.334	0.0003
(8,0)-N-SWCNT	-1.654	0.323	1.546	3.434	-0.343	-0.004
(5,5)-N-SWCNT	-0.141	-0.0004	3.050	3.370	-0.073	-0.004

Doping semi-conducting SWCNT with boron atom significantly improved the affinity towards singlet oxygen with adsorption energy almost twice the value of the intrinsic nanotubes as seen from the Table 3.3. For example (8,0) boron doped nanotube tube shows a binding energy of -1.622 eV for singlet oxygen, compared to -0.88 eV for the intrinsic case. The distances from the nanotube remain at a range of 1.46 - 1.53 Å in all the cases of semi-conducting tubes. The change in the local physical properties of the CNTs when doped with either boron atoms or nitrogen atoms through replacement of carbon atoms can also induce changes of local chemical reactivity, which in turn can change the binding energy. The charge transfer from the tube to the oxygen is found to be smaller in the doped case. Though more investigations are necessary to establish the different effects, it is understandable from the point that boron is electron deficient and that there are competing effects from both boron and the singlet oxygen towards the π electron system of the nanotube. The optimized geometry of adsorption of oxygen on (8,0) doped with boron and the corresponding ESP mapped surface are given in Figure 3.9. and Figure 3.10. respectively.

One of the most exciting features of our calculation is that we find increased affinity of ground state oxygen towards semi-conducting CNTs doped with boron. These results are highlighted in Table 3.3. The very weak physical interaction of ground state oxygen on pristine nano surfaces experimentally and theoretically predicted by various methods. However upon doping with boron the oxygen molecule is found to be at a distance of 1.5 Å. The binding energy is not great enough to form bonds chemically and this can be an added advantage for use as an oxygen sensor.

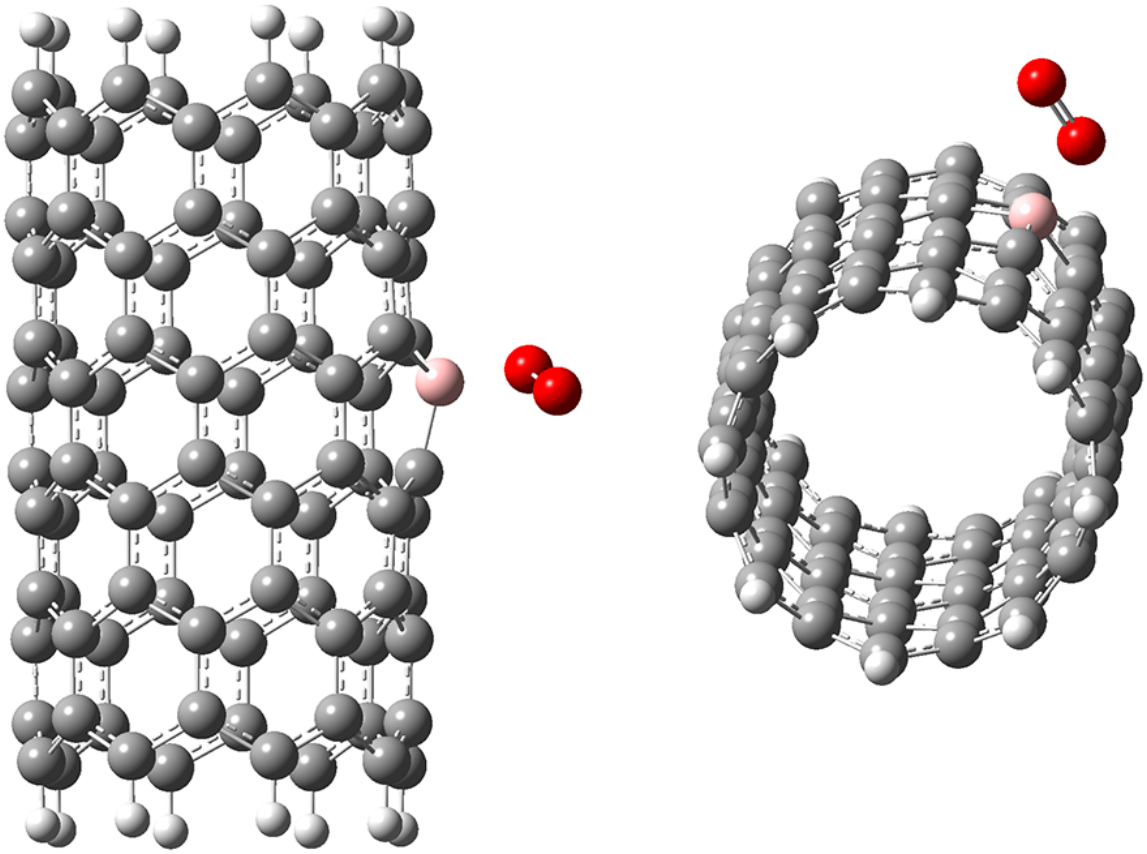

Figure 3.9. Optimized orientation of singlet oxygen with (8,0) boron doped SWCNT. Grey, white, pale pink and red colours indicate carbon, hydrogen, boron and oxygen atoms respectively. Two different orientations of optimized geometry are shown with singlet oxygen at a distance of 1.47 Å.

Nitrogen doped semi-conducting nanotubes showed a higher binding energies both for singlet and triplet oxygen, compared to the intrinsic nanotubes and the distances are of the range 1.46 - 1.54 Å. As in the case of boron doped systems, charge transfer is found to be less compared to the pristine nanotubes (Tables 3.3 and 3.4). The metallic system studied does not show any significant change upon doping.

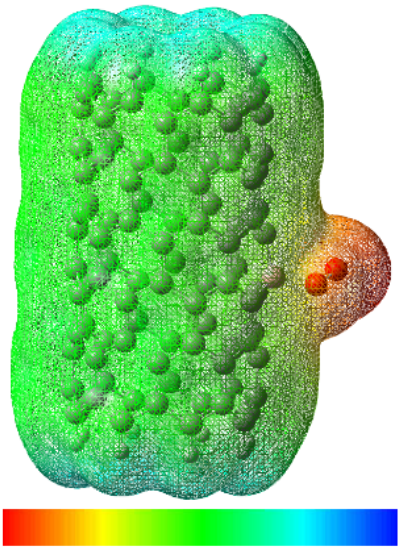

Figure 3.10. Electrostatic potential mapped surface of singlet oxygen with (8,0) boron doped SWCNT. Red to blue regions indicates the change in the electrostatic potential in the increasing order.

3.5. Conclusion

We have studied adsorption of singlet and triplet forms of oxygen molecule on both semi-conducting and conducting nanotubes. Singlet oxygen is found to be close to bonding distances of 1.47 Å near the walls of semi-conducting nanotubes. We find that there is appreciable charge transfer from the nanotube to the singlet oxygen which is also evident from the low lying LUMO of the singlet oxygen. The close proximity of the singlet near the semi-conducting tube and its dissociation to form a ring like structure is further proved by binding energy calculations. The appreciable charge transfer is also evident from the electrostatic potential energy mapped surfaces. The singlet oxygen is found to be close to the metallic nanotubes, but at distances of about 2.5 Å and the charge transfer is found to be less whereas the triplet is found at farther distances with weak interaction energies. Adsorption of oxygen on both types of nanotubes, doped with boron and nitrogen are also studied. The effect of replacing a single carbon of the semi-conducting nanotube with boron leads to almost the same distances for the singlet molecule, but with less charge transfer, as is expected. The adsorption energy is found to be more for boron doped cases compared to intrinsic and nitrogen doped SWCNTs. The most interesting effect seen with doping is the boron doped semi-conducting system where the oxygen is found to be at closer distance of

1.5 Å, with appreciable charge transfer compared to the pristine metallic tube. However the doping with nitrogen did not alter much the adsorption properties of SWCNTs.

The triplet oxygen adsorptions reported in the literature shows only weak van der Waals interactions with pristine nanotubes [10,12,13]. Our results support this and propose an idea of nanoscale sensor devices that can detect the oxygen molecule in its natural state in close proximity. The boron doped semi-conducting tubes show very good affinity towards triplet oxygen and is found to be at distances of 1.5 – 1.6 Å, whereas the existing sensing methods rely on internal doping which result in only temporary sensing capability due to weak van der Waals interaction to the doped material. Our study gives a clear understanding about how CNT can be substitutionally doped for use as a potential sensor. Since the adsorption of singlet oxygen on pristine semi-conducting and doped conducting nanotubes show interesting effects, it will be of interest to see if there are transport property changes upon adsorption.

Reference

1. J. W. Schwank, M. Dibattista. *MRS Bull.* 24, 44, 1999.
2. R. Ramamoorthy, P. K. Dutta, S. A. Akbar. *Journal of Materials Science*, 38, 4271, 2003.
3. YSI, *The Dissolved Oxygen Handbook*, YSI.com/weknowDO.
4. J. Kong, N.R. Franklin, C. Zhou, M. G. Chapline, S. Peng, K. Cho, H. Dai. *Science*, 287, 622 2000.
5. P. G. Collins, K. Bradley, M. Ishigami, A. Zettl. *Science*, 287, 1801, 2000.
6. C. K. W. Adu, G. U. Sumanasekera, B. K. Pradham, H. E. Romero, P. C. Eklund. *Chem. Phys. Lett.* 337, 31, 2001.
7. V. Derycke, R. Martel, J. Appenzeller, Ph. Avouris. *Appl. Phys. Lett.* 80, 2773, 2002.
8. M. Shim, G. P. Siddons. *Appl. Phys. Lett.* 83, 3564, 2003.
9. H. Ulbricht, G. Moos, T. Hertel. *Phys. Rev. B* 66, 075404, 2002.
10. S. H. Jhi, S. G. Louie, M.L. Cohen. *Phys. Rev. Lett.* 85, 1710, 2000.
11. D. C. Sorescu, K. D. Jordan, Ph. Avouris. *J. Phys. Chem. B.* 105, 11227, 2001.
12. J. Zhao, A. Buldum, J. Han, J. P. Lu. *Nanotechnology.* 13, 195, 2002.
13. P. Giannozzi, R. Car, G.J. Scoles, *Chem. Phys.* 118, 1003, 2003.
14. M. Grujicic, G. Cao, R. Singh, *Appl. Surface Science*, 211, 166, 2003.
15. S. Dag, O. Gülseren, T. Yildirim, S. Ciraci, *Phys. Rev. B,* 67, 165424, 2003.

16. F. J. Owens. *Nanoscale Res Lett.* 2, 447, 2007.
17. K. Kinoshita, T. Saito, I. Akira, K. Takashi, K. Yasutaka, Y. Shusuke, Y. Kizashi, O. Mitsutaka, *Polyhedron,* 30, 3249, 2011.
18. A. Tchernatinsky, S. Desai, G. U. Sumanasekera, C. S. Jayanthi, S. Y. Wu. *J. Appl. Phys.* 99 034306, 2006.
19. G. U. Sumansekera, C. K. W. Adu, S. Fang, P. C. Eklund, *Phys. Rev. Lett*. 85, 1096, 2000.
20. J. S. Murray, K. Sen, *Molecular Electrostatic Potential; Concepts and Application, Theoretical and Computational Chemistry*, vol. 3, Elsevier Science, Amsterdam, 1996.

CHAPTER 4

Adsorption of Environmentally Relevant Molecules with SWCNTs

4.1. Introduction

Gas adsorption on carbon nanotubes is an important issue of fundamental research as it is associated with many applications [1-3]. The study of adsorption of various gaseous molecules on CNTs are of importance because of its vast applications based on electronic and transport properties changes as a result of adsorption[1,2]. SWCNT based sensors have gained significant interest especially due to the modification of their electrical properties with adsorption of simple chemical species on the surface of SWCNTs due to their high surface to volume ratio can act as good sensors and also as gas storage material. For example hydrogen storage is an important area of research, since hydrogen is considered as future energy source and SWCNTs finds application in fuel cells as a storage material. U.S. Department of Energy (DOE) suggested that such an adsorbent should store 6.5 wt% of Hydrogen or 62.5 kg/m^3 for actual automotive fuel cells application [4]. Large hydrogen uptakes by light weight nanostructure carbon materials such as single walled carbon nanotubes have attracted considerable experimental and theoretical attention [1,5-7].

Many researchers have worked on the gas adsorption on SWCNTs especially with gases like Xe, CF_4, H_2, CH_4 etc [1,2,5-12]. Zhao *et al.*, [13] studied the adsorption of various gas molecules NO_2, O_2, NH_3, N_2, CO_2, CH_4, H_2O, H_2, Ar on both semi-conducting and conducting SWCNTs and SWCNT bundles employing LDA. Their studies revealed that remaining gases other than oxygen and nitrogen dioxide exhibited a weak physisorption with binding energies less than 0.2 eV and with negligible charge transfer (0.01 - 0.035e) [13]. Lithaxoos *et al.,* [14] investigated both experimentally and theoretically the adsorption of N_2, CH_4, CO and CO_2 with SWCNTs at room temperature and pressure in the range of 0.01-2.0 MPa. Adsorption of various gases is found to be in the order: $H_2 << N_2 \approx CH_4 < CO << CO_2$, in these studies [14]. The adsorption of gases at room temperature is found to be negligible with CO_2 adsorbing at around 2 wt% at normal pressure and the percentage of adsorption increasing with the increase in pressure reaching up to 12 wt% at a pressure of 13 bar [14]. Very recently Gowrishankar *et al.*, [15] investigated adsorption of various gas molecules like H_2, H_2O, O_2, CO, CO_2, NO, NO_2, NH_3, and CH_3OH along the side walls of intrinsic, boron and silicon doped (10,0) zig-zag SWCNTs employing Local density approximations. Their studies conclude that boron doped SWCNTs exhibit higher binding energies with oxygen up

to -8.64 eV. But it is not clear whether SWCNTs would exhibit such high binding energies, since it is well known fact that LDA overestimates binding energies. Most of the current literature studies are done employing LDA which make the predictions by these studies and the findings inaccurate [13-15]. Barberio *et al.*, [16] carried out an experimental study in order to understand the adsorption properties of intrinsic and silver doped MWCNTs with N_2, H_2, O_2, CH_4, C_2H_4, and C_2H_6 at very low temperatures of 35 K and they observed that silver doped MWCNTs exhibiting better adsorption capacity compared to intrinsic CNTs. Studies by various groups [17-21] concluded that intrinsic CNTs are not suitable for sensor applications and defects insertion, structural deformation, or doping methodologies are to be employed to improve the binding of low adsorption gaseous species [17]. It has been predicted by Peng and Cho [18] that boron or nitrogen doped SWCNTs exhibit good adsorption with H_2O and CO molecules, while transition metal doped SWCNTs are required to detect gases like N_2, O_2, H_2O, CO, NO, NH_3, NO_2, CO_2, and H_2S. But the major drawback of transition metal doped CNTs is that the transport properties are least affected by the adsorption of gas molecules and although they exhibit good binding properties [19-21]. In this chapter we discuss about the adsorption of different gases like H_2, N_2, CO and also gaseous H_2O with both intrinsic and boron doped zig-zag and arm-chair SWCNTs of various diameters in the DFT framework using hybrid functional employing Gaussian basis sets.

4.2. Results and Discussion

We have employed hybrid functional B3LYP with Split valence polarized Pople Basis set 6-31G (d) in the DFT framework. Semi-conducting (5,0) SWCNTs in both intrinsic and boron doped forms are considered for the study. In few cases we have also studied conducting (5,5) arm-chair SWCNTs and semi-conducting (8,0) SWCNTs. Binding energies, tube-molecule distance and charge transfer (Mulliken population analysis) of gases H_2, N_2, CO and H_2O with intrinsic (5,0) SWCNTs are calculated and shown in Table 4.1. Semi-conducting SWCNTs show a trend of weak physisorption with various gas molecules in their ground states and there is a negligible or weak charge transfer from SWCNT to the molecule. Compared to the neutral diatomic molecules polar molecules like water are shown to exhibit slightly more binding energies and charge transfers with semi-conducting SWCNTs though the values are still in the physisorption range. The higher binding energy of water compared to that of other molecules can be explained by the fact that water is a polar molecule with electro negative atoms like oxygen atoms. However in all the cases, binding was found to be weak and the charge transfer is found to be negligible.

Table 4.1. Binding energy, tube-molecule distance and charge transfer of (5,0) SWCNTs with H_2, N_2, CO and H_2O.

Gases	Binding energy(eV)	Distance (Å)	Charge transfer (e)
H_2	-0.014	3.17	-0.009
N_2	-0.011	3.54	-0.002
CO	-0.027	3.34	-0.008
H_2O	-0.146	2.55	-0.016

In order to understand it further, we have carried out similar calculations with (8,0) SWCNTs with water molecule. The same trend is repeated with weak physisorption and negligible binding energy and distances are reproduced. A binding energy of 0.081 eV, with tube-molecule distance 2.89 Å and charge transfer of -0.004e is observed with negative sign indicating charge transfer from tube to the molecule. The optimized geometry of water with intrinsic (8,0) SWCNTs is shown in Figure 4.1. From the optimized orientation, we observe that hydrogen atoms of water are oriented along the tube direction; this could be due to weak Van der Waals force of attraction between aromatic sp^2 carbons which are electronegative and electropositive hydrogens of water molecule.

Similar investigations have been carried out with arm-chair (5,5) SWCNTs are tabulated in Table 4.2. From the table we observe that intrinsic conducting SWCNTs do not show any significant effect with most of the species studied. There is a negligible charge transfer between the CNT and the gas molecules. Hydrogen is found be very weakly physisorbed with a binding energy of -0.030 eV and bonding distance of 3.19 Å and almost a negligible charge transfer of -0.007 e. Nitrogen and carbon monoxide are also found to be weakly physisorbed with binding energies -0.032, -0.023 eV respectively. H_2O molecule show a binding energy of -0.111 eV with tube-molecule distance of 2.80 Å and charge transfer of 0.024 e from the tube to the water. From Tables 4.1. and 4.2. we observe that semi-conducting and conducting SWCNTs showing a similar pattern of adsorption with various gases. All the gas molecules studied show weak physisorption with binding energies in the range -0.01 to -0.146 eV accompanied by negligible charge transfer.

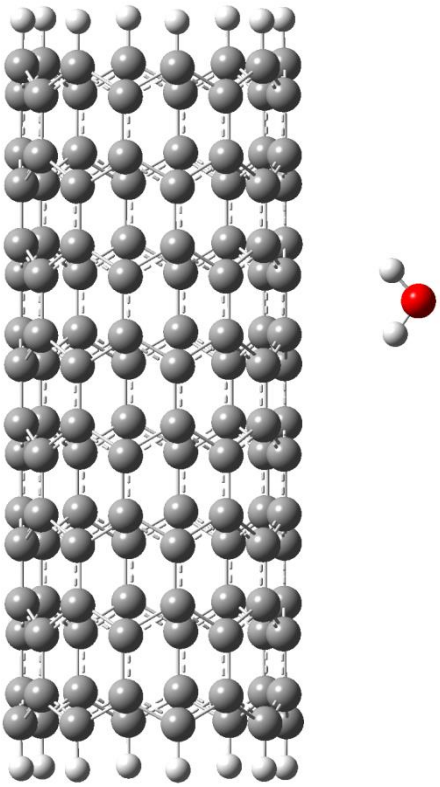

Figure 4.1. Geometry optimized structure of water near (8,0) SWCNT. Carbon, hydrogen, oxygen are represented by grey, white and red colours respectively.

Table 4.2. Binding energy, tube-molecule distance and charge transfer of (5,5) SWCNTs with H_2, N_2, CO and H_2O.

Gases	Binding energy (eV)	Distance (Å)	Charge transfer (e)
H_2	-0.030	3.19	-0.007
N_2	-0.032	3.65	-0.002
CO	-0.023	3.63	0.000
H_2O	-0.111	2.80	-0.024

4.3. Adsorption on Substitutionally Boron Doped SWCNTS

Substitutionally doping SWCNTS with boron shows an enormous impact on adsorption properties of various gaseous species with an increase in affinity of gas molecules towards the side walls. Similar studies have been carried out with boron doped SWCNTs. Gaseous

species like hydrogen, nitrogen and carbon monoxide are found to be passive even with the boron doped systems with weak binding energies and low charge transfers. The results of boron doped semi-conducting (5,0) and conducting (5,5) SWCNTs are summarized in Tables 4.3. and 4.4. respectively. Among the various gas molecules investigated, water is found to show better adsorption properties in comparison with other gas molecules which are evident from Tables 4.3. and 4.4.

Table 4.3. Binding energy, tube-molecule distance and charge transfer of (5,0) boron doped SWCNTs with H_2, N_2, CO and H_2O.

Gases	Binding energy (eV)	Distance (Å)	Charge transfer (e)
H_2	-0.018	3.09	-0.010
N_2	-0.017	3.48	0.001
CO	-0.036	3.36	0.004
H_2O	-0.239	1.85	0.160

Water exhibits a binding energy of -0.239, -0.244 eV with semi-conducting and conducting SWCNTs respectively. The charge transfer is found to be observed from the water molecule to the SWCNT. In the case of semi-conducting SWCNTs the charge transfer is found to be 0.160 e whereas in the case of conducting SWCNTs it is found to be negligible.

Table 4.4. Binding energy, tube-molecule distance and charge transfer of (5,5) boron doped SWCNTs with H_2, and H_2O.

Gases	Binding energy (eV)	Distance (Å)	Charge transfer (e)
H_2	-0.008	3.228	-0.006
H_2O	-0.244	2.539	0.017

Among the various gas molecule adsorption studied water exhibited a very good binding with boron doped SWCNTs. So we have investigated the adsorption of water with larger diameter SWCNT (8,0) with both intrinsic and boron doped forms. Binding energy, tube-molecule distance and charge transfer of intrinsic and boron doped (8,0) SWCNTs with water are shown in the Table 4.5. Since water is exhibiting very good adsorbing behavior it is of interest to see how the electronic density of this system behaves with adsorption.

Electrostatic potential mapped surfaces (ESPs) are plotted for (8,0) boron doped SWCNTs with water shown in Figure 4.2.

Table 4.5. Binding energy, tube-molecule distance and charge transfer of (8,0) intrinsic and boron doped SWCNTs with H_2O.

System	Binding energy (eV)	Distance (Å)	Charge transfer (e)
(8,0) SWCNT	0.081	2.89	-0.004
(8,0)-B-SWCNT	-0.542	1.72	0.258

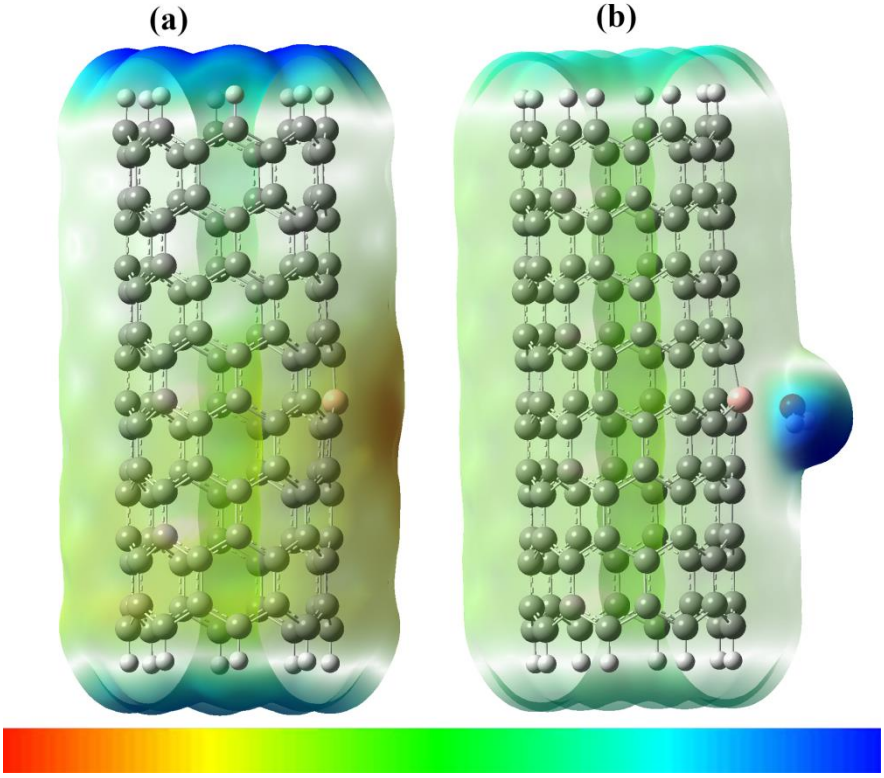

Figure 4.2. Electrostatic potential mapped surface of (8,0) boron doped SWCNT without (a) and with (b) water. Green region indicates more electron density region, blue region indicates less electron density region. Increasing potential from red to blue (colour code is shown at the bottom) Carbons, hydrogens, boron and oxygen are shown in grey, white, pale pink and blue colours respectively.

(8,0) boron doped SWCNT exhibits a binding energy of -0.542 eV with a charge transfer of 0.258 e from the water molecule to the boron doped nanotube at a distance of 1.72 Å. Since electron transfer from oxygen has already taken place, the Figure 4.2 does not show any

regions where electron density is high. As water exhibited better binding energies with appreciable charge transfers compared to other gases, we have plotted Density of states (DOS) graphs with intrinsic and boron doped (8,0) SWCNTs to probe whether CNTs are capable of sensing the moisture. From the Figures 4.3. and 4.4. we understand that DOS plots of intrinsic (8,0) SWCNTs is unaltered by the adsorption of water with band gap (HOMO-LUMO gap) remaining the same. On the other hand for boron doped (8,0) SWCNT the band gap is found to increase with adsorption of water. These preliminary investigations reveal that boron doped SWCNTs are sensitive to the presence of moisture. From the Table 4.6. we observe that intrinsic (8,0) SWCNT exhibits a band gap of 0.97 eV, upon doping with boron we observe the band gap of 0.69 eV. Intrinsic SWCNTs are insensitive to water adsorption with band gap almost remaining unaltered. On the other hand, boron doped SWCNT exhibits an increase in band gap as the charge is transferred from the water molecule to the SWCNT. From these results we can conclude that boron doped SWCNTs are sensitive to adsorption of moisture.

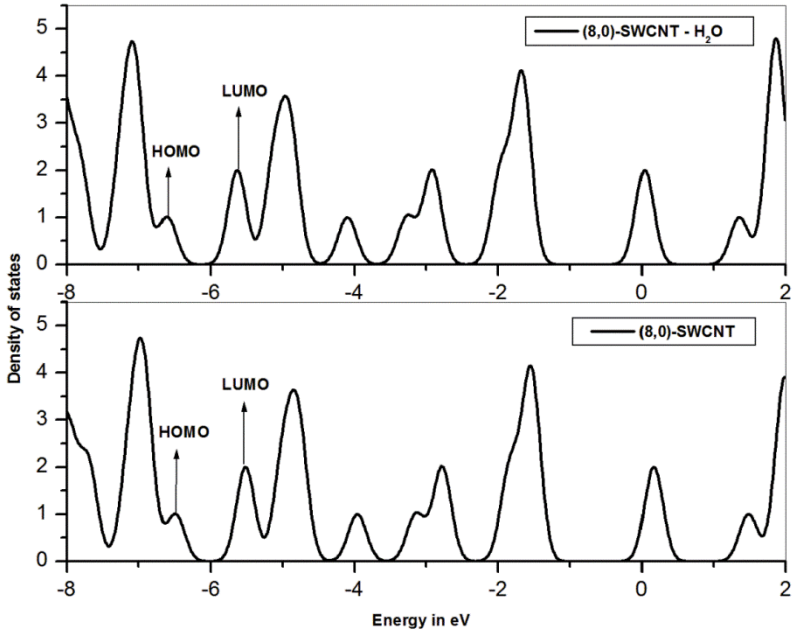

Figure 4.3. Density of states (DOS) of (8,0) intrinsic SWCNT with and without water.

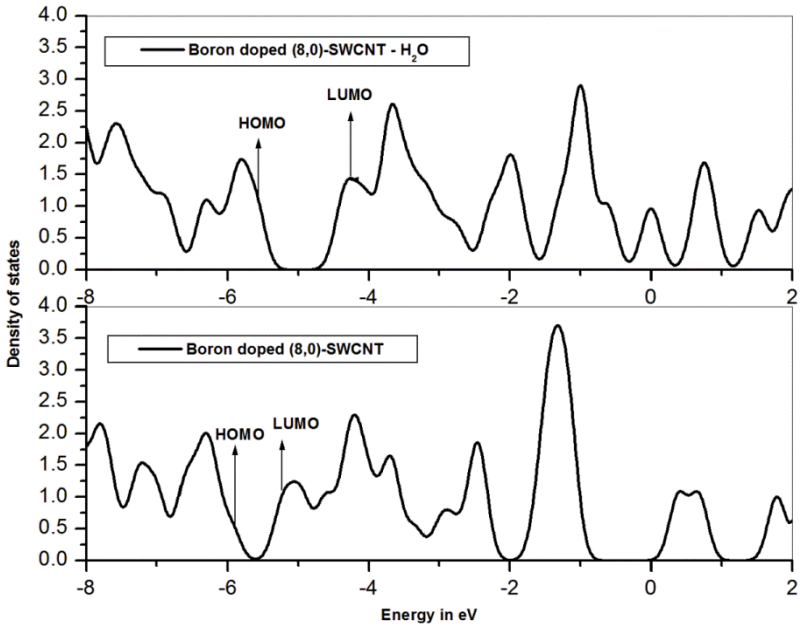

Figure 4.4. Density of states (DOS) of (8,0) boron doped SWCNT with and without water.

Table 4.6. HOMO, LUMO energies and band gaps of (8,0) intrinsic and boron doped SWCNTs with and without water.

System	HOMO (eV)	LUMO(eV)	Band gap(eV)
(8,0)-SWCNT	-6.49	-5.52	0.97
(8,0)-B-SWCNT	-5.95	-5.26	0.69
(8,0)-SWCNT-H_2O	-6.61	-5.63	0.98
(8,0)-B-SWCNT-H_2O	-5.60	-4.13	1.47

4.4. Conclusion

We have investigated the adsorption of Hydrogen, Nitrogen, Carbon monoxide and Water molecules with semi-conducting and conducting SWCNTs. Intrinsic SWCNTs both zig-zag (5,0) and arm-chair (5,5) forms did not exhibit any significant binding with these molecules. Among the adsorption of various gases studied water exhibited a binding energy of -0.146 eV with semi-conducting (5,0) SWCNT and -0.111 eV with conducting (5,5) SWCNT. Increasing the tube diameter did not affect the adsorption pattern with (8,0) SWCNT exhibiting a binding energy of 0.08 eV. In the case of boron doped systems, water exhibited a binding energy of -0.239, -0.244, -0.542 eV with (5,0), (5,5) and (8,0) SWCNTs

respectively. The charge transfer is found to be from the water molecule to the electron deficient boron doped CNT. From the density of states plots of (8,0) intrinsic and boron doped SWCNTs, we observe that the band gaps remain unaltered in the case of intrinsic SWCNTs whereas an increase in band gap is observed with doped system. This can be understood from the fact that there is negligible charge transfer between intrinsic (8,0) SWCNT and water whereas 0.258 e charge transfer is observed in the case of (8,0)-B-SWCNT. All the other gaseous molecules studied are found to be passive with respect to binding on both intrinsic and boron doped SWCNTs.

Reference

1. P. G. Collins, K. Bradley, K. Ishigami, M. Zettl. *Science*, 287, 1801, 2000.
2. C. Cantalini, L. Valentini, L. Lozzi, I. Armentano, J. M. Kenny, S. Santucci, *Sensors and Actuators B* 93, 333, 2003.
3. M. Barberio, P. Barone, F. Stranges, R. A. Romano, F. Xu, A. Bonanno. *Journal of Chemistry*, 2014, 816193, 2014.
4. J. M. Marulanda, *Carbon Nanotubes*, InTech, 2010.
5. J. Kong, N. R. Franklin, C. Zhou, M. G. Chapline, S. Peng, K. Cho, H. Dai, *Science*, 287, 622, 2000.
6. Q. Y. Wang, J. K. Johnson, *J. Chem. Phys.* 110, 577, 1999.
7. X. P. Tang, A. Kleinhammes, H. Shimoda, L. Fleming , K. Y. Bennoune, S. Sinha, C. Bower, O. Zhou, Y. Wu. *Science*, 288, 49, 2000.
8. A. Kuznetsova, J. T. Yates, J. Liu, R. E. Smalley, *J. Chem. Phys*. 112, 9590, 2000.
9. O. Byl, P. Kondratyuk, S. T. Forth, S. A. Fitzgerald, L. Chen, J. K. Johnson, J. T. Yates, *J. Am. Chem. Soc.* 125, 5889, 2003.
10. A. C. Dillon, M. J. Heben, *Appl. Phys. A.* 72, 133, 2001.
11. G. E. Froudakis. *J. Phys. Condens. Matter*, 14, 453, 2002.
12. Lubezky, L. Chechelnitsky, M. Folman. *J. Chem. Soc. Faraday Trans.* 92, 2269, 1996.
13. J. Zhao, A. Buldum, J. Han, J. P. Lu, *Nanotech*, 13, 195, 2002.
14. G. P. Lithoxoos, A. Labropoulos, L. D. Peristeras, N. Kanellopoulos, J. Samios, I. G. Economoua, *J. of Supercritical Fluids*, 55, 510, 2010.
15. P. A. Gowrishankar, K. Udhayakumar. *Journal of Nanomaterials*, 2013, 293936, 2013.
16. M. Barberio, P. Barone, F. Stranges, R. A. Romano, F. Xu, A. Bonanno, *Journal of Chemistry*, 2014, 816193, 2014.

17. L. B. Da Silva, S. B. Fagan, R. Mota. *Nano Lett.* 4, 65, 2004.
18. S. Peng, K. Cho. *Nano Lett.* 3, 513, 2003.
19. C. S. Yeung, L. V. Liu, Y. A. Wang. *Jour. Phys. Chem. C.* 112, 7401, 2008.
20. J. M. Garcìa-Lastra, D. J. Mowbray, K. S. Thygesen, A. Rubio, K. W. Jacobsen. *Phys. Rev. B.* 81, 245429, 2010.
21. G. Zollo, F. Gala. *Journal of Nanomaterials*, 2012, 152489, 2012.

CHAPTER 5

Adsorption of Ammonia on Semi-conducting Pristine and Boron Doped SWCNTs

5.1. Introduction

Ammonia is a natural gas present in trace quantities in the atmosphere being produced from the decay of nitrogenous organic waste. Currently most of the ammonia enters into the atmosphere either directly or indirectly by various human activities. The worldwide emission of ammonia per year was estimated in 1980 by the European community commission for environment and quality of life to be 20–30 Tg (1Tg = 1 million ton) [1]. Other investigations, summarized by Warneck [2], observed the values between 22 and 83 Tg. There are mainly three sources of ammonia described in the literature [2], the first pathway is atmospheric deposition of ammonia by the direct deposition of ammonium and nitrate salts which occur by the addition of particulates to the soil in the form of dissolved dust or particulates in rain water. This process is further enhanced by the agricultural sector in the form of fertilizer. The second way of nitrification is by bacterial nitrogen fixation and the third source is the combustion from both chemical plants and motor vehicles. It is also produced by the chemical industry for the production of fertilizers. The total emission of ammonia from combustion is about 2.1–8.1 Tg per year [2].

There are many ways to detect the presence of ammonia. High concentration of ammonia is easy to detect since the gas has a pungent odor. But to quantify the ammonia concentration at lower concentrations of ammonia is beyond the human perception. However, in many occasions, the ammonia concentration has to be known, even at ultra-low concentrations of less than parts per billion in air (ppb) [3]. There are mainly four areas where ammonia sensors find their applications namely, environmental analysis, automobile industry, chemical industry and also in medical science. Ammonia sensors are required in diverse areas with specified requirements, for example, sensors used in monitoring the environment need not require very fast sensing systems but in chemical industry, sensors with very fast sensitivity are required. Sensors in medical applications require the sensors to detect the concentration of ammonia in ppb, with fast sensitivity at ambient temperatures and require it to be selective.

5.2. Results and Discussion

In this chapter, we discuss the study of ammonia adsorption with semi-conducting SWCNTs of various diameters both in intrinsic and boron doped nanotubes. The Density functional calculation with hybrid functional B3LYP are performed using 6-31G (d) basis set. Nanotubes of various diameters (5,0), (7,0) and (8,0) are considered with eight layers having 80, 112 and 128 carbon atoms respectively (zig-zag SWCNTs). These nanotubes have length 15.7 Å along the tube axis and diameter 4.1, 5.6 and 6.4 Å respectively with an average C-C bond length of 1.43 Å. In the doped cases, one of the carbon atoms is replaced with boron atom and adjacent bonds of the hetero atom are made single. The dangling bonds at the ends of the tube in both cases are saturated with hydrogen in order to satisfy valence criteria. While considering other electronic properties with the help of continuous bands, we have considered infinite systems employing periodic boundary conditions.

To investigate the changes in electronic charge, we have calculated the net charge-transfer between ammonia molecule and the intrinsic and boron doped SWCNT by using Natural Population Analysis (NPA) [4] in addition to the widely used, oldest procedure of Mulliken Population Analysis [5] which makes use of the density matrix. Although widely used, it has long been recognized that the Mulliken procedure has a strong dependence on the basis set [4]. NPA procedure eliminates most of the problems associated with the Mulliken Analysis and provides a marked improvement over the same [4]. Natural Bond Orbital (NBO) Analysis [6] is also performed on the optimized orientations in order to understand the favorability of charge transfer between SWCNT and ammonia as the stabilization energies will provide more insights into the charge transfer studies.

In order to investigate the effects of an infinite system and to consider continuous bands in place of discrete molecular orbital model, we have also made use of periodic boundary condition (PBC) model [7]. The DFT-B3LYP method with 6-31G (d) basis set and the PBC function are used to generate the crystal orbitals and the band structures. For the DFT-PBC, (8,0) SWCNT is chosen for the study and we have used 3 layers with 48 carbon atoms for the unit cell and extended it along the tubular axis to infinite length. The PBC model in the Gaussian 09 package transform the Gaussian type orbitals into crystalline orbitals, using Bloch functions modulated by a phase factor e^{ikl} where k is the reciprocal lattice vector which classifies the periodic orbitals by their irreducible representations of the

infinite translation group. The direct band gaps are measured as difference of the maximum of valence band and minimum of conduction band for same k vector value.

We have investigated the interaction of a single ammonia molecule on intrinsic semi-conducting and substitutionally doped SWCNTs employing the Density functional theory. The binding energies, equilibrium tube-molecule distances, charge transfer and the band gaps are calculated to study SWCNT-NH_3 interaction. The calculations are performed for three different intrinsic and substitutionally doped (5,0), (7,0) and (8,0) semi-conducting SWCNTs. The calculated binding energy, optimized distances and charge transfer employing both NPA and Mulliken analysis are summarized in Table 5.1.

Table 5.1. Calculated binding energies (eV), equilibrium tube-molecule distance (Å) and charge transfer (e) of ammonia near the walls of the intrinsic and boron doped SWCNTs.

System type	**Binding energy (eV)**	**Distance (Å)**	**Charge Transfer (e)**	
			NPA	**Mulliken**
(5,0)-SWCNT	-0.105	2.920	0.034	-0.009
(5,0)-B-SWCNT	-1.085	1.649	0.195	0.241
(7,0)-SWCNT	-0.095	3.000	0.006	0.009
(7,0)-B-SWCNT	-0.645	1.681	0.195	0.238
(8,0)-SWCNT	0.097	3.030	0.001	-0.008
(8,0)-B-SWCNT	-0.584	1.694	0.197	0.232

The binding energy is found to be low and the charge transfer negligible for adsorption of ammonia on intrinsic SWCNTs, with equilibrium tube-ammonia distances of 3 Å or more. The calculated binding energy values are -0.105, -0.095, 0.097 eV and corresponding interaction distances are 2.92, 3.0, 3.03 Å respectively. The large distances and the small binding energy values suggest that ammonia undergoes physical adsorption on intrinsic SWCNTs due to weak van der Waals interaction. The charge transfer is found to be small indicating that there is negligible interaction between intrinsic SWCNT and ammonia. This weak binding does not result in any significant structural distortion in the nanotube and the N-H bond length remain 1.019 Å which is the same as in bare ammonia. The representative optimized configuration for the physisorption of ammonia on the (8,0) SWCNT at a distance of 3.03 Å is shown in Figure 5.1.

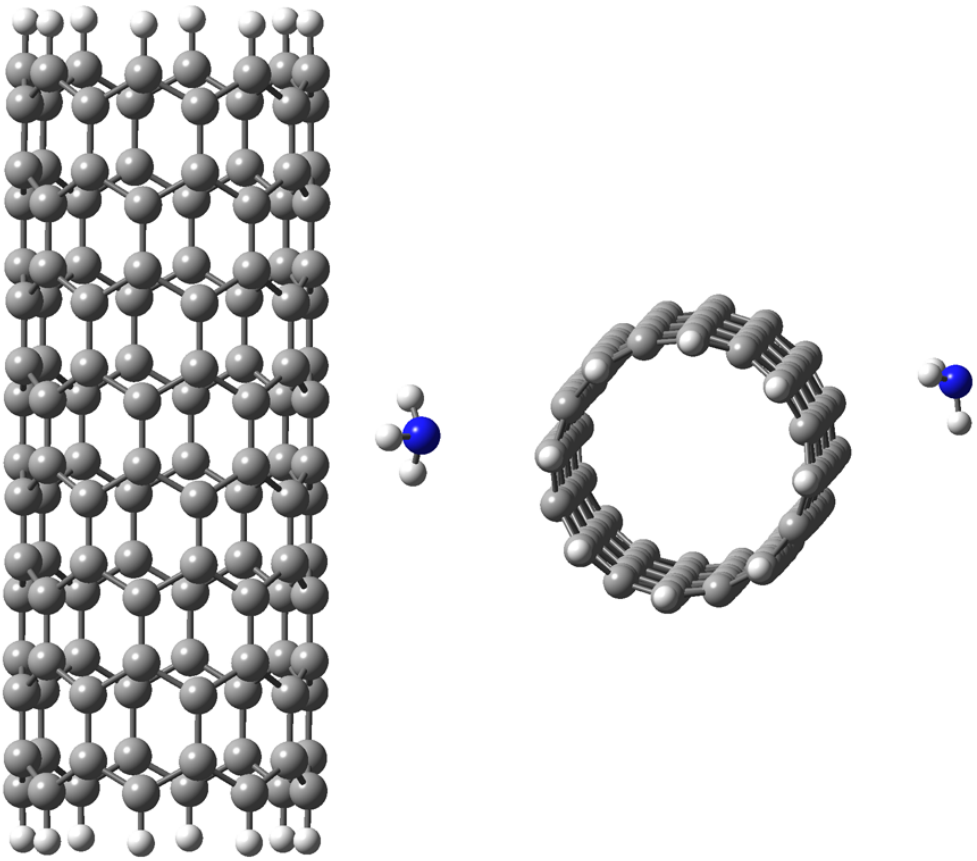

Figure 5.1. Geometry optimized structure of ammonia near pristine (8,0) SWCNT at 3.03 Å (Two different orientations are shown). Carbon, hydrogen and nitrogen are represented by grey, white and blue colours respectively.

Our theoretical calculations support the experimental findings [8] that ammonia is only weakly physisorbed on semi-conducting SWCNTs with negligible charge transfer. In all the cases studied, the charge transfer is found to occur from ammonia to the SWCNT and is varying from 0.001 - 0.034 e which is close to the previous theoretical and experimental investigations with values of 0.04 e [8,9]. Adsorption of ammonia with intrinsic SWCNTs is very weak indicating physisorption, confirming that pristine SWCNTs are insensitive to ammonia molecule. On the other hand, for the doped systems with one carbon atom of SWCNT substituted by a boron atom, appreciable changes are observed. For all the substitutionally doped SWCNTs studied, appreciable binding energies and charge transfers are found and these results are given in Table 5.1. The distance of the ammonia molecule measured with respect to the boron in the SWCNT and nitrogen of ammonia is found to be about 1.6 Å on an average. The binding energies and the distances for the substitutionally

boron doped (5,0), (7,0) and (8,0) SWCNTs are -1.085, -0.645 and -0.584 eV respectively. It is found that the binding energy values decreases as the diameter of the CNT increases. The optimized geometry for the ammonia near boron doped SWCNT is shown in Figure 5.2. The optimized orientations of ammonia near both SWCNTs are also interesting. While in intrinsic nanotube nitrogen is away from the walls, in the doped geometry optimized structure, the configuration is changed with nitrogen being closer to the boron atom. We also see that there is a noticeable change in the carbon-boron distance after binding with ammonia for the carbon atoms directly bonded with boron. Without adsorption on the (8,0) tube, this distance is 1.518 Å whereas with ammonia binding it is increased to 1.585 Å.

The ammonia, N-H distances are also changed slightly as the molecule is at a distance of 1.6 Å from the tube walls. These distortions are shown in Figure 5.3. and the values are summarized in Table 5.2. We find that the boron-carbon distance without ammonia adsorption is about 1.51 Å, which is close to typical boron-sp^2 hybrid carbon distance in boron-doped graphenes [10]. Upon chemisorption with ammonia, boron-carbon distance is increased to 1.58 Å and the N-H bond length shows slight increase to 1.022 Å. This local deformation as is envisaged by increased boron-carbon is the consequence of the appreciable binding with ammonia. The doping with the boron atom clearly changes the electronic transport properties of the SWCNT as is clear from the higher charge transfer of about 0.195e for all the doped systems from nitrogen to boron. These facts supporting Figure 5.2. indicates that the interaction between NH_3 and boron-doped SWCNT falls under chemisorption in contrast to its physisorption on intrinsic SWCNT.

Doping the SWCNTs system with boron enhanced the adsorption of ammonia along the side walls, which can be well understood by the fact that boron in its +3 oxidation state is electron deficient, readily accepts electrons and act as a very good Lewis acid. On the other hand, ammonia is a Lewis base capable of donating a pair of electrons from lone pair of nitrogen atom thus strongly interacting with each other as calculated by NPA. The charge on nitrogen atom in ammonia when adsorbed along the side walls of intrinsic SWCNT is -1.111 e (in the case of (8,0)-NH_3), while on doping the same system with boron, the charge of nitrogen in ammonia molecule is found to be -0.463 e.

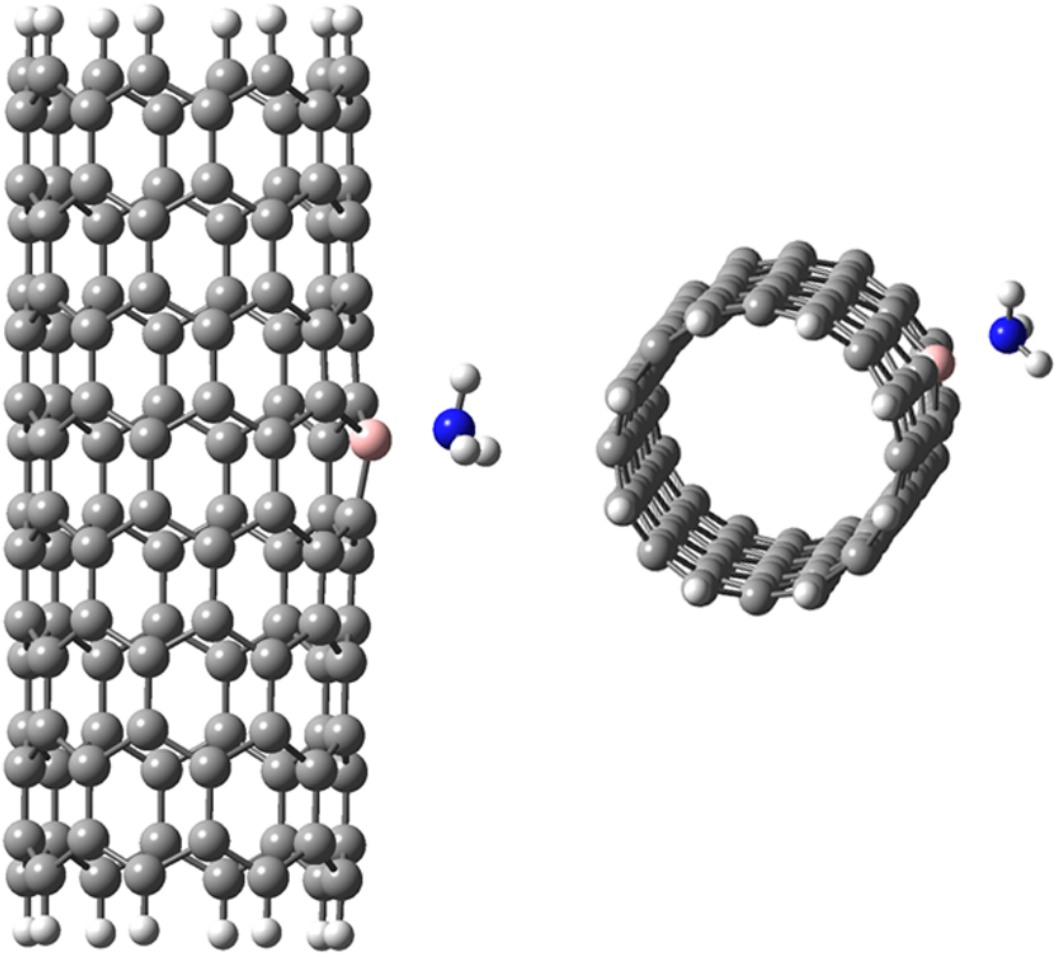

Figure. 5.2. Geometry optimized structure of ammonia near boron doped (8,0) SWCNT (Two different views are shown) at a distance of 1.69 Å. Carbon, hydrogen boron and nitrogen are represented by grey, white, pale pink and blue colours respectively.

This significant decrease in charge of nitrogen is a clear indication that doping has enhanced the affinity of ammonia towards SWCNT with appreciable charge transfer thus enhancing the binding energy. The optimized geometry with ammonia closer to the boron atom clearly facilitates this charge transfer. These results are tabulated in Table 5.1, which shows a marked difference in binding upon doping compared to that of the intrinsic systems. In order to confirm the minimum energy optimized structure and to understand the kind of adsorption, the binding energies are calculated for the nearest tube-molecule distances and are plotted in Figures 5.4, 5.5. and 5.6.

Table 5. 2. Local deformation on the walls with and without binding with ammonia, in terms of C-C and C-B bond distance and N-H distance in ammonia. The B-C bond distances mentioned in this table are for carbons directly attached to the boron.

System	**N-H bond distance (Å)**	**C-C bond distance (Å)**	**B-C bond distance (Å)**
NH_3	1.019	-	-
(5,0)-SWCNT	-	1.43	-
(7,0)-SWCNT	-	1.43	-
(8,0)-SWCNT	-	1.43	-
(5,0)-SWCNT – NH_3	1.019	1.43	-
(7,0)-SWCNT – NH_3	1.019	1.43	-
(8,0)-SWCNT – NH_3	1.019	1.43	-
(5,0)-B-SWCNT	-	-	1.537
(7,0)-B-SWCNT	-	-	1.518
(8,0)-B-SWCNT	-	-	1.518
(5,0) B-SWCNT – NH_3	1.023	-	1.606
(7,0) B-SWCNT – NH_3	1.023	-	1.589
(8,0) B-SWCNT – NH_3	1.022	-	1.585

Figure 5.4. depicts binding energy as a function of distance between the nanotube and ammonia, for three different intrinsic nanotubes. The binding energy curves shows decrease with distance and reaches to small negative values finally forming a plateau. As is evident, the curves are typical for physisorption near surface which confirms that pure ammonia is only weakly adsorbed on pristine SWCNTs by van der Waals interactions. This physisorption lead to only negligible charge transfer with no bond modification. This finding is also in accordance with the previous theoretical and experimental investigations [11,12].

Figure 5.5. explains binding energy curve of doped semi-conducting SWCNTs with respect to the tube molecule, boron-nitrogen distance. It is found that for all doped nanotubes that we have studied the binding energy curves give well defined minima at around distances of 1.6 Å. The curve with the doped case shows a remarkable minimum compared to the physisorbed case where there is not a proper minima.

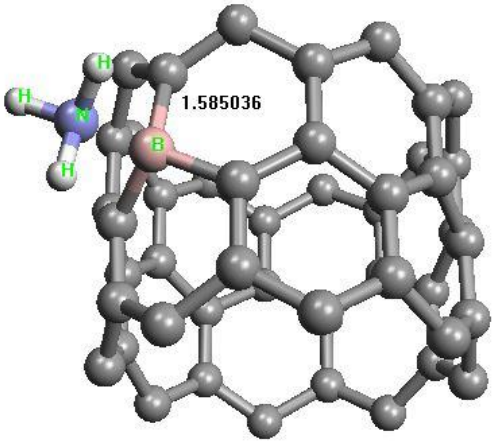

Figure. 5.3. The local structural distortions of boron-doped (8,0) SWCNT on ammonia adsorption. The boron-carbon distances have changed from 1.518 Å to 1.585 Å on binding with ammonia. Carbon, hydrogen, boron and nitrogen are represented by grey, white, pale pink and blue colours respectively.

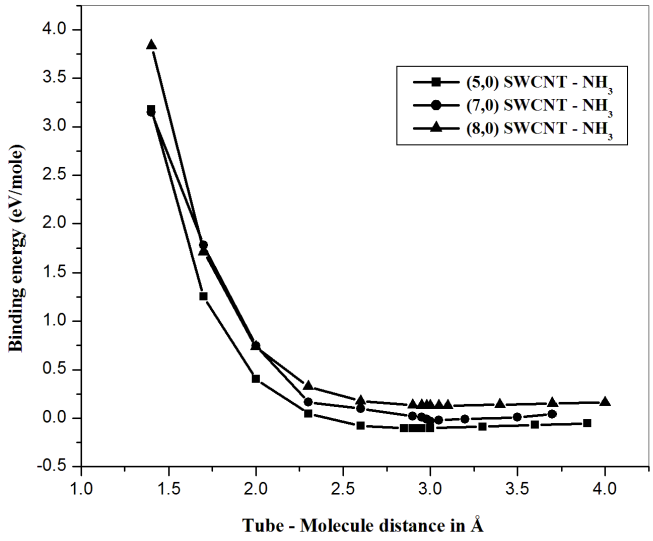

Figure. 5.4. Binding energy curve of intrinsic semi-conducting (5,0), (7,0) and (8,0) SWCNTs with respect to the tube-molecule distance.

These minima correspond to the most favorable geometry of the ammonia on boron doped SWCNT system. To get a clear picture, in Figure 5.6. the binding energy curves for ammonia on the intrinsic and doped cases are drawn together for (5,0) SWCNT where we observe the difference between both the cases and a distinct minimum for the ammonia binding on doped SWCNT.

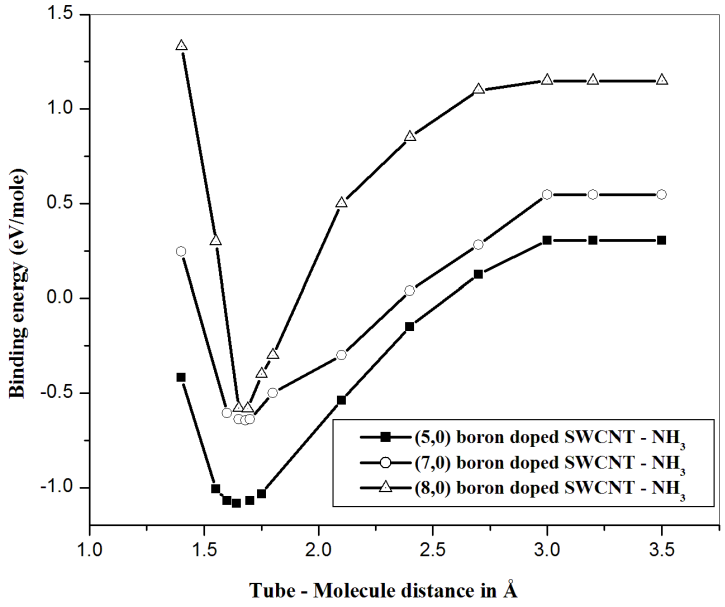

Figure. 5.5. Binding energy curve of doped semi-conducting (5,0), (7,0) and (8,0) SWCNTs with respect to the tube molecule distance.

In order to evaluate the changes in electronic properties of the intrinsic and boron doped SWCNT systems with and without ammonia, we have calculated the electronic density of states (DOS) for both these cases and are shown in Figures 5.7 and 5.8. For the finite systems, we have considered the difference between the Lowest unoccupied molecular orbital (LUMO) and Highest occupied molecular orbital (HOMO) as the energy gap (E_{gap}) and are listed in Table 5.3. In Figure 5.7. the DOS plots for the case of (8,0) intrinsic SWCNT and also for ammonia weakly physisorbed at a distance of 3.03 Å with (8,0) SWCNT are given. From the two plots in Figure 5.7, we observe that the DOS spectrum remains the same, unaffected with ammonia binding on intrinsic SWCNT.

The energy gap is found to be about 0.97 eV which is unaffected by the physisorption of ammonia. Hence we again conclude that the intrinsic SWCNTs cannot serve as sensors for detecting the presence of ammonia. On the other hand, for the boron doped case the DOS plots in Figure 5.8. show interesting effects. For the boron doped SWCNT, we find that the energy gaps near Fermi level decrease appreciably. From the electronic point of view, the electronic structure of the SWCNT contains electronic holes after doping with boron atoms.

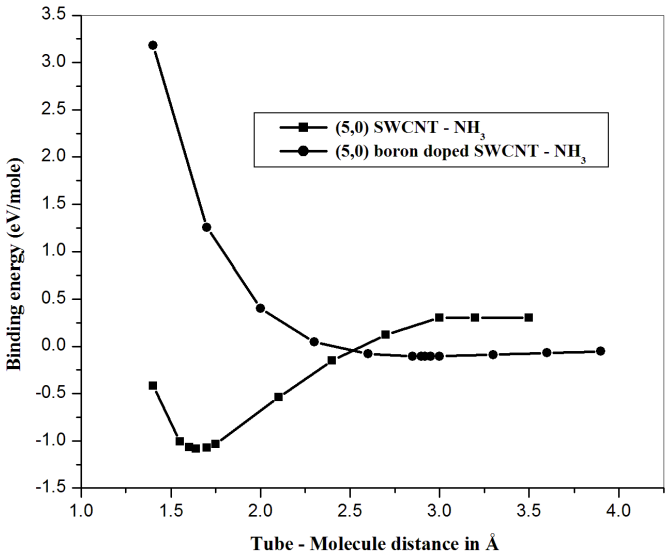

Figure. 5.6. Binding energy curve of (5,0) SWCNT with ammonia, for both intrinsic and doped systems.

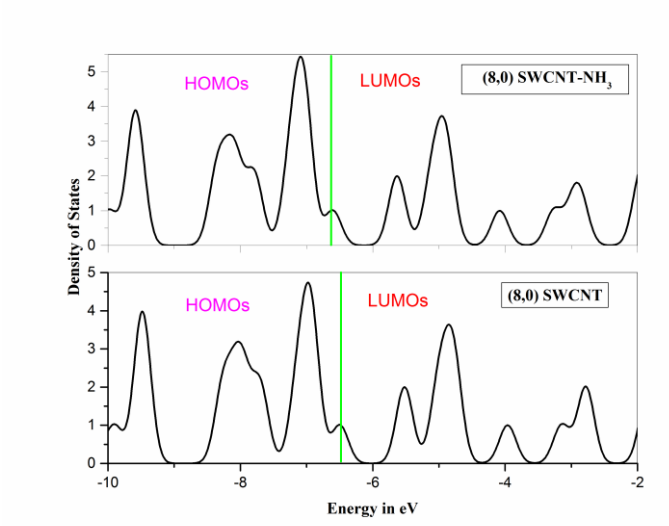

Figure. 5.7. Total density of states of (8,0) SWCNT with and without ammonia. Frontier molecular orbitals (HOMOs and LUMOs are shown). Green line indicates highest occupied molecular orbitals.

When it interacts with ammonia, the non-bonding electrons of ammonia are getting transferred to the unoccupied orbital of boron atom which changes the conductivity again. The increased number of accepting states and nearby LUMO of doped systems with HOMO of ammonia will facilitate the charge transfer more favourable in doped systems compared to

that of undoped system and enhance its affinity towards doped system. From the NPA charge transfer study it is clearly evident that the charge is being transferred from ammonia to SWCNT in both the cases. Although DOS calculated for finite length nanotubes will give an understanding about band gaps of nanotubes upon doping and adsorption, the methodology is not accurate enough to determine the exact band gaps of infinite systems like SWCNTs.

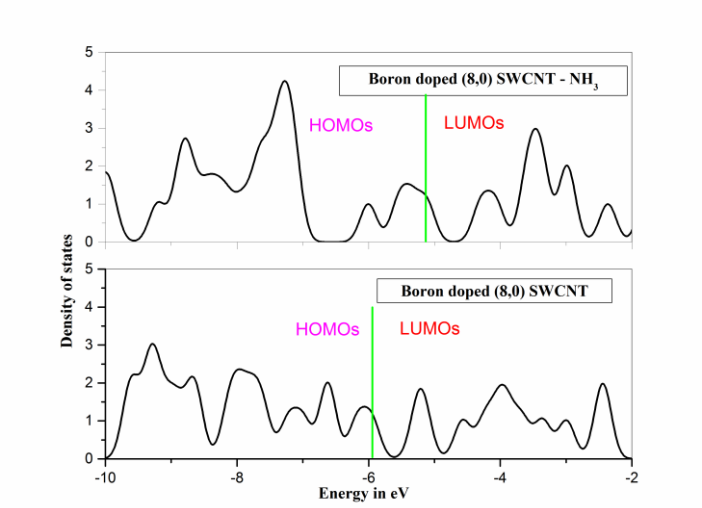

Figure. 5.8. Total density of states of (8,0)-boron-doped SWCNT with and without ammonia. Frontier molecular orbitals are shown (HOMOs and LUMOs). Green line indicates highest occupied molecular orbitals.

5.3. Band structure studies – Ammonia adsorption

In order to determine accurate band gaps of intrinsic as well as doped SWCNTs with and without ammonia, band structure calculations are performed using Density Functional Theory employing periodic boundary conditions for (8,0) SWCNT system taking a unit cell of 48 carbon atoms employing PBC conditions along the tube axis using DFT with B3LYP functional and 6-31G (d) basis set taking 80 k points along the Brillouin zone. Similar to the HOMO and LUMO of a finite system, the highest occupied crystalline orbital (HOCO) and lowest unoccupied crystalline orbital (LUCO) are defined for infinite system. In this case, the energy gap of HOCO and LUCO corresponds to the band gap and is given by the expression

$$E_{\text{band gap}} = E_{\text{LUCO}} - E_{\text{HOCO}} \qquad (5.1)$$

The calculated band gap between the highest occupied crystalline orbital (HOCO) and lowest unoccupied crystalline orbital (LUCO) using DFT for different systems are also given in the Table 5.3.

Table 5.3. HOMO, LUMO and the energy gaps for ammonia and finite SWCNTs. HOCO and LUCO for infinite SWCNTs are given. E_{gap} = (LUMO-HOMO), $E_{bandgap}$= (LUCO-HOCO).

System	**HOMO (eV)**	**LUMO (eV)**	**Gap(eV) (E_{gap})**	**HOCO (eV)**	**LUCO (eV)**	**Gap (eV) ($E_{bandgap}$)**
NH_3	-6.49	5.52	12.01			
(8,0)-SWCNT	-6.49	-5.52	0.97	-4.78	-3.33	1.45
(8,0)-B-SWCNT	-5.95	-5.26	0.69	-4.67 -4.67	-4.30 -5.81	0.365 (Direct) -1.14 (Indirect)
(8,0)-SWCNT - NH_3	-6.60	-5.63	0.97	-4.88	-3.43	1.45
(8,0)-B-SWCNT- NH_3	-5.11	-4.29	0.82	-3.98	-2.74	1.24

Band structures with few frontier crystalline orbitals, for intrinsic and doped systems with and without ammonia are shown in Figures 5.9, 5.10 and 5.11. The intrinsic (8,0) SWCNT is found to be semi-conducting with a gap of 1.45 eV, which is in good agreement with existing predictions of 1.28 eV [13]. Even after the physisorption of ammonia molecule on intrinsic SWCNT, we did not observe any change in the LUCO-HOCO energy gap, which remained at 1.45 eV as shown in Figure 5.9. indicating that the weak physisorption of ammonia does not change the transport properties of intrinsic SWCNTs confirming that intrinisic SWCNTs are insensitive to ammonia molecule. We see that doping of the nanotubes leads to lowering of the direct band gap thus making the semi-conducting SWCNT to a semi-metal SWCNT with a direct band gap of about 0.365 eV and a negative indirect band gap of –1.14 eV with the HOCO and LUCO values reduced to -4.67 and -5.81 eV respectively as shown in Figure 5.10. A semi-metal is a material with a very small overlap between the bottom of the conduction band and the top of the valence band, the overlapping region is shown in dotted line which also gives the indirect band gap as shown in Figure 5.10. The minimal-energy state in the conduction band and the maximal-energy state in the valence band are characterized by a certain crystal momentum (k-vector) in the Brillouin zone.

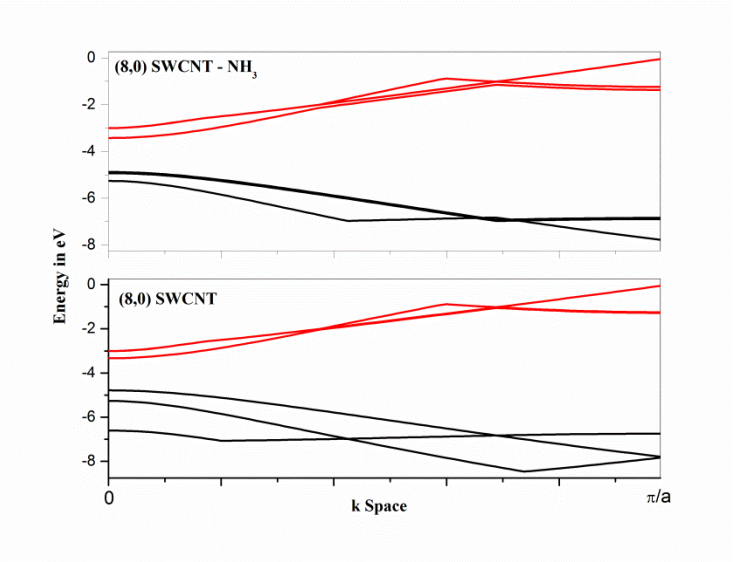

Figure. 5.9. Band structure calculations of (8,0) SWCNT, with and without ammonia. The difference of LUCO and HOCO at π/a (or Γ point) gives the band gap. Black and red lines indicate occupied and unoccupied Frontier crystal orbitals respectively.

In a semi-metal, the bottom of the conduction band is typically situated in a different part of momentum space (at a different k- vector) than the top of the valence band.

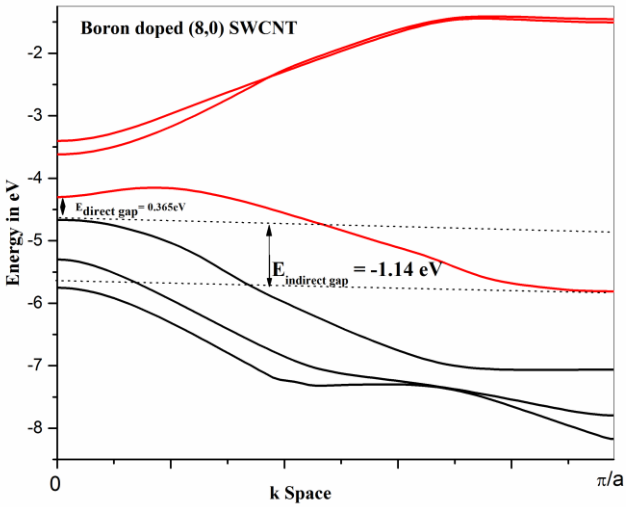

Figure. 5.10. Band structure calculations of boron doped (8,0) SWCNT. The difference of LUCO and HOCO at 0 (or Γ point) gives direct band gap, Indirect band gap is shown with dotted lines. Black and red lines indicate occupied and unoccupied Frontier crystal orbitals respectively.

We can see that HOCO at the point k=0 whereas LUCO is at nearby k=π/a (Figure 5.10). It is interesting to see that it is similar to p-type doping where increased hole concentration determine the conductivity. After binding with ammonia, as shown in Figure 5.11, the band gap opens up and the tube becomes more semi-conducting with an increase in band gap from 0.365 to 1.24 eV which can be understood by the charge transfer phenomenon. SWCNT doped with boron has hole carriers and ammonia would reduce the hole concentration by transferring its electrons to the doped SWCNT, thus increasing the band gap and reducing the conductivity. Thus by detecting the conductivity changes of the boron doped systems before and after adsorption of ammonia, the presence of this molecule can be detected. Therefore, we suggest that the boron doped SWCNTs would be a promising candidate to detect the presence of ammonia by making use of their conductivity difference.

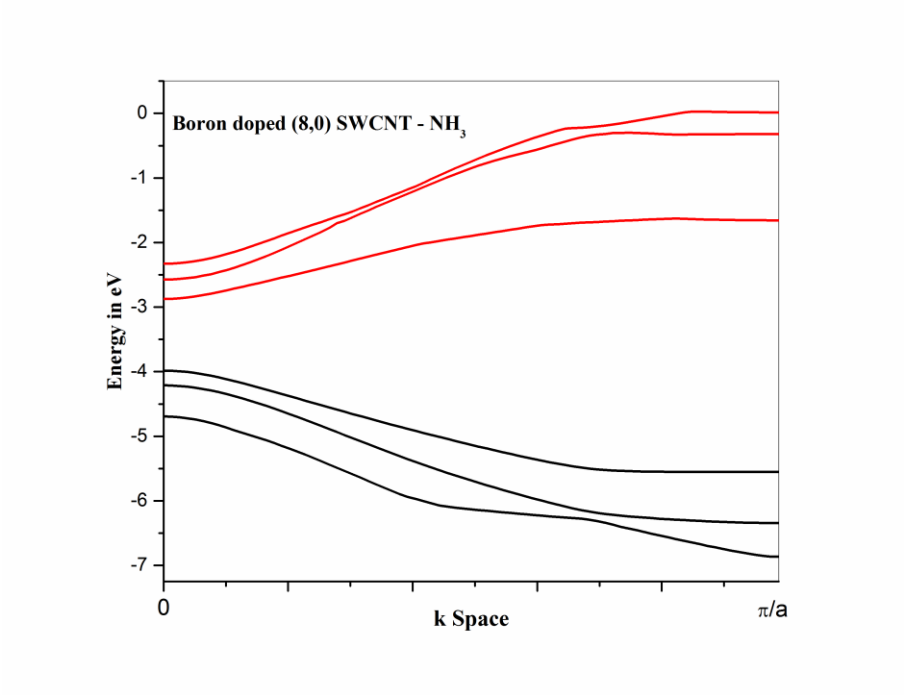

Figure. 5.11. Band structure calculations of boron doped (8,0) SWCNT with ammonia. The difference of LUCO and HOCO at 0 (or Γ) point gives the band gap. Black and red lines indicate occupied and unoccupied Frontier crystal orbitals respectively.

One of the important characteristics of the gas sensors is recovery of the device, but high binding energy implies that desorption of the adsorbate could be difficult and the device may suffer from long recovery times. Based on the conventional transition state theory, the recovery time, can be written as

$$\tau = \nu_o^{-1} \exp(-E_{bind}/kT), \qquad (5.2)$$

where, T is the temperature, *k* is the Boltzmann's constant, and υ_o is the attempt frequency. According to the above equation with an increase in binding energy E_{bind}, the recovery time would be prolonged. From Table 5.1 it is obvious that, on doping with boron and, with increase in tube diameter the binding energy being decreased from -1.085 eV to -0.584 eV for the case of doped systems from (5,0)–boron-doped SWCNT to (8,0)–boron-doped SWCNT. Thus this drawback of long recovery time could be overcome with increase in tube diameter, enhance the sensitivity of SWCNT based sensors.

5.4. Natural Bond Orbital (NBO) analysis

Natural bond orbital analysis [6] is also carried out on the geometries in order to quantify the non-covalent donor and acceptor interactions between ammonia and nanotubes. These interactions result in transfer of occupancy from the localized bonding and nonbonding orbitals to empty non-Lewis orbitals. The study provides additional insights into interaction of the ammonia with nanotubes. Results of second order perturbation theory analysis of Fock matrix for donor and acceptor delocalization interactions are observed for the systems of (8,0)-SWCNT system with ammonia and (8,0)-boron-doped SWCNT system with ammonia on the structures optimized at 6-31G (d) basis set using DFT employing hybrid functional B3LYP and these results are summarized in Table 5.4. In the first case no significant charge transfer stabilization energy is observed between ammonia and intrinsic (8,0) SWCNT system supporting earlier experimental and theoretical findings that it is inert to the nanotube.

Table 5.4. Natural bond orbital (NBO) Analysis of non-bonded charge transfer interactions between SWCNTs and ammonia.

System	Transition	Stabilization energy (kcal/mole)
NH_3→ (8,0)-SWCNT	$N_n \rightarrow C_{Ry}^*$	0.05
NH_3→(8,0)-B-SWCNT	$N_n \rightarrow B_n^*$	39.52
	$N_n \rightarrow$ C-B*	1.09
	$N_n \rightarrow$ C-C*	0.41

In the second case between ammonia and (8,0)-boron-doped system, charge transfer is observed between lone pair orbitals of nitrogen of ammonia to empty non-Lewis orbitals of boron of (8,0)-boron-doped SWCNT system with a stabilization energy of 39 kcal/mole, which is significant in magnitude. The stabilization energy clearly signifies the importance

of boron doping and its role in enhancing the interaction between ammonia and doped CNT system.

5.5. Conclusion

We have found that the electronic properties and affinity towards ammonia appreciably change upon substitutionally doping the SWCNT with boron. This is reflected in the increased charge transfer, ammonia-nanotube distance and binding energies. We find that doping of the nanotubes leads to lowering of the direct band gap thus making the semi-conducting SWCNT to a semi-metal nanotube with a direct band gap of about 0.365 eV and a negative indirect band gap of -1.14 eV. After binding with ammonia the band gap opens up and the tube becomes more semi-conducting with an increase in band gap from 0.365 to 1.24 eV which can be understood by the charge transfer phenomenon. The doped nanotubes has hole carriers and ammonia would reduce the hole concentration by transferring its electrons to the nanotube thus increasing the band gap and reducing the conductivity. Thus by detecting the conductivity changes of the boron-doped systems before and after adsorption of ammonia the presence of this molecule can be detected. We have found that the electronic charge transfer is an important mechanism in change in conductivity in the doped SWCNT upon adsorption of ammonia. It would be interesting to investigate the effect of ammonia adsorption on the transport properties of the nanotubes following the method of ab initio charge transfer transport calculations as done by Rocha *et al.* [14]. As SWCNTs with dopants like nitrogen and boron have already been synthesized, we also expect that our current theoretical prediction of ammonia being more sensitive toward doped systems would encourage experimentalists to carry out their studies in this arena.

Reference

1. J. R. Istas, R. de Borger, L. de Temmerman Guns, K. Meeus-Verdinne, A. Ronse, P. Scokart, M. Termonia. *Effect of ammonia on the acidification of the environment, European Communities* Report No. EUR 11857 EN, 1988.
2. P. Warneck, *Chemistry of the Natural Atmosphere,* Academic Press Inc, 1998.
3. J. W. Erisman, R. Otjes, A. Hensen, P. Jongejan, P.v.d. Bulk, A. Khlystov, H. M¨ols, S. Slanina. *Atmos. Environ.* 35, 1913, 2001.
4. K. B. Wiberg, P. R. Ruben. *J. Comput. Chem*. 14, 1504, 1993.
5. A. E. Reed, F. Weinhold, L. A. Curtiss. *Chem. Rev.* 88, 899, 1988.

6. F. Weinhold. *Discovering Chemistry with Natural Bond Orbitals*; Wiley: New Jersey, 2012.
7. H. W. Wang, B. C. Wang, W. H. Chen, M. Hayashi, *J. Phys. Chem. A.* 112, 1783, 2008.
8. S. Chopra, A. Pham, J. Gaillard, A. Parker, A. M. Rao. *Appl. Phys. Lett.* 80, 4632, 2002.
9. K. Bradley, J. Christophe, P. Gabriel, M. Briman, A. Star, G. Gruner, *Phys. Rev. Lett.* 91, 218301, 2003.
10. R. Faccio, L. Fernandez-Werner, H. Pardo, C. Goyenola, O. N. Ventura, A. W. Mombru. *J. Phys. Chem. C.* 114, 18961, 2010.
11. C. W. Bauschlicher, Jr., A. Ricca. *Phys. Rev. B.* 70, 115409, 2004.
12. J. Zhao, A. Buldum, J. Han, J. P. Lu. *Nanotechnology*, 13, 195, 2002.
13. Y. Matsuda, J. Tahir-Kheli, W. A. Goddard, III, *J. Phys. Chem. Lett.* 1, 2946, 2010.
14. A. R. Rocha, M. Rossi, A. Fazzio, A. J. R. da Silva. *Phys. Rev. Lett.* 100, 176803, 2008.

CHAPTER 6

Interaction of Glycine with SWCNTs in Non-ionic and Zwitter-ionic forms

6.1. Introduction

CNTs with their unique morphology exhibit fascinating electronic and mechanical properties [1-4]. Their needle like geometry helps them to penetrate deep into the cell walls and this characteristic property is exploited in employing CNTs in drug delivery and various biomedical applications [5-8]. But the main drawback associated in employing CNTs for biomedical applications is its toxicity and solubility [9,10]. In order to improve the solubility CNTs can be functionalized with various functional groups thus making them soluble and it has been reported that increase in functionalization not only enhances the solubility but also reduces the toxicity of CNTs [10,11].

Proteins are heterogeneous in their chemical nature, and exhibit a range of functional groups that allow for versatile chemical derivatisation [12]. Proteins possess the ability to rapidly respond to changes in the local environment and is an area of research interest as they associate into complexes, catalyze molecular transformations, through rapid chemical changes. The coupling of CNTs excellent electronic and mechanical properties with proteins' biological activity is pushing the frontiers of sensing, and the topic has recently been extensively investigated and reviewed [13].

In this work, we have functionalized the SWCNTs with various functional groups and studied its interaction with glycine in both neutral form and zwitter-ionic form. Since the topic of protein encapsulation in CNTs and the interaction of proteins with CNTs are attracting the attention of research community, we have focused our attention in understanding the interaction of amino acids (glycine in the current work) which are the building blocks of proteins.

6.2. Results and Discussion

The interaction of (8,0) semi-conducting SWCNT with glycine is investigated employing the Density functional theory (DFT) with hybrid functional B3LYP. The geometry optimizations are carried out with 3-21G basis set and single point energies are calculated for the optimized geometries using 6-31G (d) double zeta valence polarized basis set. The 6-31G (d) basis set is probably the most popular basis set at the present which gives good geometries and often reasonable energies. But there is no evidence that in general geometries evaluated using

higher basis sets are better than that calculated using 3-21G∗ basis set [14]. Therefore the optimizations employing lower basis set 3-21G basis set and calculating single point energies with the optimized orientations would be computationally less expensive approach. (8, 0) SWCNT with 8 layers constituting 128 carbon atoms is considered and the end carbon atoms are saturated with hydrogens to satisfy the valency. Interaction of glycine with CNTs is examined in both normal state and also in the zwitter-ionic state employing calculations in gas and water phases respectively. Polarizable Continuum Model (PCM) [15,16] has been employed to model the solvation effects of water phase. PCM has been used with the default Self-Consistent Reaction Field (SCRF) method employed in G09 suite of programs. This method creates the solute cavity via a set of overlapping spheres and an external iteration procedure is included whereby the program computes the energy in solution by making the solvent reaction field self-consistent with the solute electrostatic potential generated from the computed electron density with the specified model chemistry [15,16].

SWCNTs functionalized with various functional groups like –OH, $–NH_2$ and –COOH and double functionalized with two different functional groups $–NH_2$ and –COOH are considered in our study. Interaction of glycine with intrinsic and functionalized SWCNTs is examined by calculating binding energies, charge transfers and equilibrium distances. Charge transfer calculations are carried out by Natural population analysis (NPA) [17] since conventional procedure of Mulliken population analysis has strong dependence on the basis sets employed. Since glycine has two reactive centers amino and carboxylic acid geometry optimization is carried out with both the orientations facing towards CNT in order to confirm the best possible orientation.

The orientation for which the binding energy is highest is considered for the study and the corresponding charge transfers and optimized distances are tabulated. The interactions of amino acids with intrinsic SWCNTs have been studied employing various methods and the results are well known in the literature [19-22]. As a first step, we have looked into the possible interaction of glycine with the pristine nanotube and the geometry optimized configuration is given in Figure 6.1.

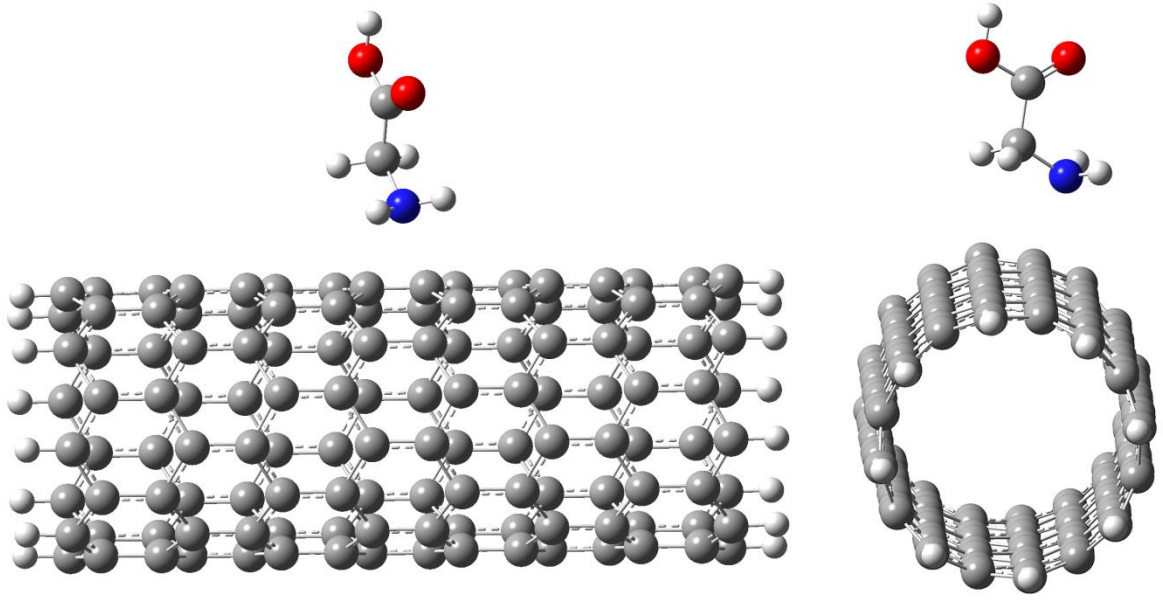

Figure. 6.1. Optimized orientation of glycine binding with intrinsic (8, 0) SWCNT in the gas phase. The optimized, nearest distance to the SWCNT walls is 3.14 Å. Grey, white, red and blue colours indicate carbons, hydrogens, oxygen and nitrogen atoms respectively.

It is found that our calculations using the hybrid functional also yield the results that the inert surface of the SWCNT interacts only with a binding energy of about 0.008 eV with a nearest distance of 3.14 Å from the side walls. This observation is in well accordance with the earlier computational results [22]. In the gas phase neutral glycine is placed along the side walls of SWCNT and optimized without any geometry constrains. From the binding energy values given in the Table 6.2. it can be seen that the interaction of glycine with intrinsic CNTs is very weak confirming the earlier studies [19-22]. This is due to passive nature of intrinsic CNTs with no reactive centers which would only result in weak physisorption with negligible binding energy and charge transfer.

Our results are coinciding with that of Sun *et al*., [21] who have investigated glycine adsorption on pristine as well as boron doped semi-conducting SWCNTs whereas there is slight disagreement with the results in binding energy and in equilibrium distance from the surface of the conducting nanotubes [19-22]. For example, even though Ganji *et al*., [22] predicts a physisorption with a binding energy value of only 0.17 eV, the equilibrium distance is found to be 2.334 Å for glycine physisorption on a (6,6) surface. These results suggest that non-ionic glycine is only weakly bound to the nanotube sidewall. Negligible binding energy, charge transfer and relatively large glycine–CNT distance suggest that only

non-covalent interactions are present in the weak physisorption. Moreover the results also show that the bond lengths in glycine are only slightly changed upon binding with CNT, with C–C, C–O and C–N equilibrium bond distances remaining 1.52 Å, 1.38 Å and 1.46 Å which is the same as in individual glycine molecule.

In order to find whether the interactions change when the surface is chemically modified we have functionalized (8,0) SWCNT with various functional groups like –OH, –NH_2 and –COOH and calculated the stabilization energy to find the favorability of functionalization. We have also doubly functionalized the SWCNT with two different groups like –NH_2 and –COOH where the functional amino and carboxylic groups are kept at a distance of 4.3 Å from each other. Functionalized SWCNTs are found to be more stable than the corresponding pristine SWCNTs and the stabilization energy E_{stab} is calculated using the formula given by (and the results are compiled in Table 6.1.)

E_{stab} = Energy of functionalized SWCNT – (Energy of SWCNT+ Energy of functional group)

Table 6.1. Stabilization energies of SWCNT functionalized with –OH,–NH_2 and –COOH in gaseous and aqueous phases.

System	**Stabilization energy (eV)**	
	Gas phase	**Aqueous phase**
SWCNT-OH	-3.447	-3.096
SWCNT-NH_2	-3.024	-2.582
SWCNT-COOH	-3.128	-2.715
SWCNT-NH_2-COOH	-2.047	-2.168

Stabilization energies in both the phases have been found to be negative in all the cases and it is concluded that functionalization on SWCNTs is a favorable process. Functionalization with one group is favored in gas phase whereas double functionalization is favoured slightly more in the water phase owing to favourable hydrogen bonding interactions.

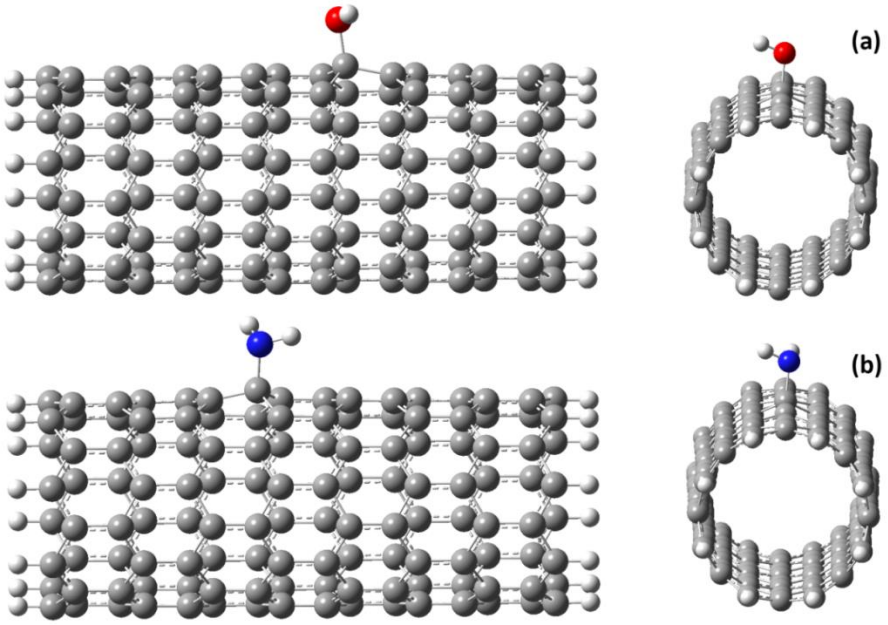

Figure. 6.2. Schematic representation of the (8,0) SWCNT functionalized with (a) –OH and (b) –NH_2 groups.

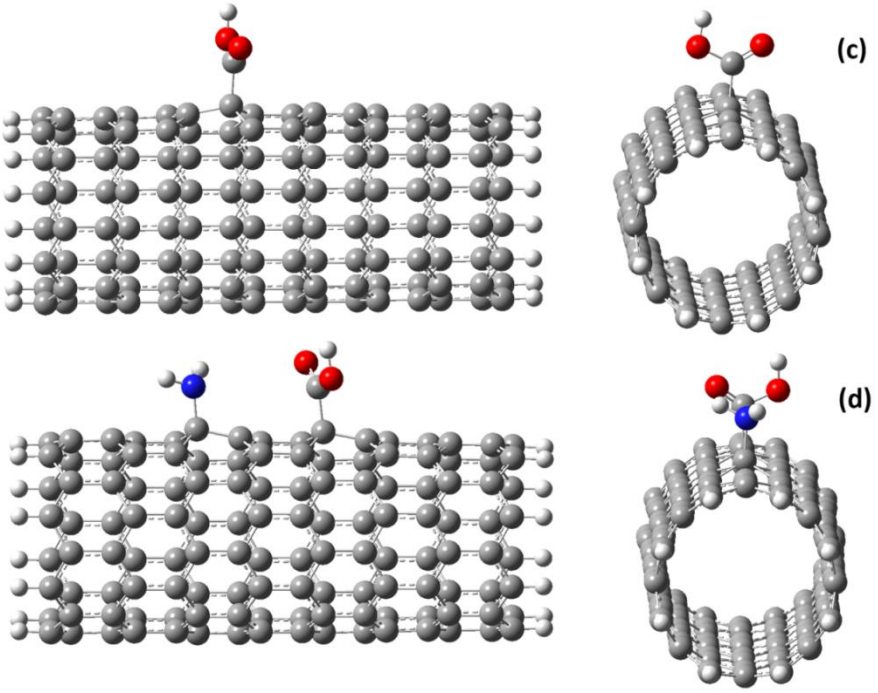

Figure 6.3. Schematic representation of (8,0) SWCNT functionalized with (c) –COOH and (d) both –COOH and –NH_2 groups.

The optimized geometries of SWCNT systems functionalized with –OH, –NH_2, –COOH and both –NH_2 and –COOH are shown in Figures 6.2. and 6.3.

6.3. Adsorption of Glycine in the Non-ionic Form

The adsorption of glycine on the functionalized SWCNT showed interesting results and the binding energies, optimized distances and charge transfers are given in Table 6.2. The optimized, functionalized SWCNTs and glycine are used for the binding process. It is interesting to see that the nearest distances in the optimized configurations are now decreased upon functionalization as shown in Table 6.2. The electronic structure and charge population are also analyzed to understand the adsorption properties.

Table 6.2. Binding energies, charge transfer and distance of glycine (In neutral form) from SWCNT in the optimized orientations in gas phase.

System	Binding energy (eV)	Charge transfer (e)	Distance (Å)
SWCNT	0.008	0.012	3.14
SWCNT-OH	-0.307	0.093	1.64
SWCNT-NH_2	-0.193	0.042	1.93
SWCNT-COOH	-0.421	0.140	1.45
SWCNT-NH_2 -COOH	-0.536	0.030	1.57

On functionalization, the binding energy of glycine with SWCNTs increased appreciably and negative binding energies and negligible charge transfer are observed. The charge transfer is found to be from glycine to the SWCNT in all cases. In the case of CNT-OH the binding energy is observed to be -0.307 eV with a weak charge transfer of 0.09 e. Similarly functionalization with amino group has shown a binding energy of −0.193 with a charge transfer of 0.042 e from glycine. Compared to hydroxyl and amino functionalization carboxylic acid functionalization has shown an increase in binding energy of −0.421 eV and slightly higher charge transfer of −0.140 e with an equilibrium distance of 1.45 Å. It is concluded that among singly functionalized SWCNTs glycine adsorption takes place preferentially on the active oxygen site of the carboxylic functional group.

Functionalizing with both –NH_2 and –COOH resulted in further increase in binding energy value of −0.536 eV with charge transfer of 0.030 e and equilibrium distance of 1.57 Å. Although binding energy in the case of doubly functionalized SWCNT increased compared to that of SWCNT-COOH case, the charge transfer and optimized distance are found to be larger which could be due to the steric effects. The order of increasing favorability of interaction of glycine with various CNTs in gas phase is as follows, SWCNT

< SWCNT-NH_2 < SWCNT-OH < SWCNT-COOH < SWCNT-NH_2-COOH. The optimized orientations of glycine with various functional groups are shown in Figures 6.4. and 6.5.

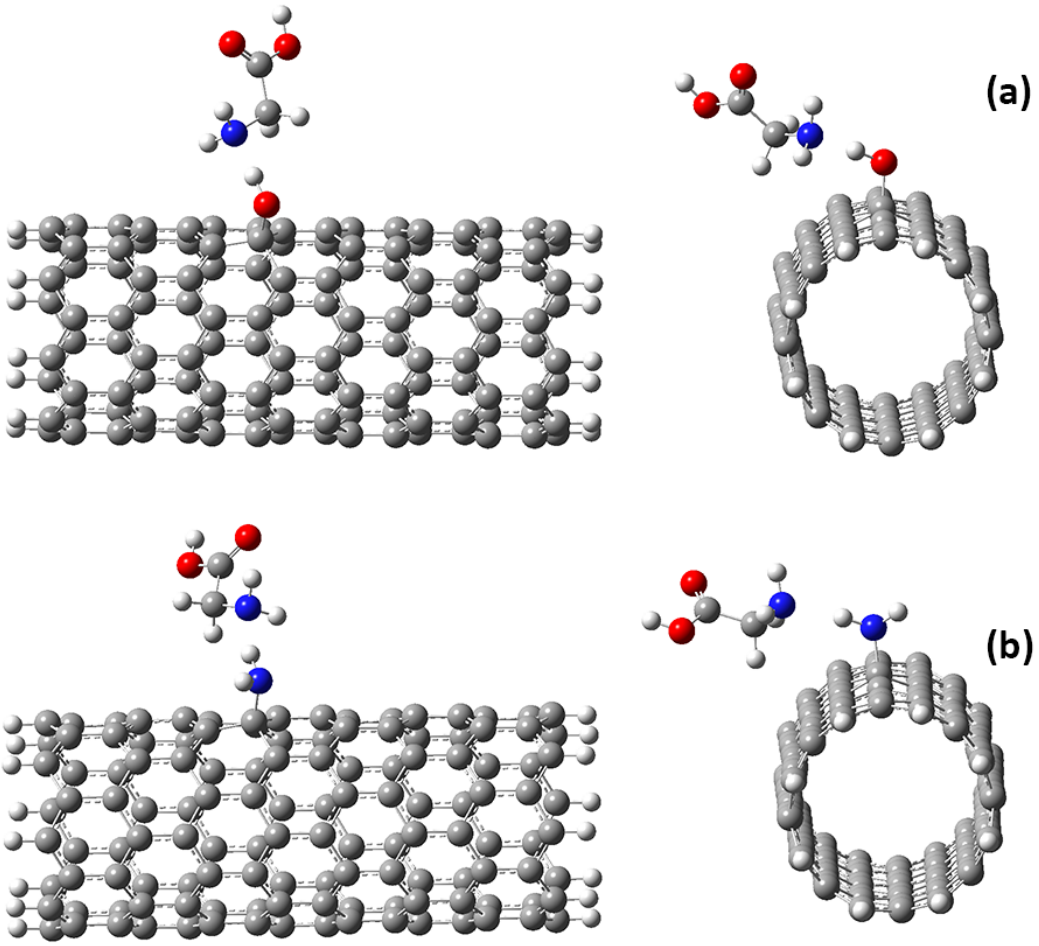

Figure 6.4. Binding of glycine on the side wall of (8,0) SWCNT functionalized with (a) –OH and (b) –NH_2 group.

The full structural optimization indicate that in all cases of non-ionic binding, the glycine is in its favorable trans configuration and that glycine interacts with its active amino nitrogen on the side walls and can be seen closer to the functional groups considered in the figures. The distances shown in Table 6.2 are of active nitrogen of glycine to H of –OH, –NH_2 and –COOH functionalized SWCNT. This is due to the possible inter-molecular hydrogen bonding between active nitrogen and electropositive hydrogen of the functional group. On the doubly functionalized SWCNT with –NH_2 and –COOH, also the nitrogen of amino group of glycine closer to the SWCNT walls at a distance of 1.57 Å. In this case, there is a

possibility of multiple noncovalent interactions between the functional groups in glycine and also on the functionalized wall of nanotube.

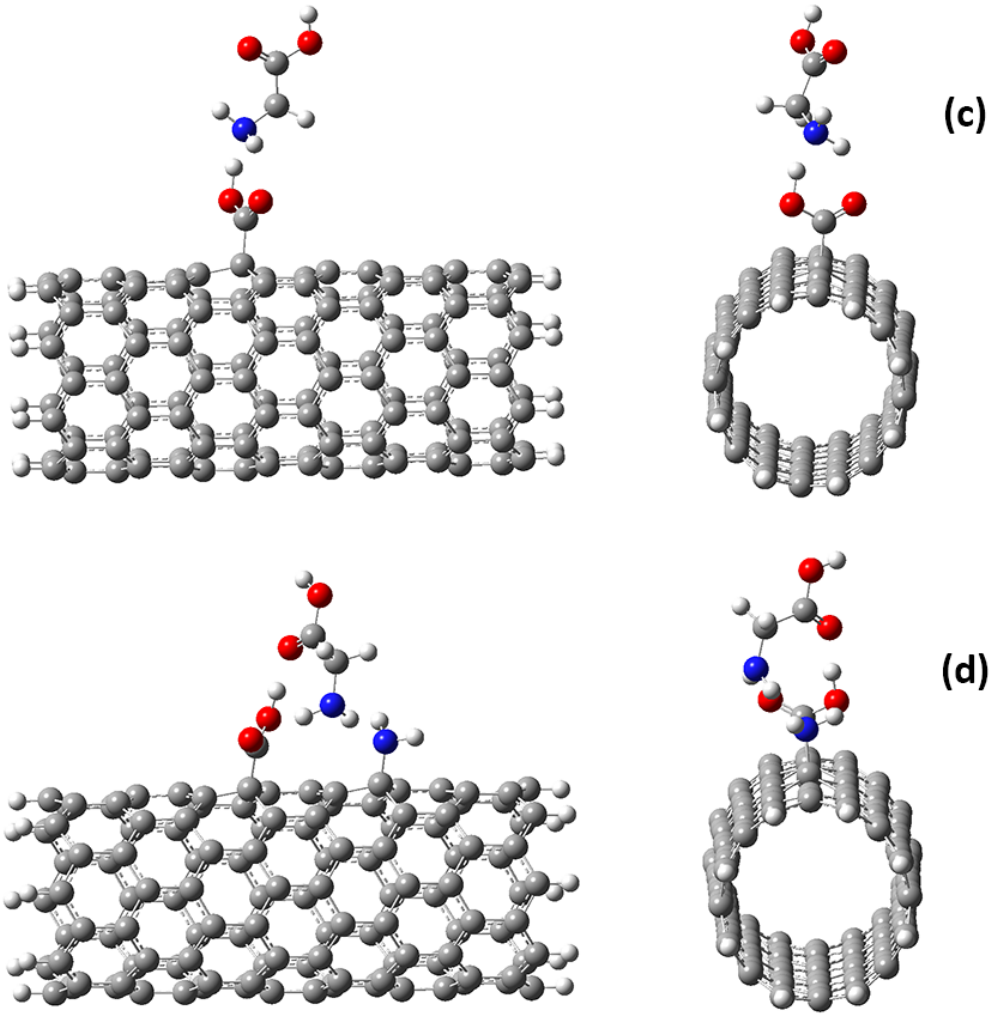

Figure 6.5. Glycine molecule physisorption on SWCNT single functionalized with (c) –COOH and on doubly functionalized with (d) –COOH and $–NH_2$ groups.

The higher interaction energy that we observe as binding is due to these multiple non-covalent interactions. As is well known all these weak interactions are effective only over a short range and require close contact between the reacting groups. It is also clear from the charge analysis that the interaction between functionalized SWCNT and glycine is appreciably stronger compared to that of intrinsic SWCNT and glycine.

6.4. Adsorption of Glycine - Zwitter-Ionic State

The binding of glycine in zwitter-ionic state on functionalized SWCNT are also considered in the aqueous phase and results are shown in Table 6.3. The schematic representations of the interactions are given in Figures 6.6. and 6.7.

Table 6.3. Binding energies, charge transfer and distance of glycine in zwitter-ionic from SWCNT in optimized orientations in aqueous phase.

System	Binding energy (eV)	Charge transfer (e)	Distance (Å)
SWCNT	-0.114	-0.001	2.84
SWCNT-OH	-0.599	0.100	1.53
SWCNT-NH_2	-0.452	0.030	1.84
SWCNT-COOH	-0.757	0.138	1.37
SWCNT- NH_2-COOH	-0.694	0.042	1.21

It is well known that amino acids contain ammonium and a carboxylate group in the zwitter-ionic form, which arise via a kind of intramolecular colour acid–base reaction. Intrinsic SWCNT which is passive with no reactive centers has shown only a negligible positive binding energy with glycine in its neutral non-ionic state. In the case of glycine in zwitter-ionic state the binding energy is slightly increased compared to that of neutral state. The polar nature of zwitter-ionic glycine induces polarizability in the intrinsic CNT thus resulting in weak binding energy. The binding energies, charge transfer and distance from SWCNT of the zwitter-ionic form are given in Table 6.3. It is seen that the functionalization enhanced the binding energy of zwitter- ionic glycine with the SWCNT appreciably.

Binding energies for mono functionalization followed a similar trend to that of gas phase where the favorability of binding followed the order COOH-CNT > CNT-OH >CNT-NH_2. Optimized distances from the walls are also decreased appreciably compared to that of neutral state. In the case of double functionalization, zwitter- ionic binding energy increased compared to that of gas phase and the optimized distance is observed at a value of 1.21 Å. The optimized orientations of zwitter-ionic glycine with functionalized SWCNT are shown in Figures 6.6. and 6.7. From the optimized orientations it is clear that for CNT-COOH glycine in zwitter-ionic state, the active oxygen site of carbonyl group of carboxylate is closer to hydrogen of –COOH group of CNT-COOH. In the case of doubly functionalized SWCNT i.e., COOH-CNT-NH_2, the zwitter-ionic species is arranged in such a way that the hydrogen of amino group of glycine interacts with oxygen of carbonyl group of carboxylate on the

walls and the hydrogen of carboxylic acid of glycine is closer to the carboxylate functional group on the walls.

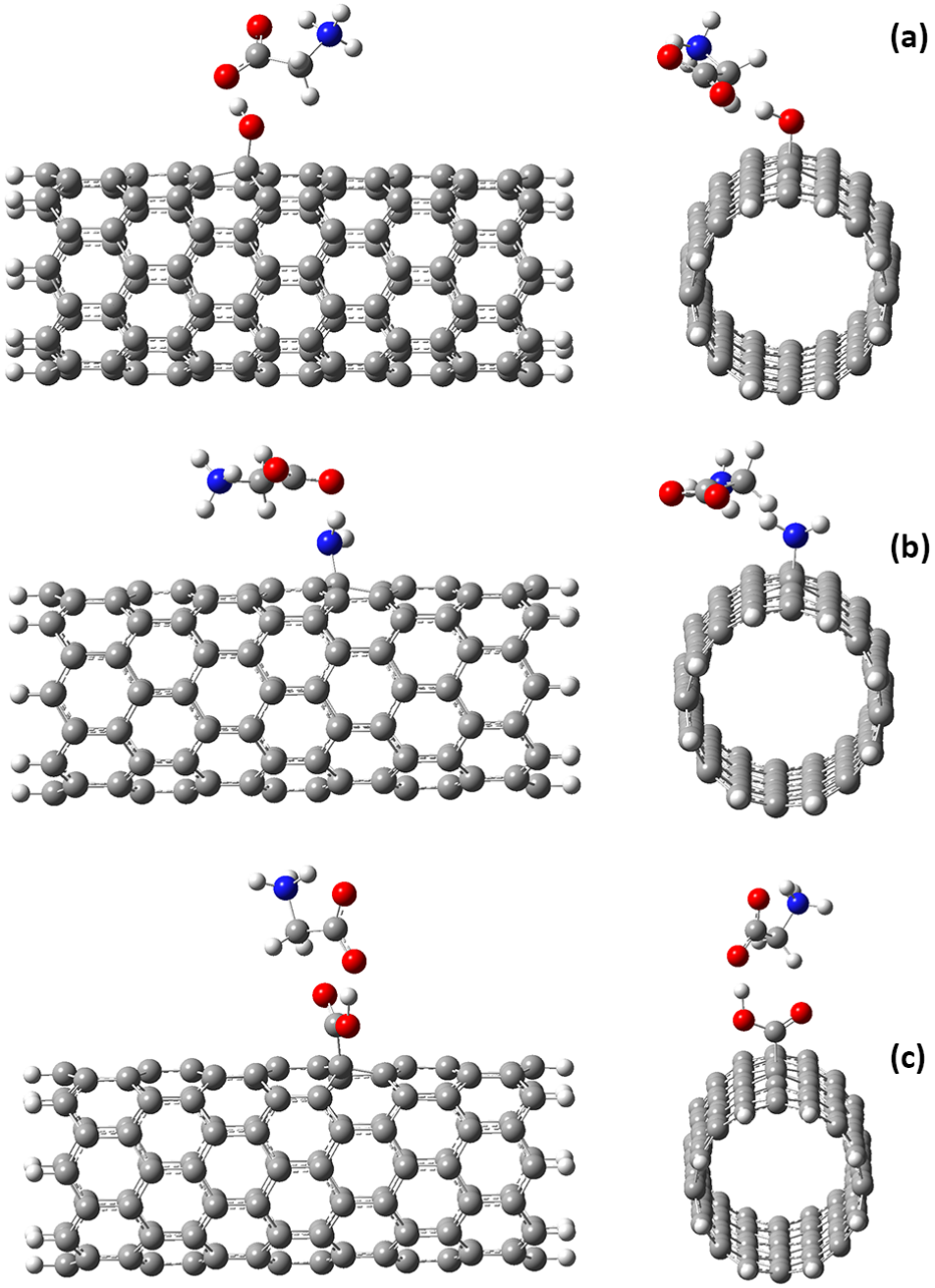

Figure 6.6. Interaction and binding of zwitter-ionic glycine on functionalized SWCNTs. (a) OH-CNT (b) NH_2-CNT (c) COOH-CNT.

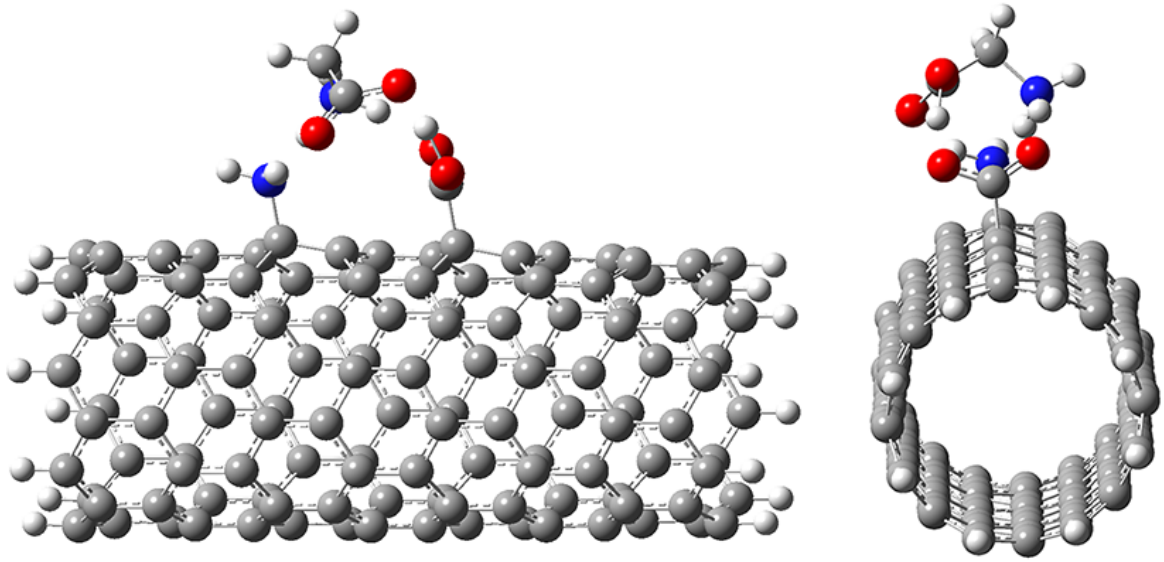

Figure 6.7. Optimized orientation of zwitter-ionic glycine bound on SWCNT functionalized with carboxylic acid and amino groups.

6.5. Electrostatic Potential Mapped Surfaces (ESPs)

In order to visualize the chargre distribution, we have plotted ESP mapped surfaces. From the Figure 6.8. it is clear that the charge distribution in glycine in the zwitter-ionic state is polarized whereas in the neutral form the polarization is observed to be less.

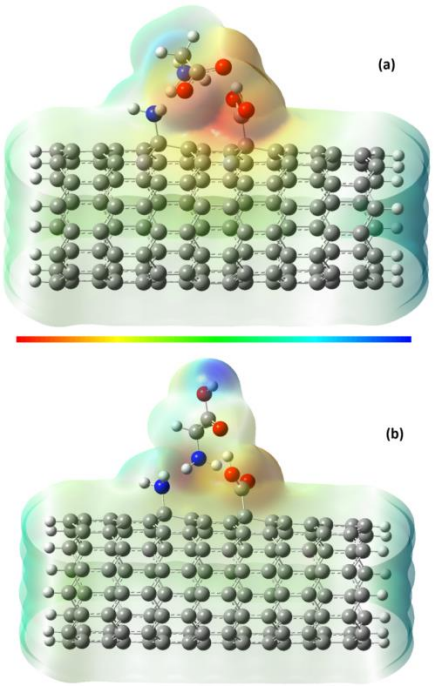

Figure 6.8. Electrostatic potential mapped surfaces (ESPs) of double functionalized SWCNT COOH-SWCNT-NH_2 with glycine in both (a) Zwitter-ionic form and (b) Neutral form. The colour code used in the mapping is also shown in the middle of the figure.

Higher polarization of charge in the zwitter-ionic state is responsible for the stronger interaction with the nanotube walls. In the case of doubly functionalized SWCNT, we observe an increased binding energy of −0.69 eV for zwitter-ionic state compared to −0.536 eV in the neutral state.

6.6. Conclusion

Interaction of glycine in non-ionic state (gas phase) and in zwitter-ionic state (aqueous phase) with intrinsic and functionalized SWCNTs have been studied employing density functional methods. Glycine in both non-ionic and zwitter-ionic states is found to exhibit weak binding energies with intrinsic SWCNT, with the latter interaction being more favourable. In the case of functionalized SWCNT, COOH-CNT exhibited higher binding energies compared to the hydroxyl and amino functionalized SWCNTs in both the phases. Doubly functionalized SWCNT exhibited higher binding energy in gas phase compared to the singly functionalized SWCNTs. In all cases charge transfer is observed to be weak, with charge being transferred from the glycine to the SWCNT. Glycine shows better interaction in both non-ionic and zwitter-ionic states with functionalized SWCNTs compared to that of intrinsic SWCNT and binding energy is found to be enhanced in the aqueous media. Zwitter-ions are found to adsorb stronger than their nonionic counterparts and physisorption is the strongest through the active carbonyl oxygen site for the zwitter-ionic-glycine amino acid, in contrast to the non-ionic case.

Reference

1. S. Ijima. *Nature* 354, 56, 1991.
2. A. Srivastava, J. Srashti, A. K. Nagawat. *Quantum Matter* 2, 469, 2013.
3. J. Kaur, N. Goel. *J. Comput. Theor. Nanosci.* 10, 48, 2013.
4. C. M. Chang, H. L. Tseng, A. D. Leon, A. P. Amarillas, A. F.Jalbout. *J. Comput. Theor. Nanosci.* 10, 521, 2013.
5. R. J. Chen, S. Bangsaruntip, K. A. Drouvalakis, N. W. S. Kam, M. Shim, Y. Li, W. Kim, P. Utz, H. Dai. *Proc. Natl. Acad. Sci.* 100, 4984, 2003.
6. K. Besteman, J. Lee, F. G. M. Wiertz, H. Heering, C. Dekker. *Nano Lett.* 3, 727, 2003.
7. A. Star, J. C. P. Gabriel, K. Bradley, G. Gruner. *Nano Lett.* 3, 459, 2003.
8. N. Venkatesan, J. Yoshimitsu, Y. Ito, N. Shibata, K. Takada. *Biomaterials* 26, 7154 2005.

9. N. Sinha, J. T. W. Yeow. *IEEE Transactions on Nanobioscience*, 4, 180, 2005.
10. M. Mananghaya, E. Rodulfo, G. Nonato Santos, A. R. Villagracia. *Jour. of Nanotech.* 2012, 780815, 2011.
11. C. M. Sayes, J. D. Fortner, W. Guo, D. Lyon, A. M. Boyd, K. D. Ausman, Y. J. Tao, B. Sitharaman, L. J. Wilson, J. B. Hughes, J. L. West, V. L. Colvin. *Nano Lett.* 4, 1881, 2004.
12. Stefanie Kellner, Salifu Seidu-Larry, Jürgen Burhenne, Yuri Motorin, Mark Helm. *Nucleic Acids Res*. 39, 7348, 2011.
13. S. Marchesan, M. Prato. *Chem. Commun.* 51, 4347, 2015.
14. E. G. Lewars. *Computational Chemistry*, Springer, New York, 2011.
15. R. Improta, V. Barone, G. Scalmani, M. J. Frisch. *J. Chem. Phys.* 125, 054103, 2006.
16. R. Improta, G. Scalmani, M. J. Frisch, V. Barone. *J. Chem. Phys.* 127, 074504, 2007.
17. K. B. Wiberg, P. R. Ruben, *J. Comp. Chem.* 14, 1504, 1993.
18. A. E. Reed, F. Weinhold, L. A. Curtiss. *Chem. Rev.* 88, 899, 1988.
19. T. Roman, W. A. Dino, H. Nakanishi, H. Kasai. *Thin Solid Films*, 509, 218, 2006.
20. A. Mavrandonakis, S. C. Farantos, G. E. Froudakis. *J. Phys. Chem. B.* 110, 6048, 2006.
21. W. Sun, Y. Bu, Y. Wang. *J. Phys. Chem. B* 112, 15442, 2008.
22. M. D. Ganji, A. Bakhshandeh. *Physica B: Condensed Matter*, 406, 4453, 2011.

CHAPTER 7

Effect of Doping on Carbon Nanotubes

7.1. Introduction

Understanding the nature of band gaps as to whether a semi-conductor has a direct or indirect gap is extremely essential since it determines the material efficiencies in LEDs, solar cells and laser applications [1-3]. In the band structure diagram, band gap represents the minimum energy difference between the valence band and the bottom of the conduction band. In a direct band gap semi-conductor, the top of the valence band and the bottom of the conduction band occur at the same value of momentum or it can also be defined as the valence band maximum (VBM) and the conduction band minimum (CBM) situated in the same direction of first Brillouin zone. Indirect band gap can be defined as the minimum energy in the conduction band and the maximum energy in the valence band occurring at different values of the crystal momentum. Schematic representations of direct and indirect band gaps are shown in the Figure 7.1 and Figure 7.2 respectively [4].

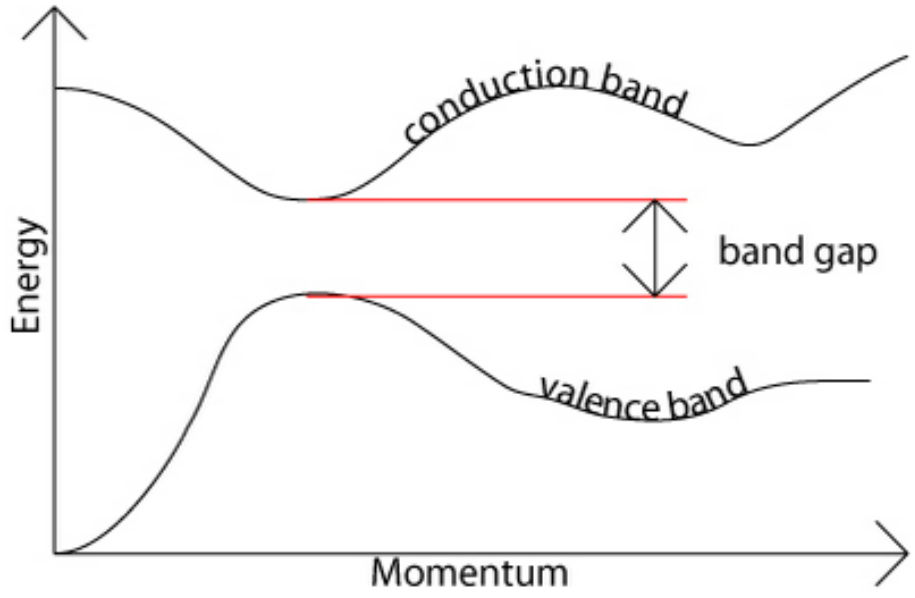

Figure 7.1. Graph plotted Energy vs Momentum showing direct band gap. [4]

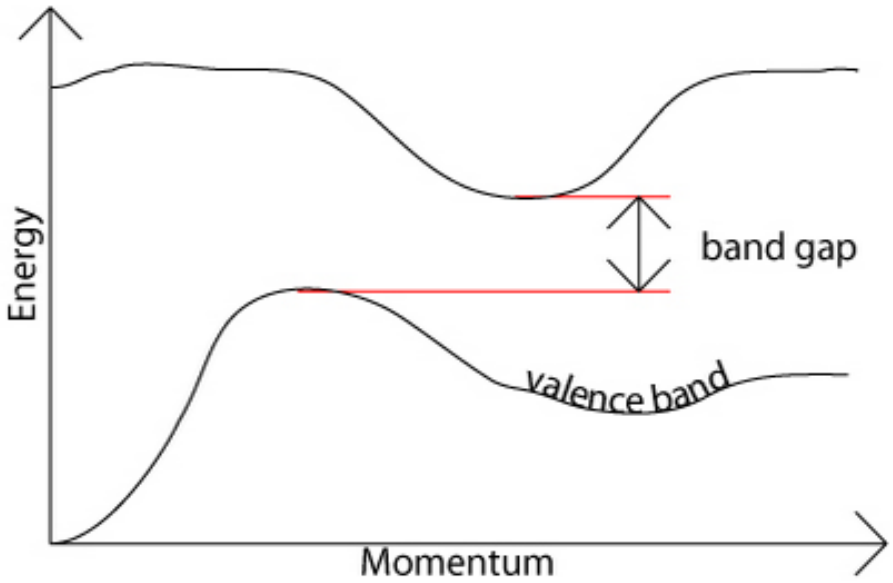

Figure 7.2. Indirect Band gap is depicted in the graph plotted between Energy Vs Momentum. [4]

A common method employed in determining whether the semi-conductor exhibits direct or indirect band gap is by absorption spectroscopy. By plotting the absorption co-efficient against photon energy we can confirm the band gap and also the nature (whether direct or indirect). If the bottom of the conduction band and the top of the valence band are assumed to have a parabolic shape, the absorption coefficient, α can be expressed as in Eq. (7.1). Here, A* is a constant and m depends on the nature of the optical transition: m =1/2 for a direct bandgap, and m = 2 for an indirect gap material. So, the plot of $(\alpha.h.\nu)^2$ vs. hν plot gives a straight line, it is indirect bandgap of material, while a plot of $(\alpha\ h.\nu)^{1/2}$ vs. hν yields a straight line, it is an in direct bandgap material [5].

$$\alpha = A^* \sqrt{h\nu - E_g}\,, \tag{7.1}$$

$$\text{where, } A^* = {q^2 x_{vc}^2 (2m_r)^{\frac{3}{2}}}\Big/{\lambda_0 \epsilon_0 \hbar^3 n} \tag{7.2}$$

Here 'ν' is light frequency, 'E_g' is the band gap energy, A^* is a frequency-independent constant, with m_e^*, m_h^* and m_r, the effective masses of the electron, hole and reduced mass

respectively 'q' is the elementary charge 'n' is the (real) index of refraction 'ε_0' is the vacuum permittivity and 'x_{vc}' is the lattice constant.

In the current chapter we discuss the effect of doping on semi-conducting (8,0) SWCNTs doping with boron and nitrogen respectively (two cases) to understand how the conductivity changes are altered upon substitution with hetero atoms. Boron doping of carbonaceous materials has become an interesting topic of research since the discovery of superconductivity in boron-doped diamond [6]. Various groups have studied the effects of boron doping on CNTs both experimentally [7-9] and theoretically [10,11]. Koretsune *et al.*, [12] carried out a systematic study on doping effects of boron on SWCNTs of various diameters in both zig-zag and arm-chair forms. Their [12] studies reveal that intrinsic semi-conducting SWCNTs band gaps decrease upon doping and substitution of boron atoms with CNTs of narrow diameter are more favored energetically. Similar studies by Kuzmany *et al.*, [13] employing tight binding calculations conclude that doping SWCNTs up to 25% semi-conducting SWCNTs are converted into metallic systems confirming the experimental observations [13]. Doping of SWCNTs with nitrogen in zig-zag and arm-chair forms results in the formation of new energy levels in both valence and conduction band thus making zig-zag SWCNTs conducting [14]. Terrons *et al.*, [15] experimentally confirmed that doping with higher level concentrations of nitrogen up to 10% SWCNTs are found to be metallic [16].

Our previous investigations in Chapter 4 reveal that doping zig-zag SWCNTs results in the formation of indirect band gap materials. In order to understand the doping effects, we have taken a unit cell (32 atoms) of (8,0) SWCNT and substituted with boron atoms and performed DFT calculations to understand the role of doping with various concentrations in determining the band gap of semi-conductor zig-zag SWCNTs.

7.2. Results and Discussion

We have performed DFT band structure calculations employing hybrid functional B3LYP using 6-31G (d) basis set. (8,0) semi-conducting SWCNT with unit cell replication of 32 carbon atoms are considered and periodic boundary conditions were applied along the tube axis to replicate the infinite crystal structure. Default k point settings were chosen as employed in G09 software. Most of the band structure calculations found in literature use plane wave basis sets in DFT framework. However in the current study we employ atom centered Gaussian basis sets. Plane wave basis sets and atom centered basis sets have their

own advantages and disadvantages. For example plane wave basis sets are mathematically simple, good at describing periodic systems and are geometry independent which makes them attractive to use widely since the calculations are computationally cheaper [17]. On the other hand the main drawbacks of plane wave basis sets is that they require large number of basis functions and their accuracy dependence on the choice of the pseudo potentials [18]. Gaussian type of basis sets which are atom centered describes well the core of orbitals and require relatively few functions but suffer with basis set superposition errors [18].

Recently Matsuda *et al.*,[19] performed bench marking calculations in order to determine the accurate band gaps of conductors, semi-conductors and insulators with various DFT methodologies like LDA, GGA along with hybrid functional B3LYP. B3LYP functional along with basis sets employing Gaussian type of orbitals have been found to predict band gaps very close to the experiments. Hence we expect our methodology chosen to probe the band gaps of intrinsic and doped SWCNTs would be more accurate compare to earlier studies employing LDA and GGA [10-13]. We have doped the (8,0) SWCNT substituting with 2, 4, 6, 8 boron atoms respectively in the unit cell and performed band structure calculations.

Table 7.1. Band gaps of boron doped (8,0) SWCNTs with various concentrations, Highest occupied crystalline orbitals (HOCO) and Lowest unoccupied crystalline orbitals energies (LUCO) are given in eV.

System	HOCO	LUCO	Band gap
(8,0)–2B- SWCNT	-3.67	-5.46	-1.79
(8,0)–4B- SWCNT	-3.76	-6.18	-2.42
(8,0)–6B- SWCNT	-4.09	-5.95	-1.86
(8,0)–8B- SWCNT	-3.73	-6.27	-2.54

Doping with boron atoms, we have observed that semi-conducting zig-zag SWCNTs converting to semi-metallic materials. Band gaps of (8,0) SWCNT with various doping concentrations of boron are given in Table 7.1. The direct band gaps of 2B, 4B, 6B, 8B-(8,0) SWCNTs are found to be 0.002, 0.010, 0.190, 0.002 eV respectively and the order of band gap is similar to the indirect band gaps. We observe that band gaps slightly increases from 4B-SWCNT to 6B-SWCNT and decreases on further doping. Perhaps this could be due to

the strain energy associated resulting from doping. Recent studies by Zade *et al.*, [20] and also our own studies [21] reveal that band gaps of cyclic molecules are sensitive to strain energies, for example in the case of 8B-(8,0) SWCNTs, the arrangement is found to be symmetrical with B-C distance in the range 1.55 - 1.57 Å, whereas nanotube doped unsymmetrically with boron atoms, 6B-(8,0) SWCNT exhibit a varied range of bond lengths of B-C in the range of 1.52 - 1.55 Å. Thus we expect that configurations which induce strain due to unsymmetrical doping would result in increase in band gaps. The optimized unit cell replications of boron doped (8,0) SWCNTs are shown in Figure 7.3. and band structure plots are shown in Figures 7.4 and 7.5.

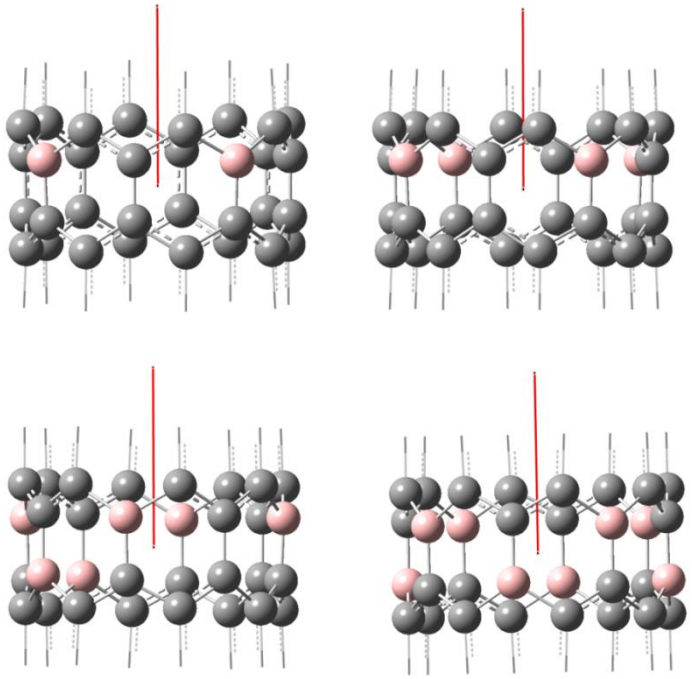

Figure 7.3. Optimized orientations of unit cell replications of 2, 4, 6, 8 –(8,0) SWCNTs. Grey colour indicate carbon atoms and light pink colour indicate boron atoms. Red line indicates PBC replication along the nanotube axis.

Similar results are obtained doping semi-conducting (8,0) SWCNTs with nitrogen. The HOCO, LUCO energies and band gaps are given in Table 7.2. Direct band gaps are found to be 0.003, 0.002 eV for 2N, 8N-SWCNTs respectively. Band structure plots of nitrogen doped (8,0) SWCNTs with 2 and 8 nitrogen atoms are shown in Figure 7.6. Increasing the doping concentration from 2 to 8 nitrogen atoms in the unit cell results in an increase of HOCO energy level from -2.11 to -1.59 eV and decrease in LUCO energy level from -4.57 to

-4.89 eV, with a decrease in indirect band gap from -2.46 to -3.30 eV, shown in Table 7.2 and also plotted in Figure 7.6.

Table 7.2. Band gaps of nitrogen doped (8,0) SWCNTs with various concentrations, Highest occupied crystalline orbitals (HOCO) and Lowest unoccupied crystalline orbitals energies (LUCO) are given in eV.

System	HOCO	LUCO	Band gap
(8,0)–2N- SWCNT	-2.11	-4.57	-2.46
(8,0)–8N- SWCNT	-1.59	-4.89	-3.30

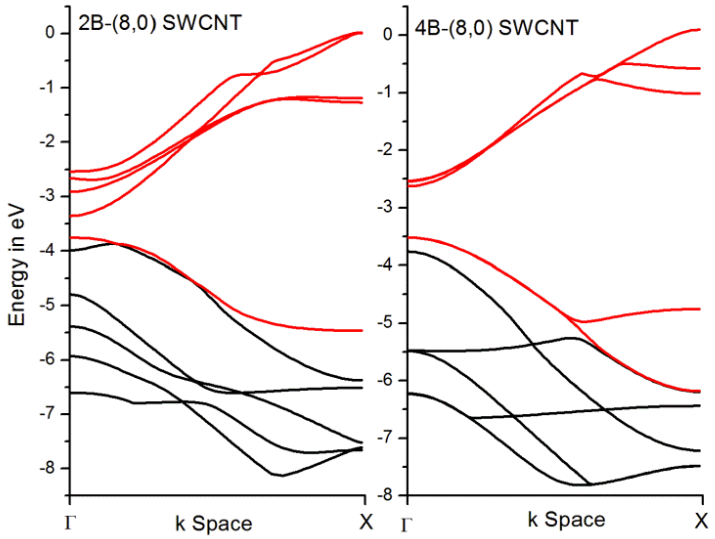

Figure 7.4. Band structure plots of 2B, 4B-(8,0) SWCNTs. Black and red lines indicate frontier occupied and unoccupied crystal orbitals respectively. ("Γ" represents 0 and "X" represents π/a in the k space of Brillouin zone).

It is well reported that LDA and GGA methodologies [19,22] are not accurate in determining band gaps of finite and also infinite crystal structures. B3LYP hybrid functional which combines the Becke GGA exchange potential based on Hartree-Fock (HF) exact exchange plus the Lee-Yang-Parr correlation functional. The inclusion of exact HF exchange helps to correct the self-energy problem with standard DFT formulations [19]. Choice of functional and basis set in DFT formulations decides the accuracy of results. Depending upon the property to be probed choice of functional is to be made.

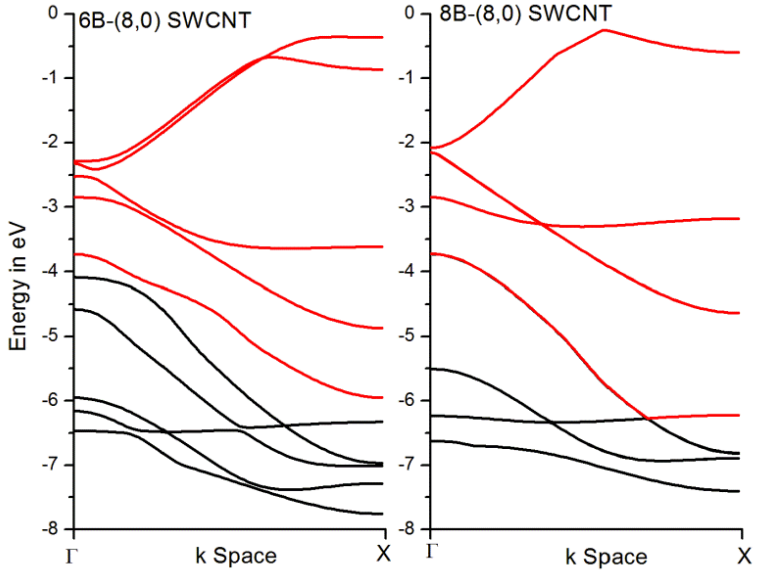

Figure 7.5. Band structure plots of 6B, 8B-(8,0) SWCNTs. Black and red lines indicate frontier occupied and unoccupied crystal orbitals respectively.

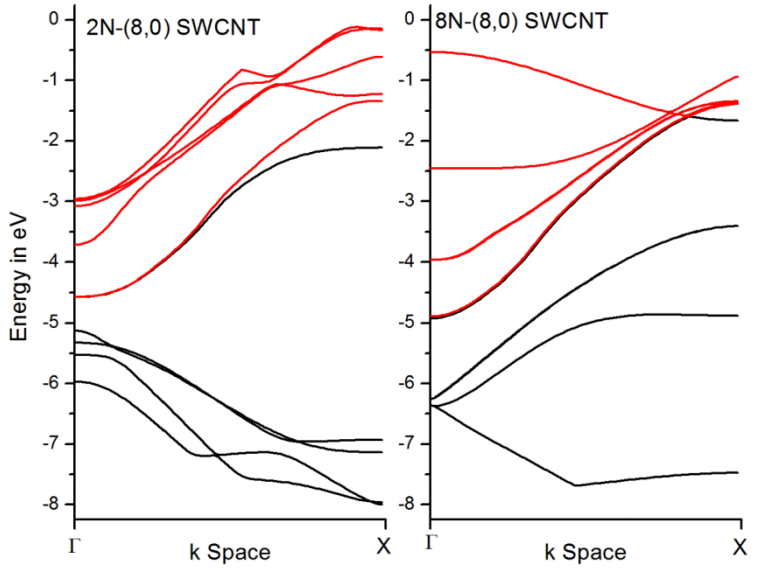

Figure 7.6. Band structure plots of 2N, 8N-(8,0) SWCNTs. Black and red lines indicate frontier occupied and unoccupied crystal orbitals respectively.

It is clear that there is no functional so far prescribed or devised which gives the exact exchange and correlation energy, hence approximations are must and finite basis sets are

employed keeping in mind the computational cost. So a proper choice of functional and basis sets which cancels out the errors arising from each other describes the properties closer to the experiment [23].

7.3. Conclusion

We have investigated the effects of doping on semi-conducting (8,0) SWCNTs with hetero atoms boron and nitrogen. We have observed that semi-conducting SWCNTs converting into semi-metallic materials upon doping. Direct band gaps are found to decrease in all the cases and the trend of band gaps are found to be similar to indirect band gaps. We expect that band gaps of cylindrical SWCNTs to be sensitive with respect to strain energy, where we observe a slight increase in band gaps associated with strain in certain configurations resulting from unsymmetrical doping.

Reference

1. D. K. Seo, R. Hoffmann. *Theor. Chem. Acc.* 102, 23, 1999.
2. Green, A. Martin *Solar Cells: Operating Principles, Technology, and System Applications*. Englewood Cliffs: Prentice-Hall, Inc., 1982.
3. X. Peng, Q. Wei, A. Copple. *Phys. Rev. B.* 90, 085402, 2014.
4. Teaching and Learning packages, DoITPoMS, University of Cambridge 2004-2015.
5. E. Rosencher, B. Vinter. *Optoelectronics*, Cambridge University Press, 2002.
6. E. Ekimov, V. Sidorov, E. Bauer, N. Mel'nik, N. Curro, J. Thompson, S. Stishov. *Nature*, 428, 542, 2004.
7. K. McGuire, N. Gothard, P. L. Gai, M. S. Dresselhaus, G. Sumanasekera, A. M. Rao. *Carbon*, 43, 219, 2005.
8. S. Numao, S. Bandow, S. Iijima. *J. Phys. Chem. C.* 111, 4543, 2007.
9. S. Bandow, S. Numao, S. Iijima. *J. Phys. Chem. C.* 111, 11763, 2007.
10. J. Y. Yi, J. Bernholc. *Phys. Rev. B.* 47, 1708, 1993.
11. H. J. Choi, J. Ihm, S. G. Louie, M. L. Cohen. *Phys. Rev. Lett*. 84, 2917, 2000.
12. T. Koretsune, S. Saito. *Phys Rev B.* 77, 165417, 2008.
13. H. Kuzmany, J. Fink, M. Mehring, S. Roth. *AIP Conference Proceedings*, 685,402, 2003.
14. A. H. Nevidomskyy, Ga´bor Csa´nyi, M. C. Payne. *Phys. Rev. Lett.* 91, 105502, 2003.

15. M. Terrones, H. Terrones, N. Grobert, W. K. Hsu, Y. Q. Zhu, J. P. Hare, H. W. Kroto, D. R. M. Walton, Ph. Kohler-Redlich, M. Rühle, J. P. Zhang, A. K. Cheetham. *Appl. Phys. Lett*. 75, 3932 1999.
16. M. Terrones, P.M. Ajayan, F. Banhart, X. Blase, D.L. Carroll, J.C. Charlier, R. Czerw, B. Foley, N. Grobert, R. Kamalakaran, P. Kohler-Redlich, M. Rühle, T. Seeger, H. Terrones, *Appl. Phys. A.* 74, 355, 2002.
17. D. C. Young. *Computational Chemistry: A Practical Guide for Applying Techniques to Real World Problems,* John Wiley & Sons Inc. 2001.
18. E. Rosencher, B. Vinter. *Optoelectronics,* Cambridge University Press, 2002.
19. Y. Matsuda, J. T. Kheli, W. A. Goddard, III. *J. Phys. Chem. Lett.* 1, 2946, 2010.
20. S. S. Zade M. Bendikov. *J. Org. Chem*. 71, 2972, 2006.
21. T. Vikramaditya, M. Saisudhakar, K. Sumithra. *Electronic structure calculations of cyclic isothionaphthenes* (Under Review).
22. T. Vikramaditya, M. Saisudhakar, K. Sumithra. *J. Mol. Str*. 1081, 114, 2015.
23. T. Vikramaditya, M. Saisudhakar, K. Sumithra. *A comprehensive evaluation of various exchange correlation functionals and basis sets on optical properties of oligothiophenes* (Under review)

CHAPTER 8

Summary

8.1. Summary

We have investigated the adsorption of various gas molecules along the side walls of intrinsic as well as substitutionally doped single walled carbon nanotubes. Among the various gas molecules studied singlet oxygen is found to bind strongly with both intrinsic and doped single walled carbon nanotubes (SWCNTs). Singlet oxygen is found to bind with a binding energy of -0.88 and -1.6 eV with (8,0) intrinsic and boron doped SWCNTs. This is a very interesting and new finding which can be further exploited in detail. It is well known that singlet oxygen can be used in photodynamic therapy to cure the tumor cells which are deficient in oxygen concentrations. Carbon nanotubes, with its special needle like geometry, can penetrate deep into the cell walls and can achieve this transport of singlet oxygen to the desired locations of the tumor cells thus helping in curing the affected areas. Intrinsic SWCNTs exhibited a weak binding with all the gases studied whereas boron doped SWCNTs are found to be sensitive with oxygen, water vapor and ammonia. Triplet oxygen, water vapor and ammonia are found to exhibit a binding energy of -0.04, 0.08, 0.09 eV with intrinsic (8,0) SWCNTs and -0.08, -0.54, -0.58 eV with boron doped (8,0) SWCNTs respectively. Our studies reveal that pure intrinsic SWCNTs are not suitable for sensor applications since there is a negligible charge transfer between intrinsic SWCNTs and the gas molecules and hence do not result in conductivity changes upon adsorption. However, SWCNTs doped with boron are found to be sensitive towards, oxygen, (in both the spin states) water vapor and ammonia. In the case of oxygen adsorption, the charge transfer is found to occur from the tube to the oxygen molecule, intrinsic (8,0) SWCNT exhibit a negligible charge transfer of -0.004 e, whereas boron doped (8,0) SWCNT exhibit a charge transfer of -0.497 e (Mulliken population analysis) (Negative sign indicate charge transfer from the CNT to the molecule adsorbed and positive sign indicate the charge transfer from the molecule to the CNT). In the case of water vapor and ammonia, charge transfer is found to occur from the adsorbed molecule to the boron doped SWCNT. Intrinsic (8,0) SWCNTs exhibit a charge transfer of -0.004, -0.008 e with water vapor and ammonia on the other hand boron doped (8,0) SWCNTs exhibit a charge transfer of 0.258, 0.235 e with water vapor and ammonia respectively (Mulliken population analysis). From these results it is clear that charge transfer is negligible in the case of intrinsic SWCNTs whereas it is appreciable when doped with dopants like boron. Another interesting finding of our research is the diameter

effect. We have observed that with the increase in diameter of the SWCNTs, the binding energy decreases, but the charge transfer almost remained the same. Boron doped (5,0), (7,0) and (8,0) SWCNTs exhibit a binding energy of -1.05, -0.64, -0.58 eV respectively whereas charge transfer is found to be almost constant of 0.2 e (Mulliken population analysis) and 0.19e (NPA population analysis) for all the SWCNTs of various diameters. This finding has an important application, if the binding energy is more than the sensor will suffer with longer recovery times and it makes the removal of adsorbed molecule difficult due to the strong binding energy between adsorbed molecule and SWCNT. By increasing the diameter of the SWCNTs, we observe the binding energy to decrease as in the case of boron doped SWCNT with ammonia improves the performance of sensors with less recovery times, without compromising on the sensitivity. The charge transferred is almost found to remain constant and in this way sensitivity is unaffected. Another interesting result of our research is that band structure calculations reveal that substitutionally doping pure intrinsic SWCNT with boron makes the semi-conducting SWCNT an indirect semi-metal.

We have also investigated the adsorption of bio-molecules like glycine with intrinsic and functionalized SWCNTs in both neutral and zwitter-ionic forms considering the solvent effects. Glycine in both non-ionic and zwitter-ionic states is found to exhibit weak binding energies with intrinsic SWCNT, with the latter interaction being more favorable. In all the cases charge transfer is observed to be weak, with charge being transferred from the glycine to the SWCNT. Zwitter-ions are found to adsorb stronger than their nonionic counterparts and physisorption is strongest through the active carbonyl oxygen site for the zwitter-ionic-glycine amino acid, in contrast to the non-ionic case. Glycine shows better interaction in both non-ionic and zwitter-ionic states with functionalized SWCNTs compared to that of intrinsic SWCNT and binding energy is found to be enhanced in the aqueous media.

Employing hybrid functional B3LYP in the DFT formalism, which is found to predict reasonable binding energies, charge transfers and band gaps nearer to the experimental results, we have investigated the adsorption of various gases on the sidewalls of SWCNTs of various diameters. We have observed that boron doped SWCNTs can sense gas molecules better in comparison to pure intrinsic SWCNTs which remain passive to many gaseous species. Since the boron doped SWCNTs are found to be sensitive to various gases, future research can be driven to achieve the selectivity with these systems. For example, we have observed that boron doped SWCNTs are capable of sensing oxygen, water vapor and ammonia. In the case of oxygen adsorption with boron doped SWCNTs charge is being

transferred from the tube to the oxygen molecule which would decrease the band gap by increasing the hole-carriers of boron doped semi-conducting SWCNTs. On the other hand with water and ammonia charge is being transferred from the adsorbed molecule to the boron doped SWCNTs. It would be interesting to probe, how the conductivity changes of boron doped SWCNTs are altered, in the presence of both the gases which are found to exhibit similar charge transfers in order to realize the selectivity with different gases.

List of Publications

1. **T. Vikramaditya**, K. Sumithra.
   New insights in the adsorption of oxygen molecules on single walled carbon nanotubes;
   Computational Materials Science, 79, 656–662, (2013).
2. **T. Vikramaditya**, K.Sumithra.
   Effect of substitutionally boron-doped single walled semi-conducting zigzag carbon nanotubes on ammonia adsorption;
   Journal of Computational Chemistry, 35, 586-594, (2014).
3. **T. Vikramaditya**, K.Sumithra.
   Effect of substitutional doping on adsorption of environmentally relevant molecules on single walled carbon nanotubes;
   Advanced Chemistry Letters, 1, 1-8, (2014).
4. **T. Vikramaditya**, M. Saisudhakar, K.Sumithra.
   Electronic structure of α-oligothiophenes with various substituents;
   Journal of Molecular Structure, 1081 114–123, (2015).
5. **T. Vikramaditya**, M. Saisudhakar, K. Sumithra.
   The adsorption of glycine in non-ionic and zwitter-ionic states on intrinsic and functionalized semi-conducting carbon Nanotubes;
   Journal of Computational and Theoretical Nanoscience, 12, 1-7, (2015).
6. **T. Vikramaditya,** M. Saisudhakar, K. Sumithra.
   A PBC-DFT study of electronic properties of substituted Polythiophenes (In press).
   Journal of Physical Organic Chemistry, *DOI: 10.1002/poc.3473.*
7. **T. Vikramaditya,** M. Saisudhakar, K. Sumithra.
   Time-dependent density functional study of the absorption and emission properties of α-oligothiophenes (Under review).
8. **T. Vikramaditya,** M. Saisudhakar, K. Sumithra.
   Electronic structure calculations of linear and cyclic isothianapthes (Under preparation).
9. **T. Vikramaditya,** M. Saisudhakar, K. Sumithra.
   Metal free organic compounds in OLED applications - A DFT-study (Under preparation).

Presentations in International and National Conferences

1. **T. Vikramaditya**, K. Sumithra. (Oral presentation by K. Sumithra)
   Doped Carbon nanotubes as sensors for oxygen and ammonia;
   International Conference on Computational Modelling of Nanostructured Materials (ICCMNM 2013) Frankfurt Institute for Advanced Studies (FIAS) Frankfurt am Main, Germany (2013).
2. **T. Vikramaditya**, K. Sumithra. (Oral presentation by K. Sumithra)
   New insights for a carbon nanotube based oxygen sensor;
   The India-Israel Meeting on Materialscience and Nanoscience (IIMMN-2013), Mahatma Gandhi University, Kerala, India (2013).
3. **T. Vikramaditya**, K. Sumithra. (Poster presentation)
   Adsorption of gas molecules on carbon nanotubes;
   Theoretical Chemistry Symposium (TCS), I.I.T, Guwahati, India (2012).
4. **T. Vikramaditya,** M. Saisudhakar, K. Sumithra. (Poster presentation)
   Electronic and structure properties of Oligothiophenes;
   Chemistry with Computers, IIIT-Hyderabad and IICT-Hyderabad, India (2014).
5. **T. Vikramaditya,** M. Saisudhakar, K. Sumithra. (Poster presentation)
   Diagnostic test to assess the role of Functional, solvent formalism and basis set in determining the optical properties;
   13th Eurasia Conference on Chemical Sciences, Indian Institute of Science, Bangalore, India (2014).
6. M. Saisudhakar, **T.Vikramaditya,** K. Sumithra. (Poster presentation)
   Effect of Substituents on the electronic properties of oligo and polythiophenes;
   13th Eurasia Conference on Chemical Sciences, Indian Institute of Science, Bangalore, India (2014).

Biography of Mr. T. Vikramaditya – Vikramaditya completed his graduation (B.Sc., with Mathematics, Physics and Chemistry) from Acharya Nagarjuna University, Guntur, Andhra Pradesh. He completed his post-graduation in Chemistry from University College, Kakatiya University, Warangal, Telangana State. After clearing Joint UGC-CSIR exam he joined in Computational Chemistry Division, Department of Chemistry, BITS Pilani, Hyderabad campus in the year 2011 as a junior research fellow. His research interests are adsorption studies of carbon nanotubes in sensor applications and also studying the optical and conductivity properties of various organic molecules which find applications in OLEDs and solar cells employing electronic structure calculations.

Biography of Prof. K. Sumithra - Prof. K. Sumithra is presently working as associate professor, Department of Chemistry in Birla Institute of technology and science, Pilani Hyderabad Campus, India where she joined in July, 2009. She received her Doctoral degree from Cochin University of Science and Technology, Cochin, Kerala. After Ph.D. she has worked briefly as a lecturer and has worked in various institutes in Germany as a post-doctoral researcher. After this, she has worked in Martin Luther University on a C1 position equivalent to Junior Professor in the Theoretical Physics division for about six years.

She has been involved in teaching and research for the past 15 years. Her research interest mainly focus on Statistical Mechanics of Polymer in disordered media, Adsorption of polymers on surfaces, Pattern Recognition and Computational Material Science. Her current research concentrates on adsorption on carbon nanotubes, band structure calculations, organic semiconducting oligomeric and polymeric systems etc. She has published several research articles in various peer reviewed international journals. Recently, she has successfully completed a project funded by DST and another project funded by CSIR is under way.